THE SIMULATED RAMAN EFFECT

Donald M. Paul

A Thesis Submitted for the Degree of PhD
at the
University of St Andrews

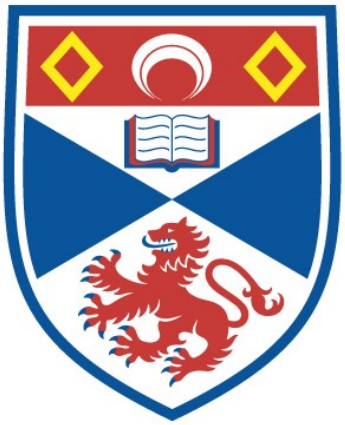

1972

Full metadata for this item is available in
St Andrews Research Repository
at:
http://research-repository.st-andrews.ac.uk/

Please use this identifier to cite or link to this item:
http://hdl.handle.net/10023/14624

This item is protected by original copyright

THE STIMULATED RAMAN EFFECT

A Thesis

presented by

Donald M. Paul, B.Sc.

to the

University of St. Andrews

in application for the Degree

of Doctor of Philosophy.

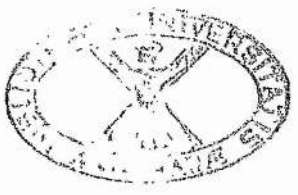

ProQuest Number: 10167165

All rights reserved

INFORMATION TO ALL USERS
The quality of this reproduction is dependent upon the quality of the copy submitted.

In the unlikely event that the author did not send a complete manuscript
and there are missing pages, these will be noted. Also, if material had to be removed,
a note will indicate the deletion.

ProQuest 10167165

Published by ProQuest LLC (2017). Copyright of the Dissertation is held by the Author.

All rights reserved.
This work is protected against unauthorized copying under Title 17, United States Code
Microform Edition © ProQuest LLC.

ProQuest LLC.
789 East Eisenhower Parkway
P.O. Box 1346
Ann Arbor, MI 48106 – 1346

Th 5934

DECLARATION

I hereby certify that this thesis has been composed by me, and is a record of work done by me, and has not previously been presented for a Higher Degree.

This research was carried out in the Physical Science Laboratory of St. Salvator's College, in the University of St. Andrews, under the supervision of Mr. A. Maitland.

Donald M. Paul

CERTIFICATE

I certify that Donald M. Paul, B.Sc., has spent nine terms at research work in the Physical Science Laboratory of St. Salvator's College, in the University of St. Andrews, under my direction, that he has fulfilled the conditions of Ordinance No. 16 (St. Andrews) and that he is qualified to submit the accompanying thesis in application for the Degree of Doctor of Philosophy.

_____

Research Supervisor

CAREER

I first matriculated in the University of St. Andrews in October 1960. I studied Mathematics and Natural Philosophy, and obtained First Class Honours in Natural Philosophy in 1964.

In October 1964, following the award of an S.R.C. Research Studentship, I was enrolled as a research student under Ordinance 12, and was transferred to Ordinance 16 in October 1965 as a candidate for the degree of Ph.D.

ACKNOWLEDGEMENTS

I would like to thank my supervisor, Mr. A. Maitland, for his encouragement and helpful advice throughout this work and also Professor J.F. Allen for making the necessary laboratory facilities available.

I would like to thank the entire technical staff, and Mr. Fritz Akerboom, who made the argon laser tube and Mr. J. McNab of the research students workshop, who deserve special praise for technical assistance and design suggestions.

ABSTRACT

THE STIMULATED RAMAN EFFECT

The present work describes a theoretical and experimental investigation of the stimulated Raman effect excited by the focused output of a slow, Q-switched ruby laser in the self-focusing liquids benzene, nitrobenzene, chlorobenzene, and carbon disulphide. Time relationships between the exciting pulse, the transmitted laser pulse, and the time resolved stimulated Raman spectra have been studied using a high speed streak camera in conjunction with fast photodiodes. The spontaneous Raman spectra of these liquids have been investigated using a photoelectric Raman spectrometer and a method is outlined for measuring the relative values of the stimulated Raman gain coefficients.

It is experimentally shown that, on a nanosecond time scale, stimulated Raman lines are not generated simultaneously but in the sequence Stokes, Anti-Stokes, and second harmonic Stokes. Further, the time delay between the start of first and second harmonic Stokes is shown to be dependent on the rate of rise of the exciting pulse. It was found that during stimulated Raman generation the laser pulse transmitted through the liquid was heavily distorted and that each liquid produced its own characteristic pulse distortion. No distortion was found in the absence of stimulated Raman generation. Time correlation were found between the duration of features of the pulse distortion and the duration of first Stokes and second harmonic Stokes. These correlatio show that forward stimulated Raman generation is controlled by the

transmitted laser pulse not the exciting pulse. The threshold for the onset of pulse distortion is shown to be dependent on the rate of rise of the exciting pulse whilst, in all the liquids, apart from carbon disulphide, the 'cut-off' threshold is dependent on the peak power of the incident pulse. Investigation of the pulse distortion thresholds for the range of liquids produced relative values which did not agree with those predicted from either the optical Kerr coefficient or the calculated stimulated Raman gain coefficients.

A theoretical model of the self-focusing of a focused beam in a medium for which both electrostriction and the optical Kerr effect are significant is presented and has been used to explain the anomalous threshold results. Within the experimental scatter of the results obtaine this model appears to explain the observed threshold effects. Since the forward stimulated Raman generation was weak in comparison to the transmitted laser pulse and followed this distorted pulse rather than the exciting pulse, it is concluded that stimulated Raman is not the dominant mechanism in the interaction. A brief review is presented of the theory and predictions of steady and non-steady state Brillouin scattering. Although the phonon lifetimes for the other liquids appear to be too short to be of significance, the results are similar in form to those of carbon disulphide. An explanation based on multiphoton absorption is suggested to explain the anomalous behaviour of these liquids. It is concluded that the observed effects in the forward stimulated Raman process depend upon the development in time of the non-linear field dependent self-focusing of the exciting beam and the strong backward scattering process.

CONTENTS

CHAPTER 1

THE RAMAN EFFECT

1.1 The Raman Effect

The Raman effect, discovered by Raman and Krishnan[1] is the inelastic scattering of light by a molecule such that when a photon interacts with the molecule some of the photon energy is distributed into the rotational and vibrational states of the molecule. The result of the interaction is that light scattered from the molecule is shifted in frequency by amounts corresponding to the particular vibrational and/or rotational states excited. The phenomenon was predicted by Smekal[2] who reasoned that a quantum of light of frequency, ν, could interact with a molecule in energy state, E_k, by an inelastic collision. Conservation of energy demands that

$$h\nu + E_k \rightarrow h\nu' + E_n, \qquad 1.1.1(a)$$

where $h\nu'$ is the energy of the scattered photon, and E_n is some definite state of the molecule after the interaction. If we have $\nu'<\nu$, the line generated is termed a Stokes line, and if $\nu'>\nu$, the line generated is an Anti-Stokes line. Then we have

$$m + h\nu \rightarrow m^* + h\nu', \ \nu'<\nu, \ \text{Stokes}$$

$$m^* + h\nu \rightarrow m + h\nu'', \ \nu''>\nu, \ \text{Anti-Stokes} \qquad 1.1.1(b)$$

where m is the molecular ground state and m^* the excited state. The Raman frequencies are given by

$$\nu'-\nu = (E_k - E_n)/h \ . \qquad 1.1.2$$

The excitation does not correspond to a straightforward absorption and re-emission of energy. A third state m_ν, which is an intermediate

state, is involved, but the incoming radiation need only satisfy the condition that

$$h\nu > E_k - E_n \quad . \qquad 1.1.3$$

The process may be written as

$$m + h\nu \rightleftarrows m_v$$

$$m_v \rightleftarrows m^* + h\nu' \quad .$$

The net process is given by

$$m + h\nu \rightleftarrows m^* + h\nu',$$

where $m_v > m^*$.

1.2 Polarisability

Placzek[3] related the Raman effect to changes in the polarisability of the molecule interacting with an optical field. When a molecule is introduced into an electric field, $\underline{E}$, an electric dipole moment, $\underline{P}$, per molecule is induced. If the polarisability of the molecule is α then the magnitude of the induced dipole is given by

$$|\underline{P}| = \alpha \, |\underline{E}| \quad . \qquad 1.2.1$$

Both $\underline{P}$ and $\underline{E}$ are vectors and for an isotropic molecule they are in the same direction and α is scalar. However, for nonisotropic molecules the application of an electric field in a fixed direction induces a moment in a different direction and α is a tensor.

The equations taking account of the different polarisabilities along the different principal axes of the molecule are

$$P_x = \alpha_{xx}E_x + \alpha_{xy}E_y + \alpha_{xz}E_z \ ,$$

$$P_y = \alpha_{yx}E_x + \alpha_{yy}E_y + \alpha_{yz}E_z \ ,$$

$$P_z = \alpha_{zx}E_x + \alpha_{zy}E_y + \alpha_{zz}E_z \ . \qquad 1.2.2$$

The tensor, α, is defined by the nine coefficients α_{xx}, ..., but since we have $\alpha_{xy} = \alpha_{yx}$, etc., there are effectively only six. These six coefficients together with the coordinates x, y, z may be used to derive the polarisability ellipsoid which is given by

$$\alpha_{xx} x^2 + \alpha_{yy} y^2 + \alpha_{zz} z^2 + 2\alpha_{xy} xy + \ldots\ldots = 1$$

Thus the components of the polarisability of the molecule are taken along the three component axes x, y, z, and the magnitudes of these components determine the polarisation ellipsoid.

The criteria for generation of Raman can be derived classically by considering the oscillating electric vector of an optical field, $E\cos 2\pi\nu t$, acting upon a molecule. For very small vibrational amplitudes the polarisability is related to the normal vibrational coordinate, q_ν, by the equation

$$\alpha = \alpha^o + (\partial\alpha/\partial q_\nu)^o q_\nu, \qquad 1.2.3$$

where the zero corresponds to the equilibrium value. This equation holds for each of the six coefficients defining α. The dependence of the normal coordinate on the vibrational frequency, ν_ν, is given by

$$q_\nu = q^o \cos 2\pi\nu_\nu t , \qquad 1.2.4$$

where q^o is the normal coordinate of the initial equilibrium position. Putting the frequency variation of E into 1.2.2 we get

$$P_x = (\alpha_{xx}E_x + \alpha_{xy}E_y + \alpha_{yz}E_z) \cos 2\pi\nu t . \qquad 1.2.5$$

From 1.2.3 and 1.2.5, we have

$$P_x = (\alpha^o_{xx}E_x + \alpha^o_{xy}E_y + \alpha_{xz}E_z) \cos 2\pi\nu t + \{(\frac{\partial\alpha_{xx}}{\partial q_\nu})_o E_x + (\frac{\partial\alpha_{xy}}{\partial q_\nu})_o Ey + (\frac{\partial\alpha_{xz}}{\partial q_\nu})_o E_z\}\cos 2\pi\nu t \cos 2\pi\nu_\nu t$$

1.2.6(a)

This equation readily gives

$$P_x = (\alpha^o_{xx} E_x + \alpha^o_{xy} E_y + \alpha^o_{xz} E_z)\cos 2\pi\nu t \qquad 1.2.6(b)$$

$$+ \frac{q_o}{2}\{\left(\frac{\partial \alpha_{xx}}{\partial q_\nu}\right)E_x + \ldots.\}\{\cos 2\pi(\nu-\nu_\nu)t + \cos 2\pi(\nu+\nu_\nu)t\}$$

The first term in 1.2.6(b) corresponds to a dipole oscillating at the frequency of the incident radiation, whilst the second term with frequency $(\nu-\nu_\nu)$ and $(\nu+\nu_\nu)$, correspond to Raman Stokes and Anti-Stokes generation.

The physical interpretation of the above expression is that, whilst the polarisability gives rise to Rayleigh scattering, it is the changes in the polarisability during intramolecular motions which are responsible for Raman generation. The criterion for Raman generation is therefore that one of the six polarisability tensors must change curing an intramolecular vibration or rotation.

This simple classical treatment indicates equal probabilities (intensities) for Stokes and Anti-Stokes which is not the case. A quantum mechanical treatment gives the correct intensities of the various Raman lines.

1.3 Semi-Classical Treatment

Although the dispersion theory of Kramers and Heisenberg (1925) can readily be extended to the Raman effect, the first analysis was presented by Placzek[3]. He postulated that the radiation from a material system is determined by the time-variation of an electric moment and solved the time-dependent Schrödinger equation under the

perturbation of the dipole moment caused by a monochromatic radiation field and hence calculated the magnitude of the electric dipole moment, F_{kn}, for a molecule making a transition from state k to state n through intermediate states r. Placzek's result is

$$F_{kn} = \sum_r \{ (A\mu_{kr})\mu_{rn} /(h\nu_{rk}-h\nu) + \mu_{kr} (A\mu_{rn})/(h\nu_{rn}+h\nu)\} , \quad 1.3.1$$

A is a complex time-independent field vector, and $\mu_{kr,rn}$ is the moment between states k and r, and states r and n. This dipole moment corresponds to scattering light at a frequency $\nu+\nu_{kn}$ (anti-Stokes) subject to the condition

$$E_k - E_n < h\nu . \quad 1.3.2$$

The intensity of the total Raman scattering can be derived from the classical dipole radiation for the transition k to n which gives

$$I_{kn} = \frac{64\pi^4}{3c^3} (\nu+\nu_{kn})^4 |F_{kn}|^2 \quad 1.3.3$$

The physical content of the above expression is that the Raman effect is an interaction whereby the molecule makes a transition (k,r,n) under the action of the radiation field. Two levels (k,n) can only exhibit the Raman effect provided that there exists a third level to which transitions are allowed. A more rigorous quantum electrodynamical treatment shows that the two terms of the electric moment correspond to two mechanisms producing the Raman effect. According to Heitler, these are the following:

(1) an absorption event followed by emission leaving the molecule in state n; and

(2) an emission event followed by absorption, the molecule again having the terminal state n.

Using the polarisation equations of paragraph 1.2 the electric moment, F_{kn}, can be related to the magnitude of the induced dipole. Designating the Cartesian coordinates x, y, z by the subscripts ρ and σ , we obtain

$$(F_\rho)_{kn} = \sum_\sigma (C_{\rho\sigma})_{kn} \cdot A_\sigma \qquad 1.3.4$$

where $(C_{\rho\sigma})_{kn}$ is given by

$$(C_{\rho\sigma})_{kn} = \sum_r \{(\mu_\sigma)_{kn} (\mu_\rho)_{rn}/(h\nu_{rk} - h\nu)\}$$

$$+ \{(\mu_\rho)_{kn} (\mu_\sigma)_{rn}/(h\nu_{rn} + h\nu)\} \qquad 1.3.5$$

It can be readily shown that

$$(C_{\rho\sigma})_{kn} = (\alpha_{\rho\sigma})_{kn} \qquad 1.3.6$$

Therefore, the magnitude of the induced dipole can be expressed in terms of the polarisability by the following

$$F_{kn} = \sum_\rho (F_\rho)_{kn} = \sum_{\rho,\sigma} (\alpha_{\rho\sigma})_{kn} \cdot A_\sigma \qquad 1.3.7(a)$$

This can be written as $F_{kn} = A \sum_{\rho,\sigma} (\alpha_{\rho\sigma})_{kn} \cdot e_\sigma$ 1.3.7(b)

where e_σ is a unit vector in the direction of the applied field for a plane polarised monochromatic exciting source .

1.4 Dirac's Scattering Theory

In Placzek's treatment, the relation between the electric moment and the scattered radiation was hypothesised, but in Dirac's treatment[4] the hypothesis is replaced by a quantum theoretical picture of the radiation field in which the molecules and the radiation field form a single system whose Hamiltonian, H, is made up of the energy of the molecule, H_m, the energy of the radiation, H_s, and the

interaction energy, H', thus we have

$$H = H_m + H_s + H'$$

The Hamiltonian of the unperturbed system consists of

$$H_o = H_m + H_s \ .$$

The interaction energy, H', is considered to be the perturbation.

To determine H_s, the radiation is imagined to be enclosed in a cavity with walls having specular reflecting surfaces so that the radiation field consists of standing waves i.e., eigenvibrations (modes) of energy, E, given by

$$E = \sum_s E_s = \sqrt{\frac{8\pi}{V}} \sum_s e_s E'_s(t) \sin\Gamma_s \qquad 1.4.1$$

In equation 1.4.1, Γ_s is given by

$$\Gamma_s = 2\pi\nu_s(k_s r)/c + \delta_s \ ,$$

and the other symbols are as follows, e_s is a unit vector in the direction of the field, E'_s is the field amplitude, ν_s the frequency, k_s the propagation vector, r the position vector, c the velocity of light, δ_s an arbitrary phase, and V is the volume of the cavity. The classical expression for the energy density of a harmonic oscillator leads to the equation

$$H_s = \tfrac{1}{2}\sum_s (\dot{q}_s + 4\pi\nu_s^2 q_s^2) \qquad 1.4.2$$

Equation 1.4.2 represents a system of oscillators with frequency ν_s and mass unity. The number of eigenvibrations in unit volume in a frequency range ν to $\nu + d\nu$ is readily shown to be

$$dN_\nu = (8\pi\nu^2/c^3)d\nu \qquad 1.4.3$$

The interaction of the radiation and the molecule is given by

$$H' = -(\mu.E) \qquad 1.4.4$$

The Schrödinger equation of the unperturbed system (molecule and radiation) is given by

$$(H_o - E)\psi = 0,$$

where $$H_o = H_m + \tfrac{1}{2} \sum_s (\dot{q}_s^2 + 4\pi^2 \nu_s^2 q_s^2)$$

The eigenvalues are the sums of the energies of the molecule and the cavity while the eigenfunctions are products

$$E_{ns} = E_n + \sum_s (n + \tfrac{1}{2}) h\nu_s$$

$$\psi_{ns} = \psi_n \prod_s U_{ns}$$

The state of the radiation field is determined by the quantum numbers n_s, which indicate the number of light quanta that occupy the individual eigenvibrations. The eigenfunctions, U_{ns}, are harmonic oscillator functions.

Let us consider next any given state of the radiation field, s_o and state k of the molecule. As long as the energy is the sum of that of the molecule and the cavity, the system remains in the same state. When H' is included, transitions are made to state s,n. Eigenfunctions of the perturbed system are developed in terms of the unperturbed system, thus we have

$$\psi = \sum_{ns} a_{ns}(t)\, \psi_{ns} \exp(-iE_{ns}t/h).$$

First order perturbation theory then gives

$$a_{ns}^{(1)} = \sum_{ns} H'^{\,ks_o} \frac{\{1-\exp 2\pi i(\nu_{nk} + \nu_{ss_o})t\}}{2(\nu_{nk} + \nu_{ss_o})} \qquad 1.4.6(a)$$

where

$$(H')_{ns}^{ks_o} = \int \psi^*_{ns}\, H'\psi_{ks_o}\, d\tau$$

and in second order

$$a_{ns}^{(2)} = \sum_{rs'} \frac{(H')_{rs'}^{ks_o} (H')_{ns}^{ns'}}{2(\nu_{rk}+\nu_{s's_o})} \times \frac{1-\exp 2\pi i(\nu_{nn}+\nu_{ss'})t}{2(\nu_{nn}+\nu_{ss'})} - \frac{1-\exp 2\pi i(\nu_{nk}+\nu_{ss_o})t}{2(\nu_{nk}+\nu_{ss_o})} \qquad 1.4.6(b)$$

By substitution of H' from equations 1.4.4 and 1.4.1 into 1.4.6, the first order perturbation theory yields processes corresponding to absorption and emission for which the atom changes its quantum state and for which the population number of the cavity oscillators changes by ±1.

To obtain the scattered radiation, the second order perturbation theory is considered. Since H' (according to 1.4.1)and 1.4.2 is linear in q_s, and since the selection rules for the harmonic oscillator are $\Delta n_s = \pm 1$, it can be seen by inspection of 1.4.6(b) that only those transitions are possible for which two cavity oscillators change by ±1, while the molecule may change or remain in the same state. Considering the cavity, three cases are distinguished. The population numbers of cavity oscillators are denoted by n_α and n_β where the subscripts α and β are particular eigenvibrations of the radiation field, s, which undergo a change of state.

1. $n_\alpha' = n_\alpha + 1$, $n_\beta' = n_\beta + 1$, double emission.

2. $n_\alpha' = n_\alpha - 1$, $n_\beta' = n_\beta - 1$, double absorption.

or 3 $n_\alpha' = n_\alpha + 1$, $n_\beta' = n_\beta - 1$.

In case 3, $h\nu_\alpha$ or $h\nu_\beta$ disappear and $h\nu_\beta$ or $h\nu_\alpha$ appear as scattered radiation. The third process is the Raman effect and we shall now consider this to obtain an expression for the probability amplitude, $|a_{nS}^{(2)}|^2$. Equation 1.4.6 along with the matrix elements shown in 1.4.1, 1.4.4, 1.4.5 and the following values for the coordinate matrices of the oscillator are employed,

$$q_{n_s,n_{s+1}} = \sqrt{\frac{(n_s+1)h}{8\pi^2\nu_s}}\exp(2\pi i\nu_s t)$$

$$\dot{q}_{n_s,n_{s+1}} = i\sqrt{\frac{(n_s+1)h\nu_s}{2}}\exp 2\pi i\nu_s t$$

$$q_{n_s,n_{s-1}} = \sqrt{\frac{n_s h}{8\pi^2\nu_s}}\exp 2\pi i\nu_s t$$

$$\dot{q}_{n_s,n_{s-1}} = \sqrt{\frac{n_s h\nu_s}{2}}\exp 2\pi i\nu_s t$$

The quantity $|a_{ns}^{(2)}|^2$ gives the probability of the molecule making a transition n to k in a time t by an interaction with the radiation field in a state $s_o(n_2,n_1 \cdot n_\alpha,n_\beta \text{ ---n;})$ which after the interaction is in a state $s(n_2,n_1, \text{ --}\underset{\alpha}{n-1}\text{-}\underset{\beta}{n+1} \text{ ---}n_j)$. For this transition we have

$$|a_{ns}^{(2)}|^2 = \frac{64\pi^2}{\nu^2} n_\alpha(n_\beta+1)\nu_\alpha\nu_\beta\sin^2\Gamma_\alpha\sin^2\Gamma_\beta|s_{kn}^{\alpha\beta}|^2\sin^2\pi\frac{(\nu_{kn}+\nu_\alpha-\nu_\beta)t}{(\nu_{kn}+\nu_\alpha-\nu_\beta)^2}$$

and

$$s_{kn}^{\alpha\beta} = h^{-1}\sum_r \frac{(e_\alpha M_{kn})(e_\beta M_{rn})}{\nu_{rk}-\nu} + \frac{(e_\beta M_{kr})(e_\alpha M_{kn})}{\nu_{rn}+\nu} \qquad 1.4.7(a)$$

To obtain the scattering of an incident spectral line of frequency ν, equation 1.4.7(a) is summed over all final states, s, and over all

eigenvibrations, α, that occur in the incident radiation. The first summation is carried out by integrating over all solid angles and emitted frequencies, $d\nu$. On consideration of the number of vibrations per solid angle, the frequency range given by 1.4.3 and the density, $\rho_{j'}(\nu',\omega')d\nu'd\omega'$, of the radiation of a given polarisation and frequency in the cavity,

where $$\rho_{j'}(\nu',\omega')d\nu'd\omega' = \sum_{\beta}^{\Delta\nu'\Delta\omega'} n_\beta h\nu_\beta/V \ ,$$

the probability may be rewritten in the form

$$|a_{ns}^{(2)}|^2 = \frac{64\pi^2}{\nu h}\cdot n_\alpha \nu \sin^2\Gamma_\alpha \sin^2\Gamma_\beta \sum_{j'} \iint (\rho_{j'}(\nu',\omega') + \frac{h\nu'^3}{c^3}) \times |s_{kn}^{\alpha,k'j'}|^2 \sin^2\pi(\nu_{kn}+\nu_\alpha-\nu')t(\nu_{kn}+\nu_\alpha-\nu')^{-2}\, d\nu'd\omega' \quad 1.4.7(b)$$

The vector e_β is replaced by the unit vector $e_{k',j'}$, which is perpendicular to the direction of propagation k' and is fixed by its state of polarisation j', $j' = 1,2$ and $s_{kn}^{\alpha\beta}$ is denoted by $s_{kn}^{\alpha,k'j'}$. The eigenfrequency, ν_β, is replaced by the continuous frequency ν' so that the probability $|a_{ns}^{(2)}|^2$ is now a continuous function of solid angle and frequency.

For large time intervals, the factor

$$\sin^2\pi(\nu_{kn} + \nu_\alpha - \nu')t/(\nu_{kn} + \nu_\alpha - \nu')^2,$$

has a sharp maximum at $\nu' = \nu_{kn} + \nu_\alpha$, and it follows that only frequencies in the immediate vicinity of the quantity ν' contribute to the value of the integral. The remaining terms are considered to be over ν', thereby giving the expression

$$\int_{-\infty}^{\infty} \sin^2\pi(\nu_{kn}+\nu_\alpha-\nu')t/(\nu_{kn}+\nu_\alpha-\nu')^2 d\nu' = \pi^2 t \ .$$

The quantity $\sin^2\Gamma_\beta$ is evaluated over all eigenvibrations. Since the phases δ_β contained in Γ_β (see 1.4.1) are independent, we have $\sin^2\Gamma_\beta = \frac{1}{2}$, and we get

$$\sum_s |a_{ns}^{(2)}|^2 = \frac{32\pi^4 t}{V^2h} n_\alpha \nu_\alpha \sin^2\Gamma_\alpha \sum_{j'} \int \{\rho_{j'}(\nu',\omega') + \frac{h\nu'^3}{c^3}\} |s_{kn}^{\alpha,j'k'}|^2 d\omega' \qquad 1.4.8$$

If 1.4.8 is integrated over all eigenvibrationsin the incident frequency, then we have

$$\rho_j(\nu,\omega)d\nu d\omega = \sum_\alpha^{\Delta\nu,\Delta\omega} n_\alpha h\nu_\alpha/V$$

and, finally, we get

$$W_{kn}(\nu,\nu') = \frac{16\pi^4}{h^2} \sum_{j,j'} \iiint \rho_j(\nu,\omega)\{\frac{h\nu^3}{c^3} + \rho'_{j'}(\nu',\omega')\}$$

$$\times |s_{kn}^{kj,k'j'}| \, d\nu d\omega d\omega' \qquad 1.4.9$$

The probability per unit time for the transition of a molecule from state k to state n under the influence of the radiation field and for a quantum $h\nu'$ of undetermined polarisation and direction tc be scattered is given by W_{kn}, i.e.,

$$h\nu \rightarrow h\nu' = h(\nu \pm \nu_{kn})$$

This probability, as is clearly shown in 1.4.9, is increased when radiation of frequency $\nu \pm \nu_{kn}$ is present, i.e., induced emission. Two special cases of equation 1.4.9 are discussed below.

Case 1

It is assumed that $\rho'(\nu',\omega') = 0$ and that the exciting beam is

plane polarised and monochromatic.

Then we have

$$\iint \sum_j \rho_j(\nu,\omega)\,d\nu d\omega = \frac{\overline{E^2}}{4\pi} = \frac{|A|^2}{2\pi} ,$$

and equation 1.4.9 becomes

$$W_{kn}(\nu,\nu+\nu_{kn}) = \frac{16\pi^4(\nu+\nu_{kn})^3}{hc^3} \cdot \frac{|A|^2}{2\pi}$$

$$\times \int \frac{1}{h^2} \sum_{j'} \left| \sum_r \frac{(e_o M_{kr})(e_{k'j'} M_{rn})}{\nu_{rk} - \nu} + \frac{(e_{k'j'} M_{kr})(e_o M_{rn})}{\nu_{rk} + \nu} \right|^2 d\omega' .$$

Vector e_o is a unit vector in the direction of the incident radiation.

The integral may be written as follows

$$\int \sum_{j'} |e_{k'j'} V|^2 d\omega' ,$$

where V is a vector (see diagram).

If components are chosen such that $e_{k1'}$ is in the plane formed by k and v and e_{k2} is perpendicular to it then we have

$$\int \sum_{j'} |e_{k'j'} V|^2 \, d\omega' = 2\pi \int_o^\pi |e_{k\ell} V|^2 \sin\theta d\theta$$

$$= 2\pi \int_o^\pi |V|^2 \sin^3\theta d\theta = \frac{8\pi}{3} |V|^2 ,$$

and

$$W_{kn} = \frac{64\pi^4}{3c^3} \cdot \frac{|A|^2}{h} \cdot \nu' \left| \sum_r \left\{ \frac{(e_o M_{kr})(M_{rn})}{\nu_{rk} - \nu} + \frac{M_{kn}(e_o M_{rn})}{\nu_{rn} + \nu} \right\} \right|^2 . \quad 1.4.10$$

The scattering intensity is given by

$$I_{kn} = h(\nu + \nu_{kn}) W_{kn}$$

Equation 1.4.10 represents the intensity emitted by a classical dipole

oscillator as in equation 1.3.3. By comparison, therefore, with equation 1.3.3 and 1.3.7(b), this can be written

$$I_R = \frac{2^7\pi^5}{3c^4} \cdot \nu_R^4 \cdot I_s \cdot \alpha_{kn}^2 ,$$

where I_s is the intensity of the exciting beam. Placzek further showed that if the system was averaged over all molecular orientations, a factor $\frac{1}{3}$ was introduced. The normal Raman effect is therefore given by

$$I_R = \frac{2^7\pi^5}{3^2c^4} \cdot \nu_R^4 \cdot I_s \cdot \alpha_{kn}^2 \quad . \qquad 1.4.11$$

Case 2

In the presence of radiation density, $\rho_{j'}(\nu', \omega')$, of significant value it can be shown from equation 1.4.9 that

$$W_{kn} = \rho_j(\Delta\nu) \{A_{kn} + B_{kn} \rho_{j'}(\Delta\nu_R)\} , \qquad 1.4.12$$

where A_{kn} and B_{kn} are termed the probability coefficients for a spontaneous and stimulated Raman scattering (analagous to Einstein coefficients). The stimulated Raman effect is discussed in Chapter 2.

It is concluded from this simple analysis that the possibility of stimulated Raman scattering (as with stimulated emission) was inherent in the basic scattering equations.

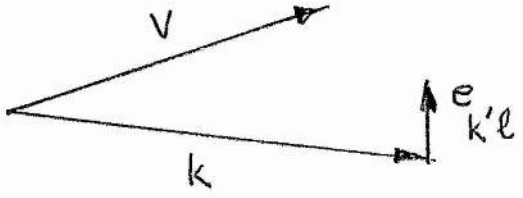

CHAPTER 2

THE STIMULATED RAMAN EFFECT

2.1(a) Intra-Cavity Stimulated Raman Spectra

The stimulated Raman effect was discovered with the development of the Q-switched laser[5] of McClung and Hellworth using a nitrobenzene Kerr cell. Woodbury and Ng[6] found that radiation appeared at 7670Å which did not correspond to any of the emission lines of ruby and yet its power was 15% of the main ruby emission at 6943Å . The new line was in the same direction as the laser output and was investigated by Eckhard, et al[7], who identified the line as a strong Raman vibration in the nitrobenzene and correctly deduced that it was generated by stimulated Raman scattering. These authors investigated a range of liquids with a cell inside the laser cavity and summarised the main properties of the effect as follows.

1. There is a threshold for the process, which when exceeded, causes the power output in the Raman line to increase to values in the range 1% - 10% of the primary laser pulse.

2. The lines excited correspond to the excitation of Raman vibrations in the liquids studied.

3. The emission consists of not only the Raman lines, but also their harmonics given by $\nu - n\nu_{RV}$, where n is an integer and ν_{RV} is the Raman vibration frequency.

4. Only the strongest lines in the Raman spectrum are excited.

5. Only Stokes lines are observed.

6. The Raman emission has the same beam divergence as that of the laser.

7. The line width of the stimulated Raman line is very much less than that of the normal Raman line.

The above phenomena correspond to one type of stimulated Raman spectra and are described by their method of generation which is called intra-cavity generation. The second type is termed extra-cavity generation and this occurs when the Raman cell is outside the laser resonator.

2.1(b) Extra-Cavity Stimulated Raman Spectra

It was found by Terhune[8] that stimulated Raman spectra could also be generated by focusing the output of a Q-switched laser into a Raman cell outside the cavity. The effect was investigated by Stoicheff[9] and the following effects were found.

1. There is a threshold for the process, not only in the intensity of the laser, but also in the path length in the liquid used.

2. Both Stokes and anti-Stokes are generated and the Raman lines are given by $\nu \pm n\nu_{RV}$, where n is an integer.

3. When threshold is exceeded by a small amount, the harmonic lines are generated, so that it was concluded that threshold was the same for both fundamentals and harmonics. (However, the work described in this thesis shows that this is not the case).

4. For each liquid the spectrum consisted of only one or two lines and their harmonics and the lines generated corresponded to totally symmetric vibrations in the normal Raman spectrum. As

symmetrical vibrations have the highest intensity and the narrowest line widths, they are expected to have the lowest threshold (see Section 2.2).

5. The angular distribution was investigated and it was found that, whilst Stokes emission occurs within angles of 4^{o}-5^{o} about the laser beam, the anti-Stokes emission occurred at discrete angles of a few degrees to the beam direction.

6. The line widths of both Stokes and anti-Stokes lines are narrower than the more usual unstimulated Raman lines.

7. The generation of harmonics could not be explained on an iterative basis as the threshold for both was the same. In experiments using two cells and two liquids no lines were generated corresponding to sum and difference frequencies so that again an iterative mechanism did not seem possible.

2.2 Stimulated Raman Gain

Theoretical treatments of stimulated Raman scattering have fallen into two categories. There were the treatments of Hellwarth[10,11] based on the individual molecular process of Raman scattering and on normal Raman emission. Alternatively the treatment of Garmire et al[12] assumed the model of intense coherently driven molecular oscillations which modulate the original light and its Raman scattered radiation, producing many ordersof Stokes and anti-Stokes lines. Both treatments lead to similar results for first Raman Stokes generation but differ in their mechanisms for extra-cavity harmonic production. The single

molecule picture requires separate thresholds for each harmonic whilst the multi-molecule scheme bases its treatment on the modulation of the dielectric constant of the medium by the optical fields of laser and first Stokes radiation requiring no further threshold condition. It will be shown in this thesis that separate thresholds do exist an expression for stimulated Raman gain, based on the single molecule scattering equations of Placzek and Dirac shown in Chapter 1, is derived below.

It was shown, using Dirac's scattering theory that the probability of stimulated Raman scattering could be separated into two parts, one proportional to the energy density of the exciting radiation, and another proportional to the energy densities of the excited and scattered radiation. Following this treatment, the probability, W, of Raman scattering per molecule can be written as (cf. eq 1.4.12)

$$W = I_L(A_{mn} + B_{mn}I_R) \quad , \qquad 2.2.1$$

where, as shown previously, A_{mn} and B_{mn} correspond to spontaneous and stimulated scattering, and the intensities of the laser and the stimulating Raman radiation are I_L and I_R, respectively.

The relation between A_{mn} and B_{mn} is given by

$$A_{mn} = (2h\nu_R^3/c^2)B_{mn} \qquad 2.2.2$$

The intensity due to Raman scattering is given by

$$I(R) = I_L A_{mn} h\nu_R + I_L I_R B_{mn} h\nu_R \qquad 2.2.3$$

The coefficient, A_{mn}, may be obtained from the intensity of spontaneous Raman scattering given by 1.4.11

$$I_R = (2^{>}\pi^5/3^2c^4)\nu_R^4\ \alpha_{mn}^2 \qquad 2.2.4$$

By comparing 2.2.4 with the equation 2.2.3 which accounts for spontaneous scattering, it is clear that we have

$$A_{mn} = (2^{>}\pi^5\nu_R^3/3^2hc^4)\alpha_{mn}^2 \qquad 2.2.5$$

and, therefore we get

$$B_{mn} = (2^6\pi^5/3^2hc^2)\alpha_{mn}^2 \qquad 2.2.6$$

With high laser intensities, the spontaneous Raman component can be neglected with respect to the stimulated scattering, so that the Raman intensity due to stimulated scattering is given by

$$I_R\delta\nu_R = I_L I_R\ B_{mn} h\nu_R \ . \qquad 2.2.7$$

If N is the number of molecules per unit volume, the number of molecules in a cylinder of unit area and length dx, is Ndx; therefore, the increase in intensity in a length dx is given by

$$dI_R = (NI_L I_R/\Delta\nu_R)\ B_{mn} h\nu_R dx \ , \qquad 2.2.8$$

where the stimulating intensity, I_R, is generated by spontaneous scattering into the frequency range $\Delta\nu_R$ (the line width for spontaneous scattering). Substituting the value for B_{mn} into 2.2.8 we obtain

$$dI_R/I_R = (2^6\pi^5 N\nu_R/3^2hc^2\Delta\nu_R)\alpha_{mn}^2\ I_L\ dx \ . \qquad 2.2.9$$

Integrating over a distance ℓ and taking the initial value of I_R to be $I_R^{\,o}$ gives

$$\ell n(I_R/I_R^{\,o}) = (2^6\pi^5 N\nu_R/3^2hc^2\Delta\nu_R)\alpha_{mn}^2 \cdot\ I_L \cdot \ell \ .$$

Finally, the expression obtained for the gain, G, is

$$G = (I_R/I_R^{\,o}) = \exp\{(2^6\pi^5 N\nu_R/3^2hc^2\Delta\nu_R)\alpha_{mn}^2\ I_L\ \ell\} \qquad 2.2.10$$

Threshold for Raman laser action therefore occurs when the above gain

is greater than the cavity losses.

2.3 Directionality of Anti-Stokes Emission

The directionality can be explained on the basis of the momentum matching condition in a dispersive medium. Both momentum and energy are conserved in an interaction between radiation and matter. When a single photon 'collides' with a molecule, the molecule recoils to conserve momentum. When a coherent beam interacts with the molecules of the medium, the difference of momentum is taken up by an optical phonon. The directions in which anti-Stokes and Stokes radiation are emitted are readily obtained in terms of wave vectors, k. The condition for Stokes emission is given by

$$\underline{k}_L = \underline{k}_{s1} + \underline{k}_p \,, \qquad 2.3.1$$

where $\underline{k}_L$, $\underline{k}_{s1}$, $\underline{k}_p$ are the wave vectors for the laser and Stokes radiation and the optical phonon, respectively. Since the magnitude of $\underline{k}_{s1}$ is fixed by conservation of energy, the above relationship is satisfied at all points on a circle of radius k_{s1} (see Fig 1). As the Stokes beam gets away from the laser direction, the coupling between the two decreases and therefore the Stokes emission decreases, i.e. Stokes emission is confined to a diffuse cone with an apex angle slightly larger than that of the exciting laser.

For anti-Stokes generation the condition given by

$$\underline{k}_{As1} = \underline{k}_L + \underline{k}_p \qquad 2.3.2$$

must be satisfied.

It is clearly shown in the figure (1)b that the three vectors

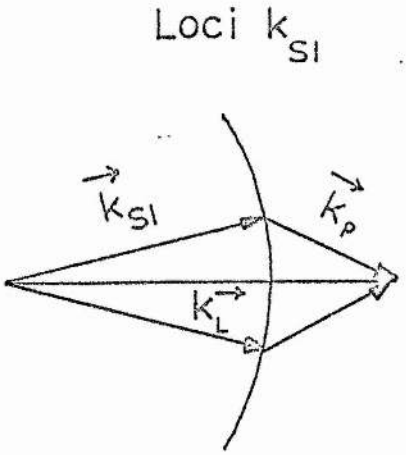

Fig 1(a)

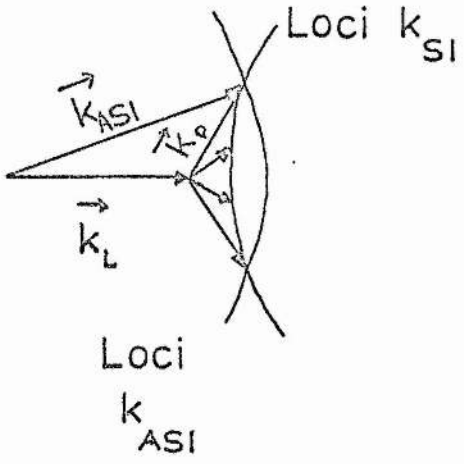

Fig 1(b)

Fig 1 (a) Vector diagram of Stokes emission

(b) Vector diagram of Anti-Stokes emission

can only satisfy 2.3.2 for particular directions. Generation of anti-Stokes radiation is, therefore, only possible in a direction at a fixed angle to the exciting beam.

The fact that anti-Stokes emission only occurs outside the cavity is thus explained by the vector model since the model shows that momentum matching condition cannot be satisfied at the same time as the directionality conditions for Raman laser action inside the cavity.

From this simple analysis a number of the features of the stimulated Raman effect can be explained.

1. Lines in the normal Raman spectrum with a high scattering probability and narrow line width will have the highest gain and the lowest threshold.

2. Intra-cavity generation of Raman spectra can be explained on the basis of a Raman laser in which stimulated Raman occurs when the Raman gain exceeds the cavity losses for the Raman line[10,11].

3. The directionality and narrowing of the stimulated Raman lines are explicable in terms of laser theory (Cain narrowing).

4. The threshold for the process (i.e. when the gain equals the cavity losses) is dependent not only on the laser intensity, but also on the length of the cell used in the cavity.

5. The generation of harmonics could be explained on the basis of iterative generation.

2.4 The Raman Laser

It is clear from paragraph 2.2 that intra-cavity stimulated Raman radiation can be treated in terms of rate equations in which the laser acts as a pump for the generation of the Raman radiation. From 2.2.1 the probability of stimulated Raman scattering can be expressed as

$$p_R = k\, n_m V\, B\, n_L\, n_R \,, \qquad 2.4.1$$

where n_L and n_R are photon densities at the ruby and Raman laser frequencies, k is the filling factor, V is the volume of the optical resonator, and n_m is the number of Raman active molecules per unit volume.

The loss of photons from the resonator can be expressed as $\omega_R(W_R/Q_R)$, where Q_R is the quality factor of the laser at the Raman frequency, and W_R is the stored radiation density.

The rate equation for Raman laser action is therefore given by

$$dn_R/dt = k\, n_m\, B\, n_L\, n_R - (\omega_R\, n_R)/Q_R \quad . \qquad 2.4.2$$

The threshold for the Raman laser, therefore, is given by

$$n_{Lth} = \omega_R/(k\, n_m\, B\, Q_R) \quad . \qquad 2.4.3$$

From this it is clear that threshold is inversely proportional to the Raman scattering cross section. Using this expression Takuma and Jennings[13] found that the experimental threshold agreed within experimental error with that predicted from spontaneous Raman data for benzene. In this experiment, however, it was found that the efficiencies of the harmonics was far greater than expected on the

bases of an iterative scheme, that is, n_R generates n_{2R} and the intensities of the harmonics were found to be comparable with that of the fundamental. This was explained on the basis of saturation. The rate equation of the Ruby laser is given by

$$dn_L/dt = B_L\, n\, n_L - kn_m\, Bn_L\, n_R - \omega_L n_L/Q_L, \qquad 2.4.4$$

where B_L is the stimulated emission probability, and n is the population inversion. Under saturation conditions, we have $dn_L/dt = 0$ and so from 2.2.4 we obtain

$$n_R = nB_L(1 - n_{th}n^{-1})/kn_mB, \qquad 2.4.5$$

where $n\, B_L$ $(= \omega_L/Q_L)$ gives the threshold value of n for ruby laser action. It is clear, therefore, that n_R can be very large since under stimulated Raman conditions we have $n >> n_{th}$ and $kn_mB << n\, B_L$.

Similarly, n_R can saturate in the presence of the second harmonic, n_{2R}. The rate equation to be considered is

$$dn_R/dt = kn_mBn_Ln_R - kn_mBn_Rn_{2R} - (\omega_Rn_R/Q_R). \qquad 2.4.6$$

Under saturation conditions with n_L, n_R, n_{2R}, we have

$$n_{2R} = n_L\left(1 - \frac{n_{Lth}}{n_L}\right) \qquad 2.4.7$$

which shows that the second harmonic can be as intense as the laser line. The above is at least qualitatively correct since the peak power output of the Raman laser was found to be comparable to that of the power necessary to produce stimulated Raman.

Near-field patterns were taken which showed that the Raman laser only operated in a few small filaments and that the bulk of the laser radiation did not contribute to Raman generation.

In spite of these anomalous effects Takuma and Jennings[13] found that the input electrical power necessary to produce second harmonic Raman generation was found to be 1.7 times that of the fundamental suggesting that the process was iterative and should therefore be dependent on stimulated Raman gain.

2.5 Anomalous Gain and Threshold

When experiments were performed to investigate stimulated Raman gain and to predict thresholds for stimulated Raman, results were obtained which did not agree with those of Takuma and Jennings[13].

McClung (unpublished) found that the threshold for Raman in nitrobenzene was an order of magnitude less than that predicted. This result was explained by Bloembergen[14] who, in a semi-quantitative analysis, showed that the multimode nature of the ruby output beam led to gains in certain modes which could be up to an order of magnitude greater than the average gain. Lallemand and Bloembergen[15] showed experimentally that the Stokes intensity could be explained on the multimode theory. Their experimental results (Fig 2) could be represented by the equation

$$I_s = \sum_i c_i (I_L - I_{i,\text{threshold}}), \qquad 2.5.1$$

where i refers to a mode and c_i is the mode dependent cross-section. The expression indicates that there is a threshold distribution explicable in terms of mode structure. The generation of the second harmonic Stokes radiation was explained on the iterative scheme with the first Stokes line acting as a pump. It was proposed that as soon as threshold is exceeded in a filament the intensity of the Stokes

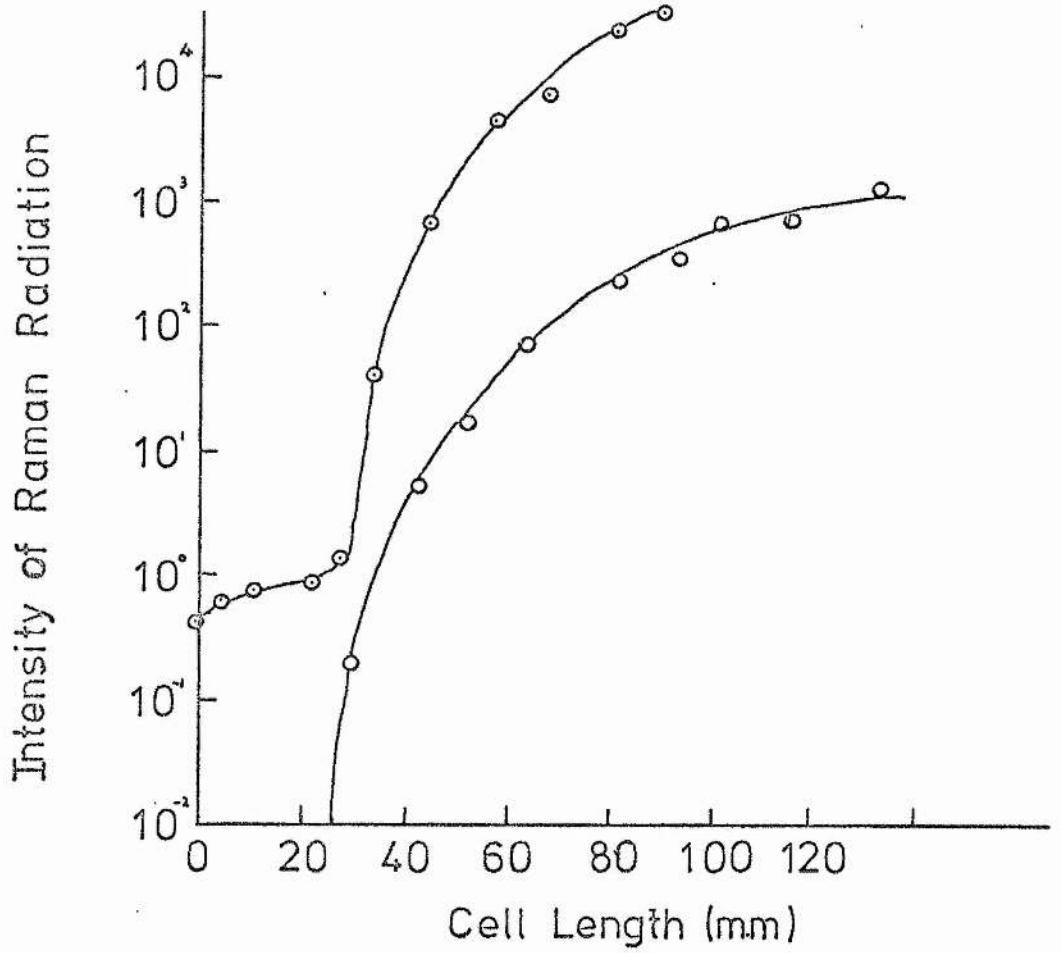

Fig 2 Intensity of 1st and 2nd Stokes Radiation in Nitrobenzene as a function of cell length for a constant laser intensity.

⊙ 1st Stokes, o 2nd Stokes.

radiation increases rapidly, so depleting the laser power in the filament. The Stokes second harmonic is then created in this filament whilst other harmonics are still below threshold. As the gain is increased, more Stokes modes go above threshold and the higher order intensities increase in a similar manner.

McClung et al[16], however, showed that the conversion into stimulated Raman radiation was mode-independent by using a single mode ruby laser with which it was shown that the conversion efficiency was the same as a multimode system. It was clear, therefore, that the anomalous results could not be explained by mode structure and possible effects leading to beam distortion in the Raman active medium were considered.

Chiao[17] showed that the interaction between the high optical field and the medium led to an intensity dependent refractive index which could lead to beam deterioration and self-trapped filaments. The effect was termed self-focusing (see Chapter 3).

It was shown by Shen and Shaham[18], by using two cells that the threshold for the generation of stimulated Raman radiation in the second cell was dependent on the length of the first and of the particular liquid used (Fig 3). This was explained by beam distortion and the multimode theory. A similar set of results was found by Lallemand and Bloembergen[19], who further showed that the beam breaks into filaments as the laser intensity is increased. Good correlation was found between the self-focusing effect and the intensity dependent

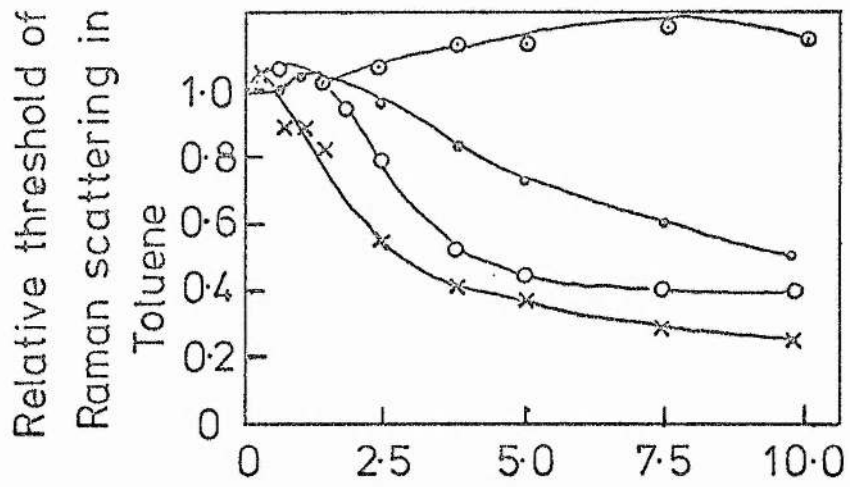

Fig 3 Raman Threshold in Toluene versus the Cell Length of a Scattering cell in front of Toluene cell. The scattering cell was filled with water, benzene, acetophenone or nitrobenzene.
∘ Water, • Benzene, ∘ Acetophenone, × Nitrobenzene.

index of refraction. It was suggested that the threshold for stimulated Raman was more dependent on the self-focusing coefficient than the Raman scattering cross section. This is discussed in Chapter 3.

CHAPTER 3

NON-LINEAR EFFECTS

3.1(a) Self-Trapping

Because of the high fields produced by Q-switched lasers, non-linear, intensity dependent terms must be considered in the interaction of the radiation with the liquid.

The phenomenon leading to a self-trapped beam can be described in terms of refractive index, by an expansion, given by

$$n = n_o + n_2 E^2 + \ldots, \qquad 3.1.1$$

together with the interaction of a diffraction limited beam with the non-linear medium.

For a beam diameter D, the beam has an angular divergence given by

$$\theta = 1.22\lambda/n_o D \qquad 3.1.2$$

If the non-linear term of 3.1.1 increases, the refractive index within the beam becomes such that the angle for critical reflection is exceeded so the beam ceases to expand. The threshold condition for this to occur has been obtained by Chiao[17] and is given by

$$P_{cr} = (\pi D^2/4)(n_o E^2 c/8\pi) \geq (1.22\lambda)^2 c/64 n_2). \qquad 3.1.3$$

3.1(b) Self-Focusing and Self-Trapping

From the simple analysis above it is clear that, at a certain critical power level, the beam is trapped and does not spread, and that the threshold power level decreases with λ^2. For a more detailed treatment of the effect, the following non-linear wave equation 3.1.4 must be solved (Kelly[21])

$$\nabla^2\vec{E} - \frac{\varepsilon_o}{c^2}\frac{\partial^2\vec{E}}{\partial t^2} - \frac{\varepsilon_2}{c^2}\frac{\partial^2}{\partial t^2}(E^2\vec{E}) = 0. \qquad 3.1.4$$

Kelley assumed a linearly polarised wave of frequency ω propagating along the z axis, so that

$$\underline{E} = (\underline{e}/2)\{E' \exp i(kz - \omega t) + c.c.\}, \qquad 3.1.5$$

where E' is the slowly varying field amplitude.

Substituting 3.1.5 into 3.1.4 and neglecting the third harmonic term then gives

$$2ik\frac{\partial E'}{\partial z} + \nabla^2 E' + \frac{\varepsilon_2' k^2}{\varepsilon_o}|E'|^2 E' = 0 \qquad 3.1.6$$

where $\varepsilon_2' = (3\varepsilon_2/4)$.

The term in the second derivative of z is assumed to be small so that we get

$$2ik\frac{\partial E'}{\partial z} + (\nabla^2_x + \nabla^2_y)E' + \frac{\varepsilon_2' k^2}{\varepsilon_o}|E'|^2 E' = 0 . \qquad 3.1.7$$

As a first approximation, transverse E' components are neglected to give the simple solution

$$E' = E_o \exp(i\, n_2'\, k|E'|^2 z/n_o) . \qquad 3.1.8$$

This equation shows that the non-linearity produces an intensity dependent phase change. Applying Huygens principle to a uniphase beam, it can be shown that a focusing action is produced.

Assuming that the transverse second derivative of E' in 3.1.7 depends upon the axial distance through the variation of intensity in the exponent 3.1.8, this solution can be used to obtain a characteristic focusing distance. An appreciable change of intensity occurs along the axis at the point given by

$$z = z_{focus} = (1/2)\ a\ (n_o/n_2)/E_m'$$

where a is the transverse radius of curvature of the input intensity and E'_m is the peak field value. Equating z_{focus} to the diffraction length an approximate threshold for cylindrical beam trapping is obtained, this is given by

$$P_{cr} = (1.22\lambda)^2 c/(512\ n_2') = (1.22\lambda)^2 c/(256 n_2). \quad 3.1.9$$

This more detailed analysis gives a factor 4 lower in threshold than equation 3.1.3 which was obtained by Chiao's simple analysis. The net focusing distance after correcting for diffraction is given by

$$z_{net} = (a/2)(n_o n_2')^{\frac{1}{2}}\ (E_m' - E_{cr})^{-1}\ , \quad 3.1.10$$

where $E_{cr} = (1.22\ )/8a(n_2' n_o)^{\frac{1}{2}}$

The treatment was further extended by Wang[22] who showed that Kelly's equation 3.1.10 could be written in the form

$$\ell = \frac{n_o}{4}\ (\frac{a^2}{f})\ (\frac{c}{n_2})^{\frac{1}{2}}\ /\ \{P^{\frac{1}{2}} - P_{cr}^{\frac{1}{2}}\} \quad 3.1.11$$

The equation has been modified by the introduction of the factor f which is the ratio of the radius of the beam, a, to a characteristic transverse radius of curvature of the input intensity. Equation 3.1.11 can be written in the form

$$^{\frac{1}{2}} = \ _{cr}^{\frac{1}{2}} + (\alpha/\ell)$$

where $\alpha = \frac{n_o}{4}\ (\frac{a^2}{f})(\frac{c}{n}\ )^{\frac{1}{2}}$, $\quad 3.1.12$

This gives the threshold power for the information of filaments in a liquid column of given length. Results confirming 3.1.12 were obtained by Wang[22] and are shown in Fig 4(a).

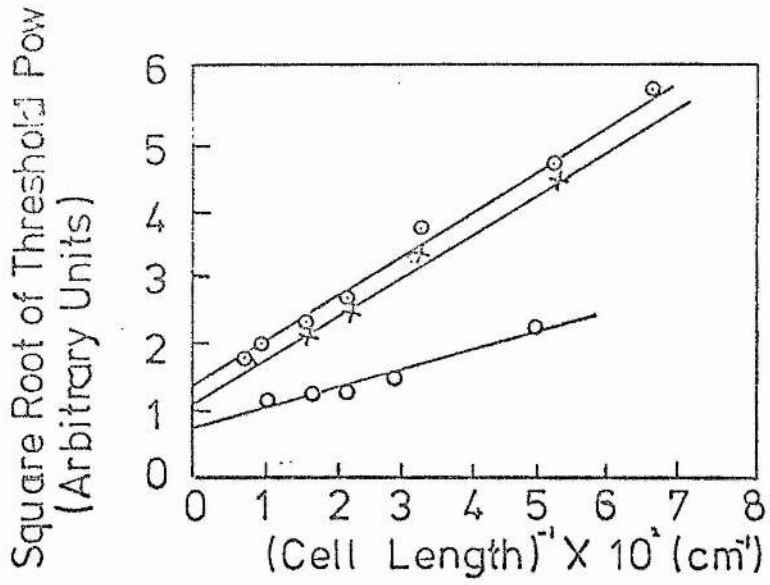

Fig 4 (a)

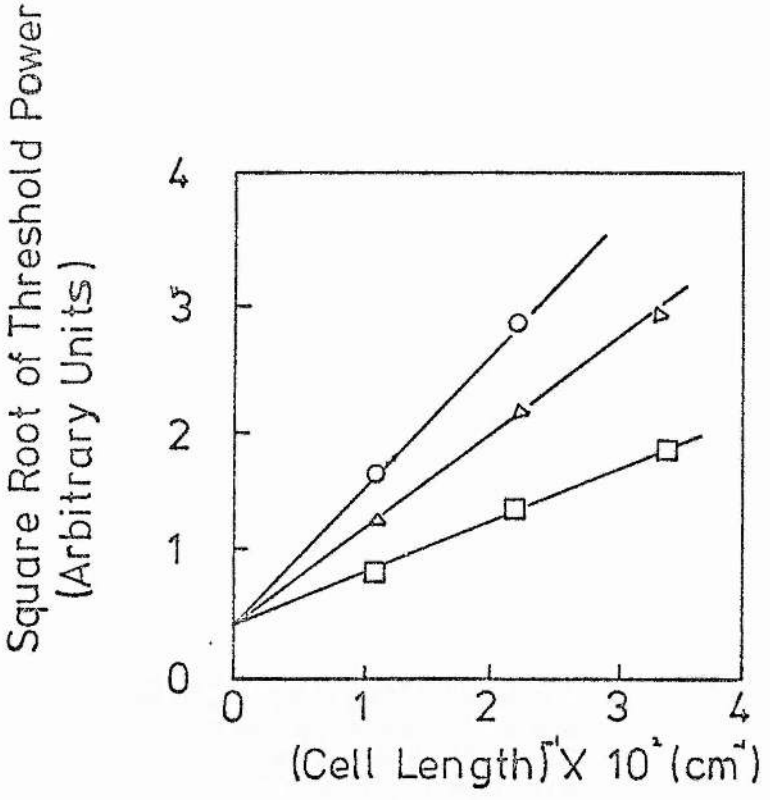

Fig 4 (b)

Fig 4 (a) Plot of the square root of threshold laser power as a function of inverse cell length for benzene ⊙, toluene × and nitrobenzene ○.

(b) Same plot for benzene, but with beams of different cross sections. ○ 1.25×10^{-2} cm^2, 0.78×10^{-2} cm^2 △, □ 0.48×10^{-2} cm^2.

Although the threshold for self-focusing is a function of the beam area, that of self-trapping is not. This was experimentally verified by Wang as is shown in Fig 4(b). From these results Wang attempted to make absolute measurements of P_{cr} but could not check his results because of lack of information on the values of the non-linear coefficients, n_2.

From the above, we see that the threshold for stimulated Raman is dependent primarily on the value of n_2, rather than Raman gain. For this reason some consideration must be given to these coefficients.

3.2(a) Electrostriction and the Optical Kerr Effect

Since it has been shown in paragraph 3.1 that the non-linear refractive index in the presence of the high optical fields available from Q-switched lasers lead to self-focusing and could lead to a threshold for stimulated Raman it is necessary to determine the magnitude of the self-focusing coefficient. The two effects causing the non-linearity are electrostriction and the optical Kerr effect.

Shen[23] determined the relative importance of the two effects by use of the Clausius Mossotti relation[24]. The change in refractive index is given in terms of variations in density, $\Delta\rho$, and polarisability,

$$\Delta n = (\Delta n)_\alpha + (\Delta n)_\rho = \frac{(n_o^2-1)(n_o^2+2)}{6n_o(n_o^2+2)}\left[\frac{\Delta\rho}{\rho_o} + \frac{\Delta\alpha}{\alpha_o}\right] \qquad 3.2.1$$

Electrostriction $(\Delta n)_\rho$

By solving the driven acoustical wave equation in an optical field given by, $E = E(r)\cos(kr - \omega t)$

$$(-\nabla^2 + \frac{1}{V^2}\frac{\partial^2}{\partial t^2} - \frac{2\Gamma}{V^2}\frac{\partial}{\partial t})\Delta\rho = -\frac{1}{8\pi}\cdot\frac{\gamma}{V^2}(\nabla^2 E^2) \qquad 3.2.2$$

where the medium only responds to the slowly varying part of the field Shen found that

$$(\Delta n)_\rho = k_\rho \lambda(\tfrac{1}{2}E^2) \qquad 3.2.3$$

where $$k_\rho = \gamma^2\beta/8\pi\, n_o\lambda \qquad 3.2.4$$

β is the isothermal compressibility, $\gamma = 2n_o g_o(\partial n/\partial\rho)$ and the velocity $V = (\rho_o\beta)^{-\frac{1}{2}}$.

Optical Kerr Effect $(\Delta n)_\alpha$

The change in polarisability was assumed to come from the orientation of anisotropic molecules and was calculated using the theory of Langevin[25]. Again, the medium only responds to the slowly varying part of the field, and, for a linearly polarised wave, Shen found

$$(\Delta n)_\alpha = 2/3\; k_\alpha \lambda(\tfrac{1}{2}E^2), \qquad 3.2.5$$

where the optical Kerr constant is given by

$$k_\alpha = \{(n_o^2+2)(n_o^2-1)(\varepsilon+2)/(\delta+2)^2(\delta-1)\}(K_{DC}) \qquad 3.2.6$$

The dielectric constant is ε, and δ is given by the Debye relation

$$(\delta-1)/(\delta+2) = \{(\varepsilon-1)/(\varepsilon+2) + \frac{4\pi\rho_o\mu^2}{9nkT}\} \qquad 3.2.7$$

where μ is the permanent dipole moment of the molecule.

The table below gives the values of optical Kerr constants and electrostrictive constants for a range of liquids.

It is clear that if the threshold for stimulated Raman depends upon self-focusing, then the relative thresholds should be in the

TABLE 1

Electrostrictive coefficients, K_ρ, optical Kerr constants, K_α, and the d.c. Kerr constants, $(K_1)_{dc}$, calculated at the wavelength of the sodium D line for various liquids. In calculating these constants, n_o is obtained from the International Critical Tables and β and δ from the Handbook of Chemistry and Physics. All physical constants are taken at 20°C if possible.

LIQUID	$K_\rho \times 10^7$	$K_\alpha \times 10^8$	$(K_1)_{dc} \times 10^8$ (esu)
Carbon-tetrachloride	1.21	0.67	0.74
Carbon-disulphide	2.53	32.6	32.26
Hexane	1.06	0.45	0.45
Cyclohexane	1.06	0.78	0.74
m-xylene	1.20	7.59	8.58
Benzene	1.33	5.73	5.93
Toluene	1.25	6.55	7.53
Chlorobenzene	1.20	9.93	91
Bromobenzene	1.50	14.35	91
Nitrobenzene	0.92	26.4	2560
Aniline	1.00	3.22	-12.3
Chloroform	1.03	1.70	-33.2
Acetone	0.75	1.03	163
Methyl alcohol	0.58	0.17	9.7
Ethyl alcohol	0.66	0.21	7.68
Butyl alcohol	0.64	0.41	-36.5

inverse ratio of their non-linear coefficients.

In practice the interaction between a medium and a giant pulse must be considered and $E(r)$ must be replaced by $E(r,t)$. The interaction of a giant pulse of the form

$$E^2(r,t) = A\, e^{-\alpha^2 r^2} t, \quad t \lesssim \Lambda$$

$$E^2(r,t) = A\, e^{-\alpha^2 r^2} (2\Lambda - t), \quad t \gtrsim \Lambda$$

with the medium is considered below.

A rough estimate of the magnitude of the two effects can be made by substitution of the above into the driven acoustical wave equation neglecting the transverse variation of $\Delta\rho$. This is valid for $r < \alpha^{-1}$ and $\alpha < 10^{-2}$. The equation is a linear differential equation whose solution is

$$\Delta n_\rho = {}^1/_3\, K_\rho \alpha^2 V^2 (1-\alpha^2 r^2) t^3\, A\, e^{-\alpha^2 r^2} \quad . \qquad 3.2.8$$

The total change in refractive index, therefore, is given by the addition of the optical Kerr component. The reorientation time τ_k is typically $\sim 10^{-10}$ sec so that the Kerr-dependent change in refractive index accompanies the pulse and so we have

$$\Delta n = \Delta n_\rho + \Delta n_\alpha = \{K_\rho (1-\alpha^2 r^2) (\frac{t}{\tau_\rho})^2 + K_\alpha\}\, E^2(r,t), \qquad 3.2.9$$

where $\tau_\rho = (\alpha V)^{-1}$ is the response time of the system to a density wave. It is clear from the above that the change in refractive index only accompanies the giant pulse provided τ_ρ is large in comparison with the pulse width so that electrostriction can be neglected. This a function of the form of the exciting pulse and the geometry of the system, depending upon whether the excitation is by a parallel or a

focused beam. The ratio of the two coefficients, R_{EK} is given by

$$R_{EK} = \frac{K_s}{K_\alpha} (1-\alpha^2 r^2)(t/\tau_\rho)^2 , \qquad 3.2.10$$

which must be considered for all conditions of excitation.

3.2(b) Parallel Excitation

With the typical values $\alpha=30cm^{-1}$, and pulse width 20n sec, the maximum value of R_{EK} is $10^{-2}K_\rho/K_\alpha$ which indicates that electrostriction can be ignored. Kaiser and Maier[26], using this system investigated a range of liquids and found that the thresholds of carbon disulphide, benzene, nitrobenzene and toluene were in the inverse ratio of their non-linear Kerr coefficients. Even if a pulse of double the width were used it would still be valid to use the optical Kerr coefficient.

3.2(c) Focused Excitation

If we consider the focusing of a diffraction limited beam, it is well known that the beam focuses to a cylinder whose dimensions are

$$D = \frac{f\lambda}{na} \qquad 3.2.11$$

where n is the refractive index of the medium and a is the diameter of the input beam. It is clear, therefore, that the time response of the medium under these conditions is such that electrostriction cannot now be eliminated, since $\tau_\rho = \frac{D}{V}$ and D can be of the order of a few wavelengths. The coefficient R_{EK} can be expressed in the form

$$R_{EK} = \frac{K_\rho}{K_\alpha} \cdot \frac{(1-\alpha^2 r^2)}{(A\tau_\rho)^2} E^2(t) , \qquad 3.2.12$$

where A is the rate of rise of the pulse which indicates that the electrostrictive term is a function not only of the field but also the

rate of rise of the pulse.

This result will be discussed further in Chapter 5. Direct observation of self-focusing using a focused system was observed by Pilipetskii and Rustamov[27] who found that filaments were formed ahead of the lens focus.

Conclusions

From the above we see that an intensity dependent refractive index leads firstly to self-trapping followed by self-focusing which produces filaments inside the beam envelope where the beam intensity can be very large. It would appear that, with unfocused excitation, the threshold for stimulated Raman corresponds to the self-focused threshold due purely to the index change caused by the optical Kerr effect. It is not clear what dictates threshold in a focused excitation system. The dynamics of filament formation have not been studied in any great detail although Chiao et al[28] have shown that the filament approaches a terminal size after which it increases, possibly due to two photon absorption. This result is of significance to the results found during our experiments and will be discussed in Chapter 5.

CHAPTER 4

STIMULATED AND SPONTANEOUS RAMAN SPECTRA (EXPERIMENTAL ASSESSMENT).

4.1 Introduction

Papers published up to October, 1964 indicated that many of the features of the stimulated Raman effect were not understood. One of the reasons for this was that thresholds for the effect could not be theoretically determined because of the lack of data on the line widths of spontaneously emitted Raman lines and the scattering cross sections needed for calculation of Raman gain coefficients. The simultaniety of harmonic generation could not be explained on the basis of stimulated Raman gain using an iterative generation scheme. It was proposed therefore to investigate stimulated Raman by setting up both stimulated and normal Raman spectrometers, so that all the information necessary for a theoretical analysis would be available. The projected investigation was therefore in two parts, A, the study of stimulated Raman spectra and B, normal (spontaneous) Raman spectra.

The aim of the investigation of stimulated Raman spectra was to construct a spectrometer based on a Q-switched ruby laser and to develop methods for measuring thresholds for a range of liquids and to compare the thresholds obtained with the predicted values calculated from spontaneous scattering data. It was also proposed to investigate the possibility that stimulated Raman spectra may be iteratively generated.

To study spontaneous Raman spectra a conventional Raman spectrometer was to be constructed to assess the possibility of measuring cross sections and line widths with a photo-electric detection system in conjunction with a CW gas laser.

Since the investigation started with an empty room and this was an ambitious investigation it was decided to pursue both projects with the proviso that the investigation of spontaneous Raman spectra would be suspended if either it was no longer possible to complete it in the available time or if it was no longer worthwhile in the light of developments in the field.

A. Stimulated Raman Spectra

The ruby laser for the investigation was purchased from Barr and Stroud in 1965. A rotating prism Q-switched unit was chosen as this generated a slow pulse (typically 40 nanoseconds) suitable for the proposed time resolution experiments. It was specified that it should produce pulses ~20 Mwatt. Before setting up any experiment it was necessary to develop instrumentation and techniques to align and measure the power output of the device. These are discussed below.

4.2(a) The Ruby Laser

The unit consists of a 7.5 K Joule condenser bank with a charging unit, trigger circuitry for discharging the bank into the flash tube, and an air blower for cooling the ruby. The laser head consists of a ruby rod (6" x ½" dia) mounted in a cylindrical cavity parallel with a xenon flash tube. The head is mounted on an adjustable platform

with screws giving a three dimensional movement. The cavity mirrors are (a) a roof prism which is rotation at 15,000 rpm and a dielectric mirror with a reflectivity of 30% at 6943Å . The ruby rod is cut at 90° to the crystal axis so that the output is plane polarised.

The ruby can be operated in either the non Q-switched or Q-switched modes by locking the prism in the aligned position or permitting it to rotate at 15,000 rpm. Triggering in both cases is effected by the application of a hgih voltage pulse to a trigger wire wound round the flash tube. In the Q-switched case the trigger pulse is generated by a pointer mounted on the rotating prism passing a magnetic pick-up and the system is synchronised such that the high Q_0 lasing position occurs during the peak of the flash tube pump pulse.

The unit is mounted on an optical bench 2 metres long which is itself mounted on a heavy iron girder. This ensures a fixed calibrated reference axis with a stable mounting. A schematic diagram of the system is shown in Fig 5 and the actual unit can be seen in Plate 1.

4.2(b) Output Pulse Characteristics

The laser was aligned by using the autocollimator described in section 4.3. A photodetector (90 CV) was used to investigate the beam scattered off a block of MgO. The response-time of the photodetector was reduced by operating it at 300 volt in the circuit shown in Fig 6. A typical pulse train is shown in Fig 7(a) in which the system operates with laser output (lases) in two separate periods suggesting a pre-lasing action in which output is obtained before the prism is in a high Q-position. It was found that the system lased with the

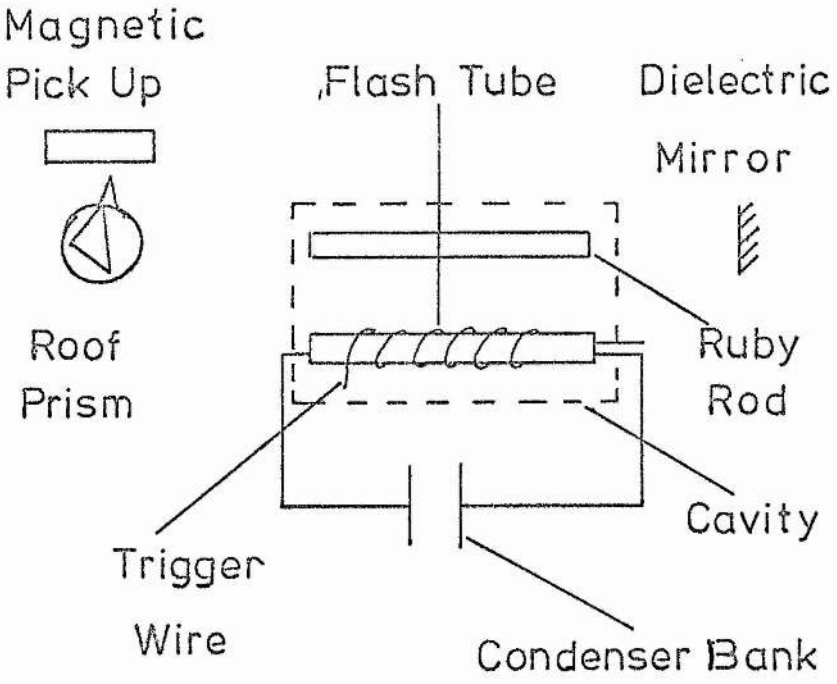

Fig 5 The Ruby Laser

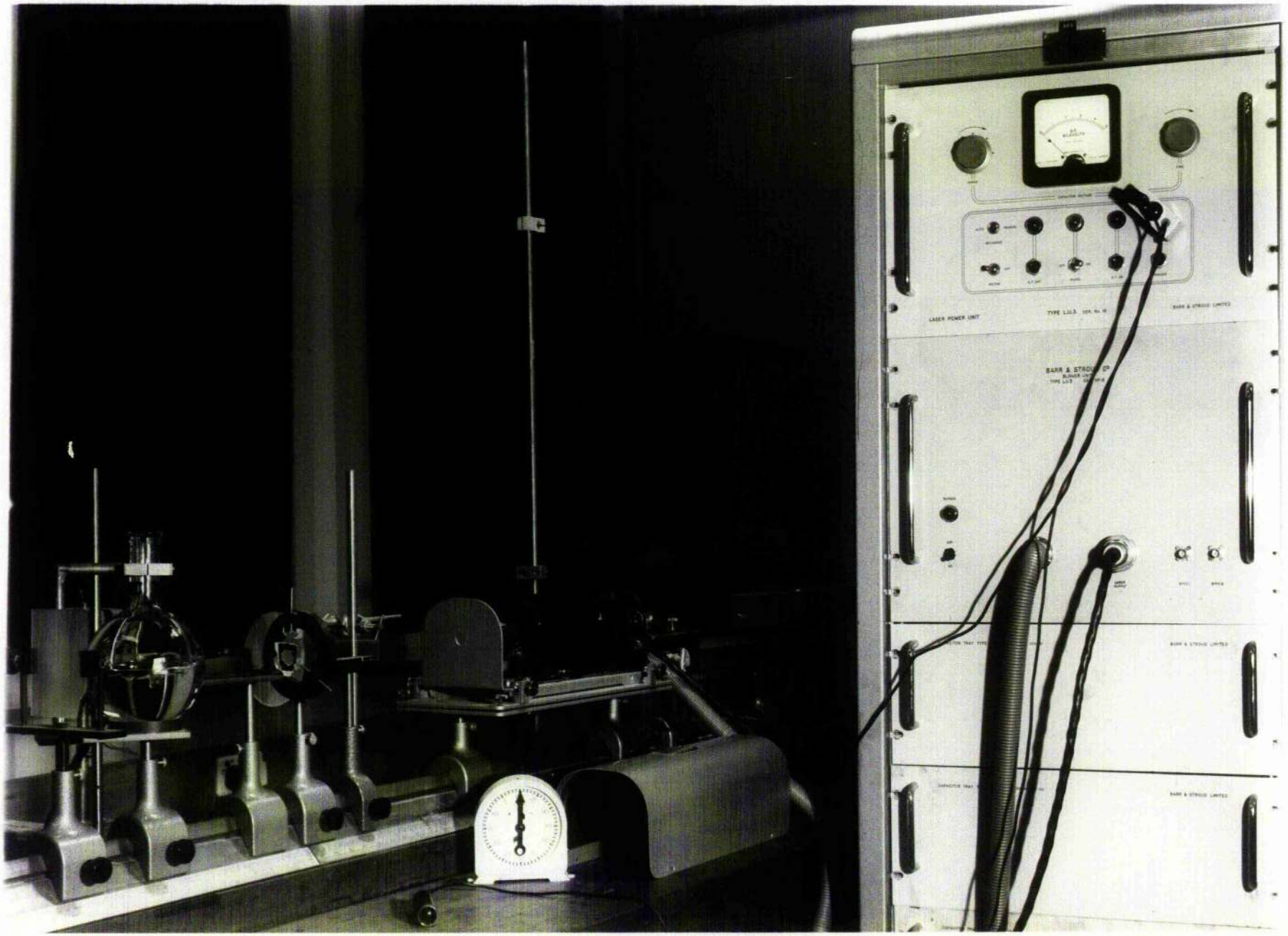

Plate 1. The Ruby Laser

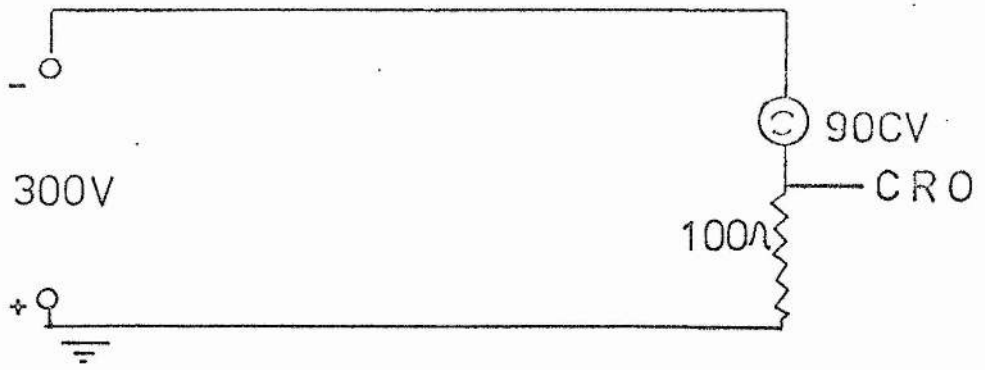

Fig 6 Circuit of 90CV Detector

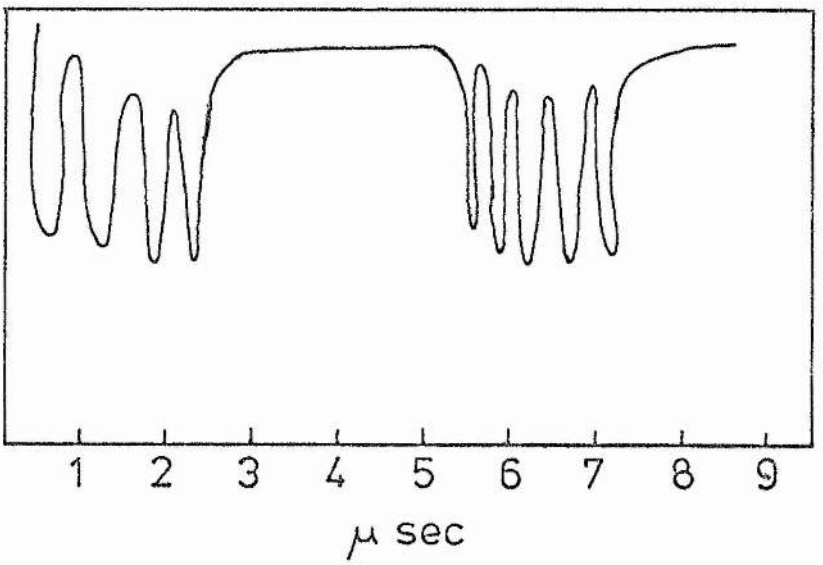

Fig 7(a)

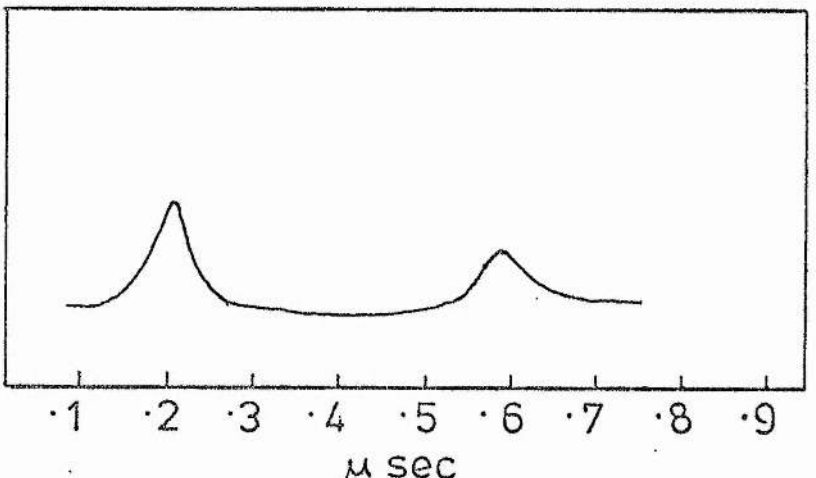

Fig 7(b)

Fig 7(a) Output of Original Ruby on 90C.V. Detector.
(b) Output of Replacement Ruby on HP 4203.

the rotating prism removed suggesting that the gain was too high to produce a Q-switched pulse output. Examination of the ruby rod showed discontinuities which would lead to an increased beam divergence. The ruby was returned to the makers who, after some time, agreed with our findings and replaced it. The new rod was found to operate satisfactorily with a typical pulse output of the form shown, Fig 7(b) taken with a HP4203 photodiode as discussed in section 4.5.

4.3(a) The Autocollimator

The ruby rod and the mirror system must be aligned to within a few seconds or arc. To do this an autocollimator was designed and constructed. The unit is shown in Fig 8.

The light source S, is a 50 watt Phillips projection lamp which focuses onto the pin-hole, P. The pin-hole is at the focus of the lean, L so that a collimated beam is produced whose diameter is variable by means of the iris, I. The parallel beam then passes through a beam splitter over which is mounted a telescope adjusted to receive parallel light. Light from the autocollimator striking two reflecting surfaces passes back into the field of view of the telescope and the separation of the two spots gives a measure of their angular orientation with respect to the beam. In operation a reference beam is set up by reflecting the beam back along the axis into the field of view of the telescope. Other reflecting surfaces are then orientated perpendicular to this reference by adjustment screws until all the reflected spots are coincident.

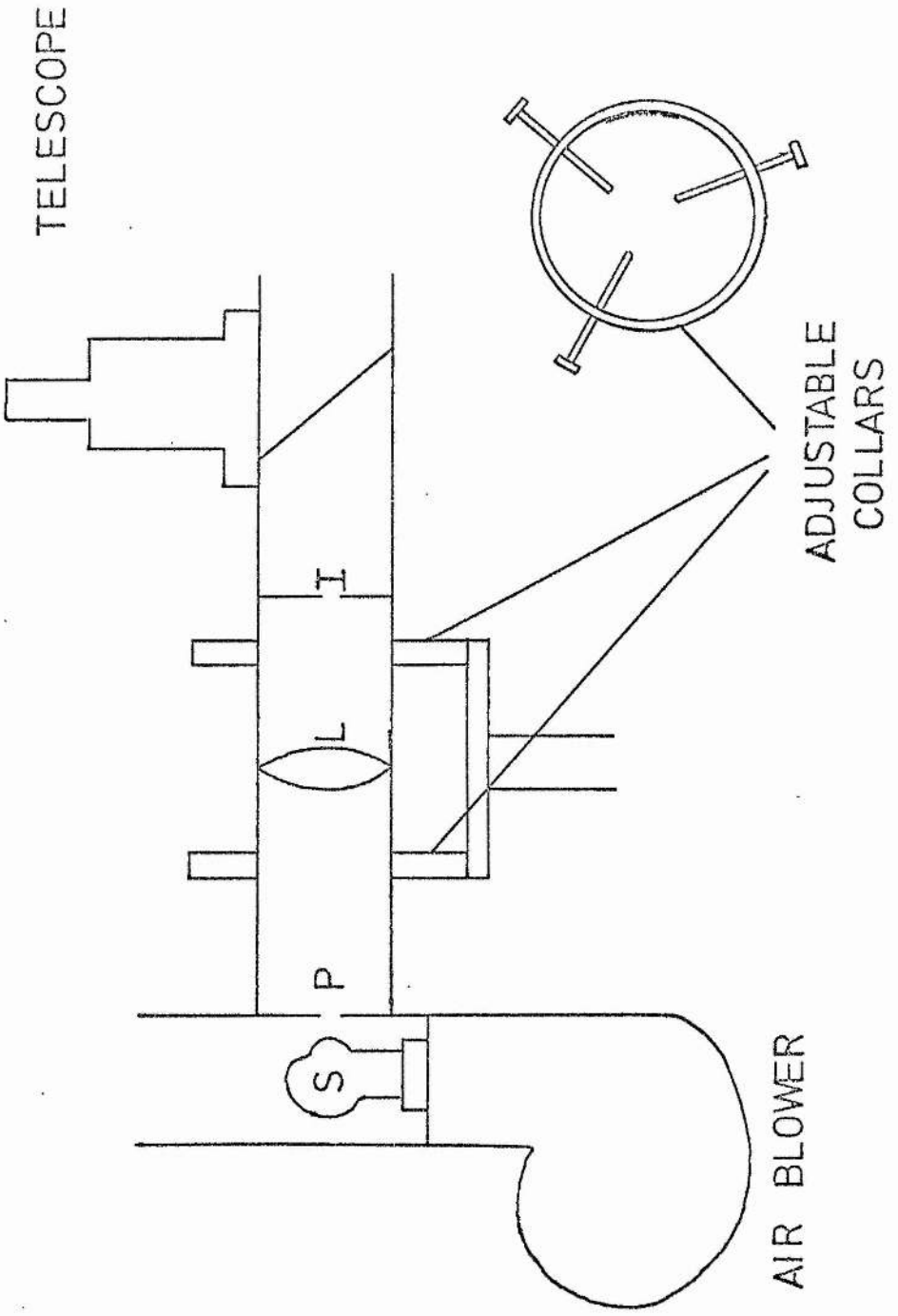

Fig 8 The Autocollimator

4.3(b) Autocollimator Resolution

The beam divergence of the unit constructed was measured over a distance of 5 metres and found to be 6 mins. of arc. This was checked by using the mirror mount with the autocollimator and finding the rotation of a single control which moved the spot one diameter. The control had to be turned $\frac{1}{8}$ of a turn which corresponded to an angular rotation of 4 mins. of arc. Since the smallest screw movement the operator is capable of making corresponds to approximately one fifth of the spot diameter, the collimator is capable of alignment within the capabilities of the adjustment controls.

4.3(c) Alignment Technique

The procedure for aligning the ruby laser is as follows.

1. With the iris aperture set at minimum, the collimator is aligned along the optical bench by means of the adjustment screws until the beam passes through a 2 mm pin-hole over the one metre length of bench that is to contain the ruby laser cavity.

2. The reference beam is then formed by means of the roof prism which is adjusted with respect to orientation and height until the collimator beam striking centrally on the roof edge is reflected back through the pin-hole placed immediately in front of the collimator. The prism is then locked in this position.

3. The ruby unit is then placed on the bench and the beam is aligned centrally on the ruby face nearest the collimator.

4. The rod is then aligned perpendicular to the reference beam

by the adjustment screws of the ruby laser head until the spot reflected from the front surface of the ruby coincides with the reference spot in the field of view of the telescope.

5. The iris aperture is now increased and, if accurate alignment has been achieved, a red circular spot of the same diameter as that of the ruby rod should be visible on a white card inserted near the roof prism. If this is not the case, further alignment adjustments are necessary.

6. The dielectric mirror is then inserted and after aligning it such that the beam is centrally placed on the mirror surface and the reflected spot is coincident with the reference spot, the system should be in a lasing condition.

7. The ruby unit is then tested in this non Q-switched arrangement and should lase at the minimum voltage of the condenser bank.

8. The prism is released from its locking screw and the system may now be operated in the Q-switched mode.

4.4(a) The Rat's Nest Calorimeter

To measure the power from the laser it is necessary to measure the energy output in the Q-switched pulse. Following a paper by Baker[29] a bolometer unit was constructed.

In this system the beam energy is trapped and absorbed in a bundle of fine insulated copper wire termed a Rat's Nest. The change in resistance of the wire is proportional to the energy absorbed and is independent of the distribution of incident light. This method was

chosen because of its advantages over others in which the energy is absorbed in a liquid or a solid and the temperature rise is measured by means of a thermocouple. These systems, apart from problems of measurement of absorption coefficient and heat capacity, suffer from the defect that thermal equilibrium must be reached before any measurement is made and as a result errors are caused due to loss of energy during this period and the final temperature is a function of the heat loss. In using the Rat's Nest there is no need to wait for equilibrium. That this is so is shown by Baker's analysis which is given below.

Construction

The Rat's Nest consists of approximately 1,000 ft. of fine insulated copper wire of resistance 1000Ω (measured on an avometer) contained in a silvered beaker. The disturbance caused by air effects is avoided by covering the end of the beaker with a glass plate sealed on with araldite. The measurement circuit is a conventional Wheatstone bridge and to maintain thermal equilibrium two of the bolometers are used in the measurement arm. The two units are contained in a metal cylinder and are isolated from the walls by means of a plastic foam cushion. See Fig 9.

4.4(b) Theory

When a pulse of energy is incident on the Rat's Nest, light is successively scattered and absorbed by the individual wires and the total energy absorbed appears as a temperature rise in the wire. The

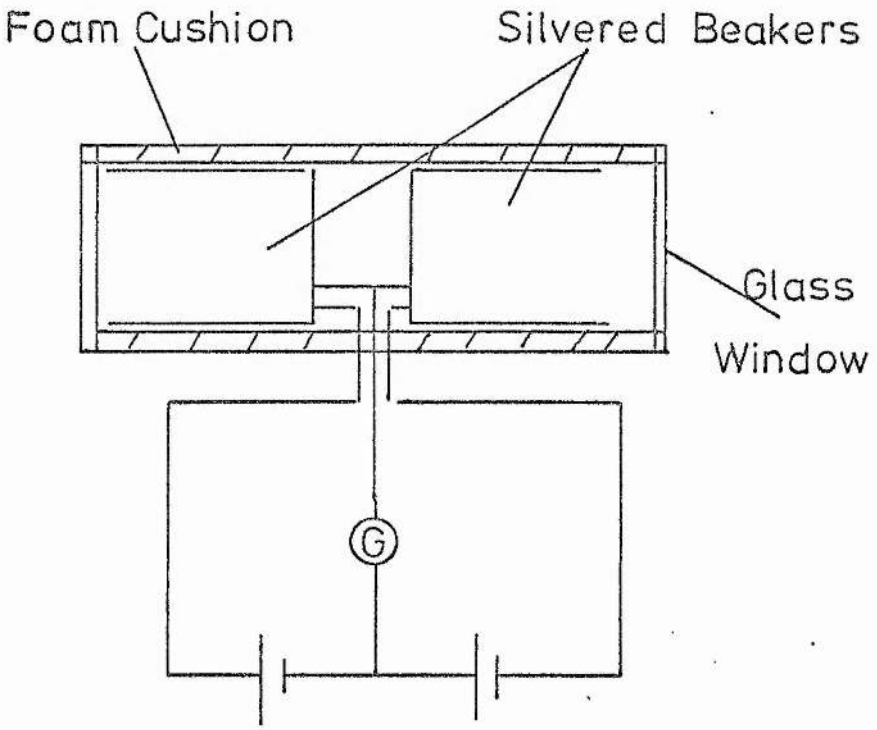

Fig 9 The Rats Nest Bolometer

change in resistance of an element of wire, $\Delta R_o'$, is given by

$$\Delta R_o' = \alpha R_o' E' / (4.2\ M' C) \quad , \qquad 4.4.1$$

where R_o' is the resistance of the element, E' is the energy absorbed, M' is the mass of the element, C is its specific heat, and α the temperature coefficient of resistance. The total resistance change is summed over all elements of the wire.

If the wire is of uniform cross section, then we have

$$R_o'/M' = R_o/M \quad , \qquad 4.4.2$$

where R_o, M are the corresponding total resistance and total mass of the wire. The total change in resistance is therefore

$$\Delta R = \alpha R_o/(4.2\ MC)\Sigma E' = \alpha R_o/(4.2\ MC)\ E, \qquad 4.4.3$$

where E is the total energy absorbed.

The energy dumped into the Rat's Nest is therefore given by

$$E = (4.2\ MC/\alpha R_o)\Delta R \quad , \qquad 4.4.4$$

where MC is the thermal capacity of the wire.

4.4(c) Corrections

Since some of the incident energy is reflected back by both the glass plate and the wire itself, a correction must be made. Baker found this to be 28% and this figure has been used as being probably accurate enough for our purposes. The wire is covered in a layer of Lewmex insulation whose heat capacity is not known so that the value of MC was determined experimentally by discharging a condenser of known energy into the system and measuring the temperature rise. The final expression obtained from 4.4.4 by substituting appropriate values is

$$E = 2.4\Delta R \text{ joules} \qquad 4.4.5$$

4.4(d) Measurement Circuit

In Baker's system the circuit is an equal arm Wheatstone bridge which although not in the most sensitive arrangement has the advantage of thermal stability. In consultation with Mr. H.A.T. Cairns of this department a new bridge was constructed which maintained thermal stability but had an increased sensitivity. This is discussed in Appendix A.

4.4(e) Energy Output

The total output energy as a function of time between shots was monitored to check reproducibility. Figure 10 shows that there is a rapid decrease in energy output from the laser for the first few pulses which is followed by a slow decay as the ruby rod increases in temperature. The output energy fluctuations can therefore be minimised if the first few pulses are neglected and the laser unit is operated at regular intervals. The energy was also monitored with a microscope slide in the beam so that a photo-diode could be calibrated by sampling a known fraction to give the power output directly. The 90 CV is basically not a fast diode and was found to give erratic results. Consistent results were obtained with the photo-diode described in the next section.

4.5 Photo-diode Unit

In order to monitor the pulses generated by the Q-switched ruby laser a fast photo-diode is necessary.

Silicon p.i.n. photo-diodes (Hewlett-Packard type HP4203) which

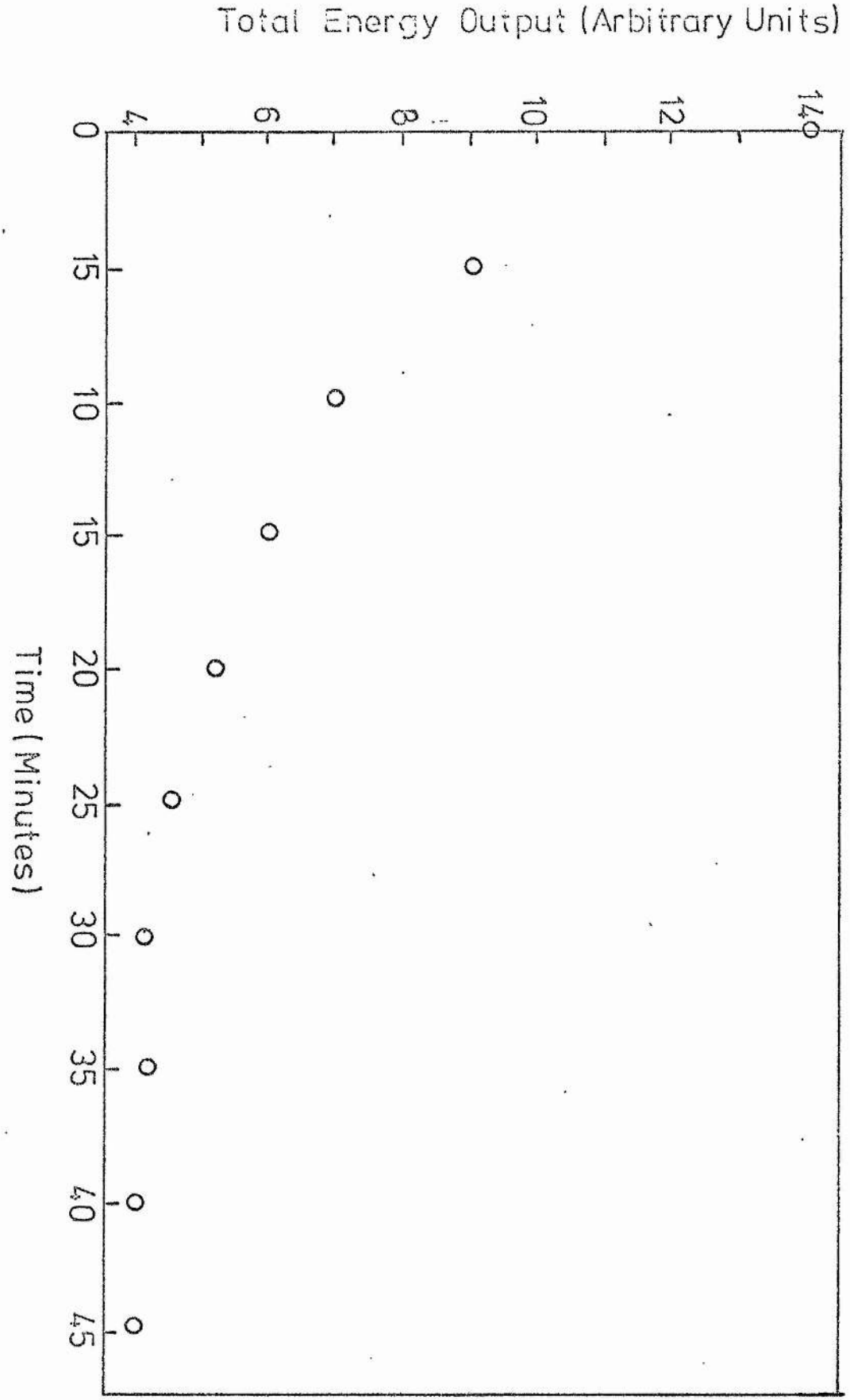

Fig10 Energy Output of Ruby Laser as a function of Time at Constant Input Energy

have a rise-time of less than one nanosecond have been found to be suitable. The advantages of these photo-diodes are as follows.

1. They are inexpensive.

2. They operate at voltages of -10 to -20 volts, Ever Ready batteries, type PP3, are used.

3. Voltage signals up to 10 volts can be obtained

4. They are small, enabling the construction of compact units.

The basic circuit is shown in Fig 11. The same basic unit was used throughout the investigation either singly or in multiples. The signal was recorded directly through a 50Ω cable by an oscilloscope (Tektronix type 555).

4.6(a) Time Resolution of Stimulated Raman Spectra

The experimental arrangement used to study the temporal development of stimulated Raman Spectra is shown in Fig 12. The streak camera used was an image converter type manufactured by Space Technology Laboratories.

The camera equipment consists of the head, the streak unit, the control console, and the trigger delay generator. The camera head is shown in Fig 13.. Light from a source is imaged on to a photocathode where the photon image is converted into an electron image. The electrons emitted are then accelerated through a voltage of 15 KV , and focused, by means of an electron lens, on to a fluorescent screen where the resultant photon image, intensified by the acceleration, is photographed by means of a polaroid camera.

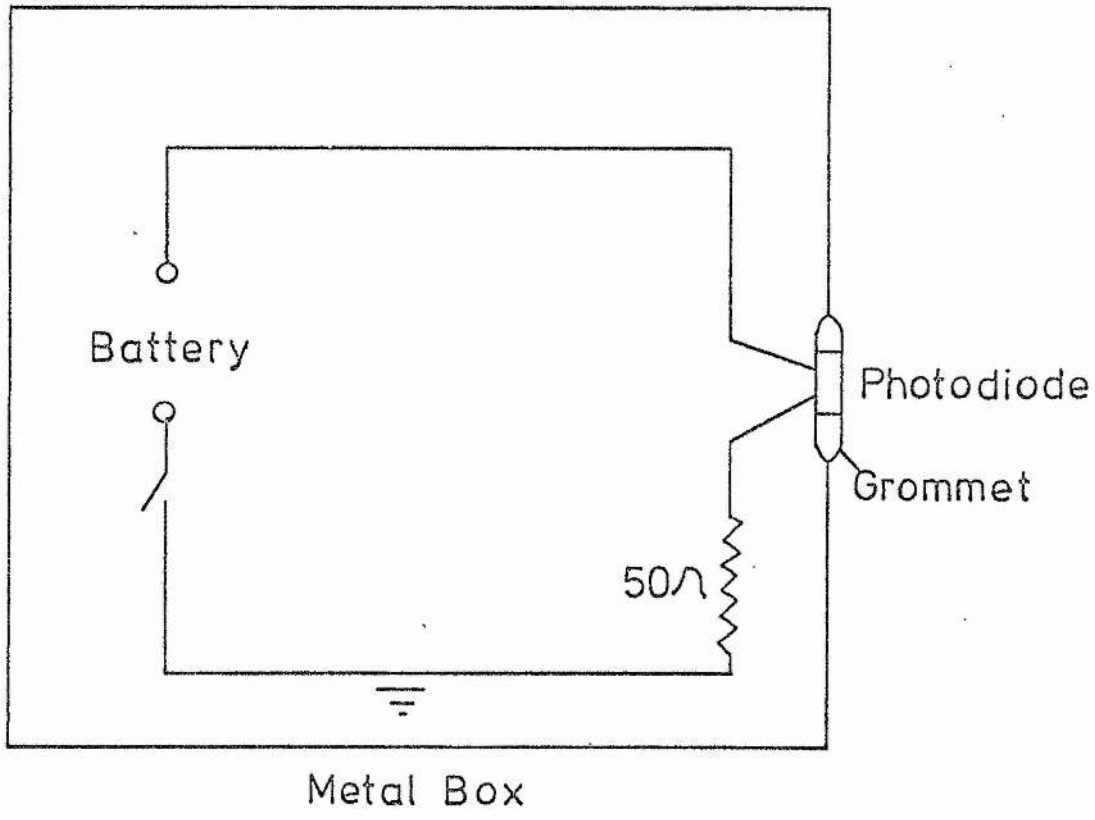

Fig 11 The Photodiode Unit

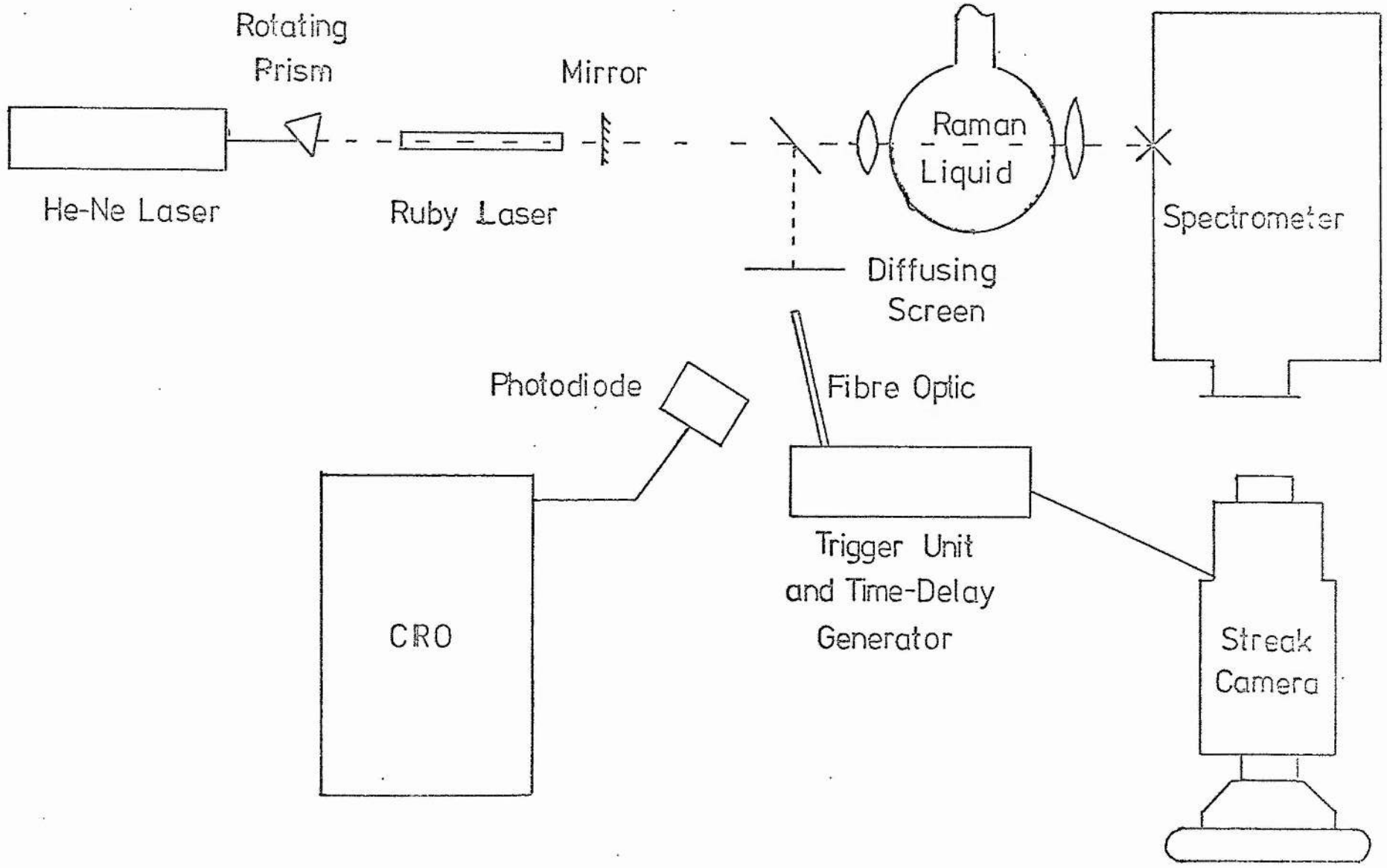

Fig12 The Stimulated Raman Spectrometer.

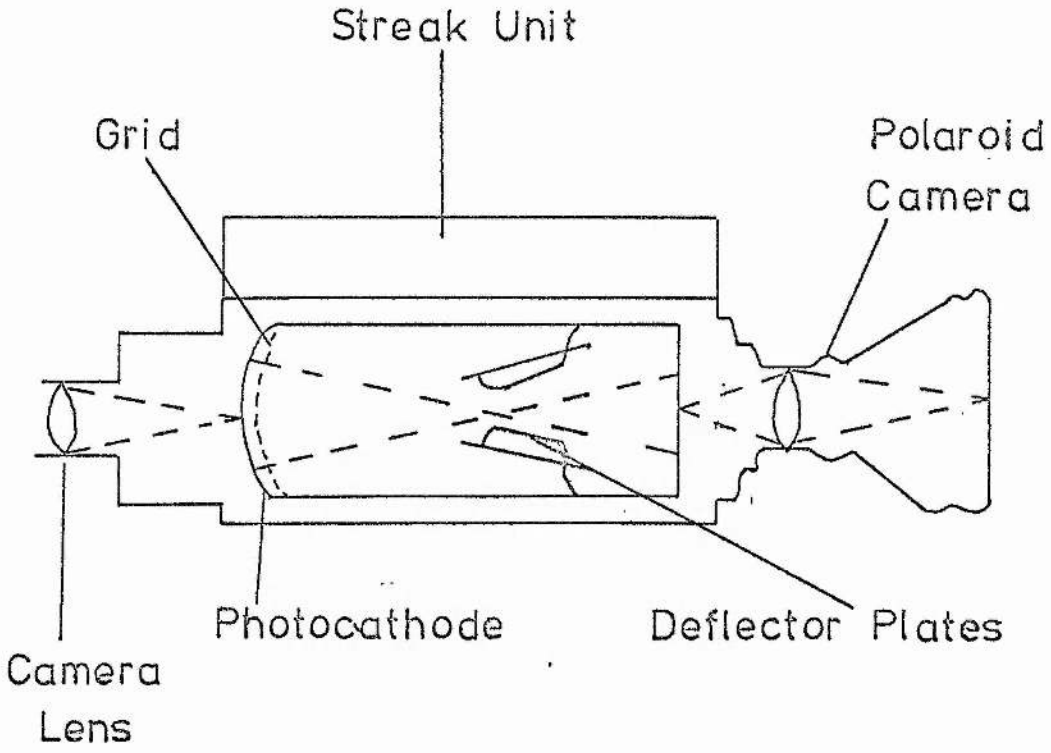

Fig 13 The Image Converter Camera

The camera shutter is electronic in that the instantaneous potential of the grid with respect to the photocathode permits or prevents the passage of electrons. A pair of deflection plates at the cross over of the beam permits the image to be moved across the fluorescent screen.

The camera can be operated in either the sweep mode or the framing mode. In the sweep mode, a positive pulse is applied to the grid for the duration of the exposure whilst the image is deflected linearly by means of a ramp voltage applied to deflection plates. Two streak units were used in the investigation; the wide range unit, and the high speed unit. The photocathode has an S 20 response. The source can be imaged from 12" to infinity by means of a focusing control and the aperture of the instrument is variable from f/22 to f/1.9. The resolution of the instrument when operated with 10,000 ASA Polaroid is 10 line pairs/mm so that with the wide range streak unit with a maximum streak speed of 10 n sec/mm two events separated by 1 n sec are resolvable. The equipment requires a trigger pulse of 300 volts with a rise-time of 10 n sec. The minimum time delay in the equipment is 12 n sec.

4.6(b) Triggering

The trigger pulse is generated by the time delay generator which accepts either an optical or electrical signal and produces the required 300 volt pulse with a rise time of 10 n sec. The optical input consists of a photodiode with a rise time of 1 n sec which is

fed by means of a 5 ft x ½ inch diameter fibre optic bundle. The spectral response of the photodiode is S11.

The optical input can be monitored but it was found that the photodiode circuit is unsuitable for laser pulses as the RC decay time is large. The electrical input accepts pulses from 1 to 500 volts provided the rise time is greater than 1 volt/μsec. The triggering level is variable from 1 to 200 volts with the input signal fed into a 50Ω input impedance. The output voltage is variable from 50 to 500 volts in 50 volt steps and is set at 300 volts to operate the camera. The pulse rise time is 10 nsec with a fall time of 500 nsec. For both optical and electrical inputs the resulting output can be delayed from 00.00 to 99.99 μsec with an accuracy of 1 nsec. The time delay chosen is displayed on a digital scale. The minimum time delay on zero delay setting is 30 nsec. The maximum repetition frequency for both inputs is 100 pulses per sec.

It was clear from these specifications that, if the camera was triggered by means of the time delay generator, the minimum time delay is 42 nsec. Delays for the fibre optic and co-axial cables give a total of approximately 50 nsec for the system. The laser pulse has a rise time (from lase to peak) of 40 nsec. To photograph the whole laser pulse and events within the pulse it is necessary to trigger the camera at least 50 nsec before the signal arrives at the camera so that it may be recorded.

Triggering the camera by means of the flash tube light pulse or any of the discharge circuit was not possible because of the time

delays involved (3 msec). In any case, the jitter on the time between the flash tube and the laser was prohibitive. The trigger pulse has to be constant with respect to the onset of laser action to within 0.2 μsec to ensure a picture within the 0.5 μsec streak time. A time of flight delay in the system was considered but since this would require an optical distance of 15 metres and would mean deflecting the beam across the laboratory this method was rejected. It was discovered that double pulses could be obtained from the laser and it was decided to trigger the camera by the first pulse and to take streak photographs of subsequent pulses by appropriate adjustments of the time delay generator.

The laser output energy as a function of time showed that the energy output was fairly constant provided there was sufficient time between shots for the ruby to reach thermal equilibrium, see Fig 10. The pulse output under equilibrium conditions, shown in Fig 7 satisfied the jitter requirements so that triggering of the laser was possible. The output pulse was monitored as is shown in Fig 12 by deflecting a fraction of the beam by menas of a microscope slide on to a ground glass screen behind which a fast photodiode was mounted. The diode was protected from overload by means of an ON.30 neutral density filter mounted on the diode unit. The output was fed into a Tektronix 545B oscilloscope, triggering being effected by the signal. The screen also acted as source for the fibre optic feeding the time delay generator.

4.6(c) Helium-Neon Alignment Laser

This was incorporated to align all the components of the optical train along the same axis as that of the ruby laser. The laser was D.C. excited by a power pack constructed in the electronics work-shop which produced 1 KV up to 25 ma and included a trigger circuit for striking the discharge. The laser tube was a commercial unit and delivered up to 3 mw multi-mode. The laser was contained in 2" channel iron section and was mounted on an independent 1 metre optical bench.

4.6(b) Optical Train

The beam was focused into the flask with a lens of focal length 15 cms and the focal region was imaged by means of a second lens into the slit plane of the spectrometer. After dispersion in the spectrometer a point spectrum was formed at a ground glass screen for presentation to the image converter camera. It was found that if the beam was not focused into the centre of the flask a dielectric breakdown occurred which could clearly be seen as a flash of white light followed by a cloud of black discharge products, presumably carbon. Breakdown could be avoided with correct alignment. It should be noted that after this has occurred it is very difficult to stop breakdown and as a consequence no Raman spectra are produced. This is probably caused by the dispersed carbon.

4.6(e) The Spectrometer

The spectrometer was built at Harwell at the instigation of S.R.C. on the grounds of economics. Unfortunately because all of the

components had to be ordered and because of constructional delays the instrument was delivered over one year from the date of order.

The instrument (see Fig 14) is an "over and under" Czerny-Turner with a 600 line/mm grating blazed for 7200Å. The two mirrors are figured to $\lambda/4$ and parabolically corrected to produce a true line focus. The mirrors are concave with a focal length of 1 metre and of diameter 6" and 8" respectively. The wavelength range exposed at the photographic plate is 1600Å. It should be noted that this range limits the observations, e.g. with benzene (Raman shift 992 cm^{-1}), only the Stokes lines can be recorded (see Plate 2). The aperture of the instrument is dictated by the useful area of the collimator mirror which is apertured by the grating, so that it is f/10.

The system was calibrated with a Philips neon lamp chosen because of the number of strong spectral lines in the region of interest (4000-9000Å). Spectra were recorded on Kodak I.R. E R plates which have a flat spectral response from the visible into the near infra red. The lamp was aligned with the spectrometer by using the method of conjugate images such that the image was focused on the slit for the two lens positions. A calibration chart for neon was available up to 6500Å and, using known lines from this, the system was calibrated to 8500Å with a Hilger comparator. The disperions is 16.3 Å/mm. Plate 2(a) shows a typical spectrum with the line identification. Plate 2(b) shows the calibration spectrum with the stimulated Raman spectrum of benzene. The lines were identified as the Stokes fundamental at 992 cm^{-1} from the exciting line and the second harmonic at 1984 cm^{-1}.

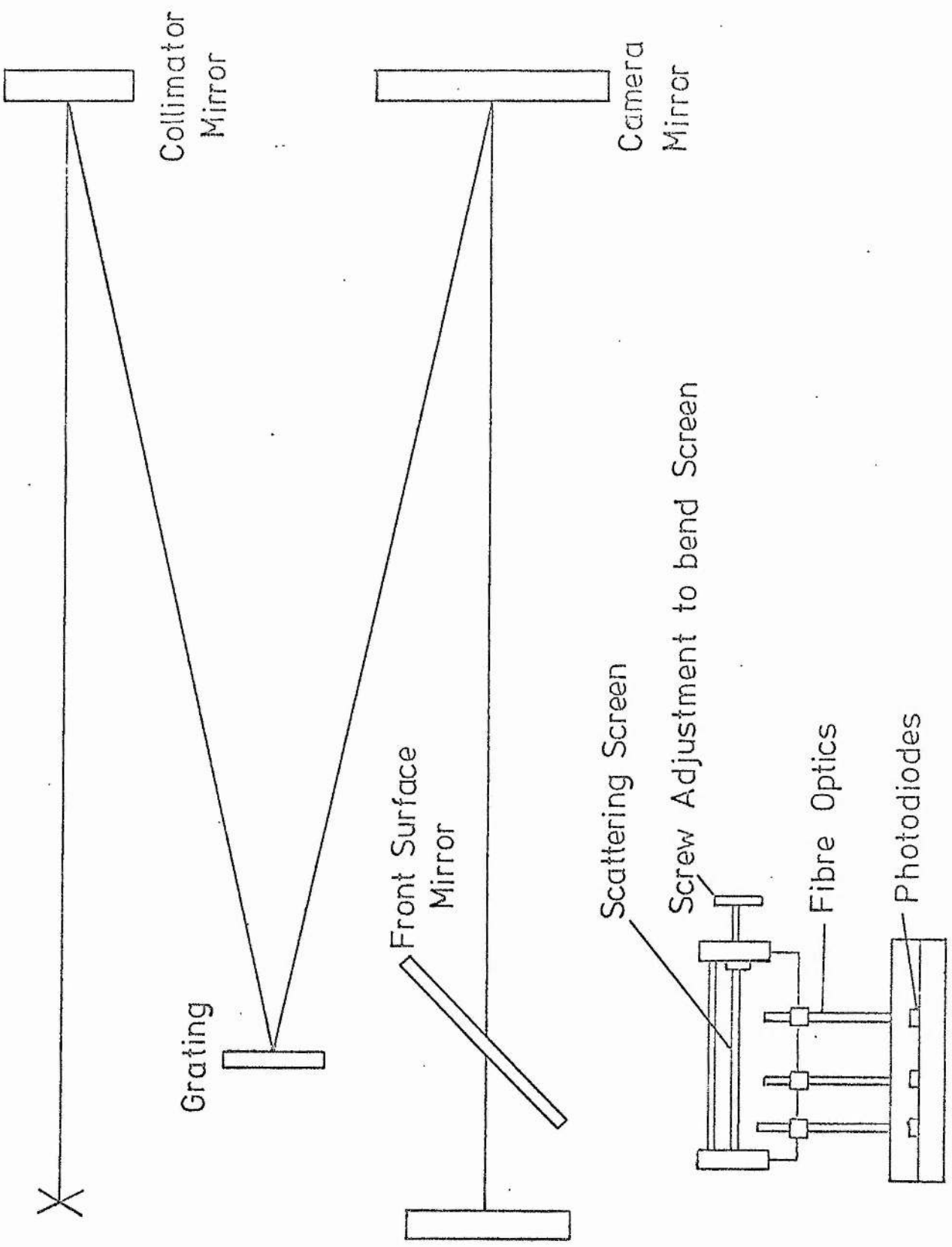

Fig14 Schematic of the Spectrometer and the photodiode system

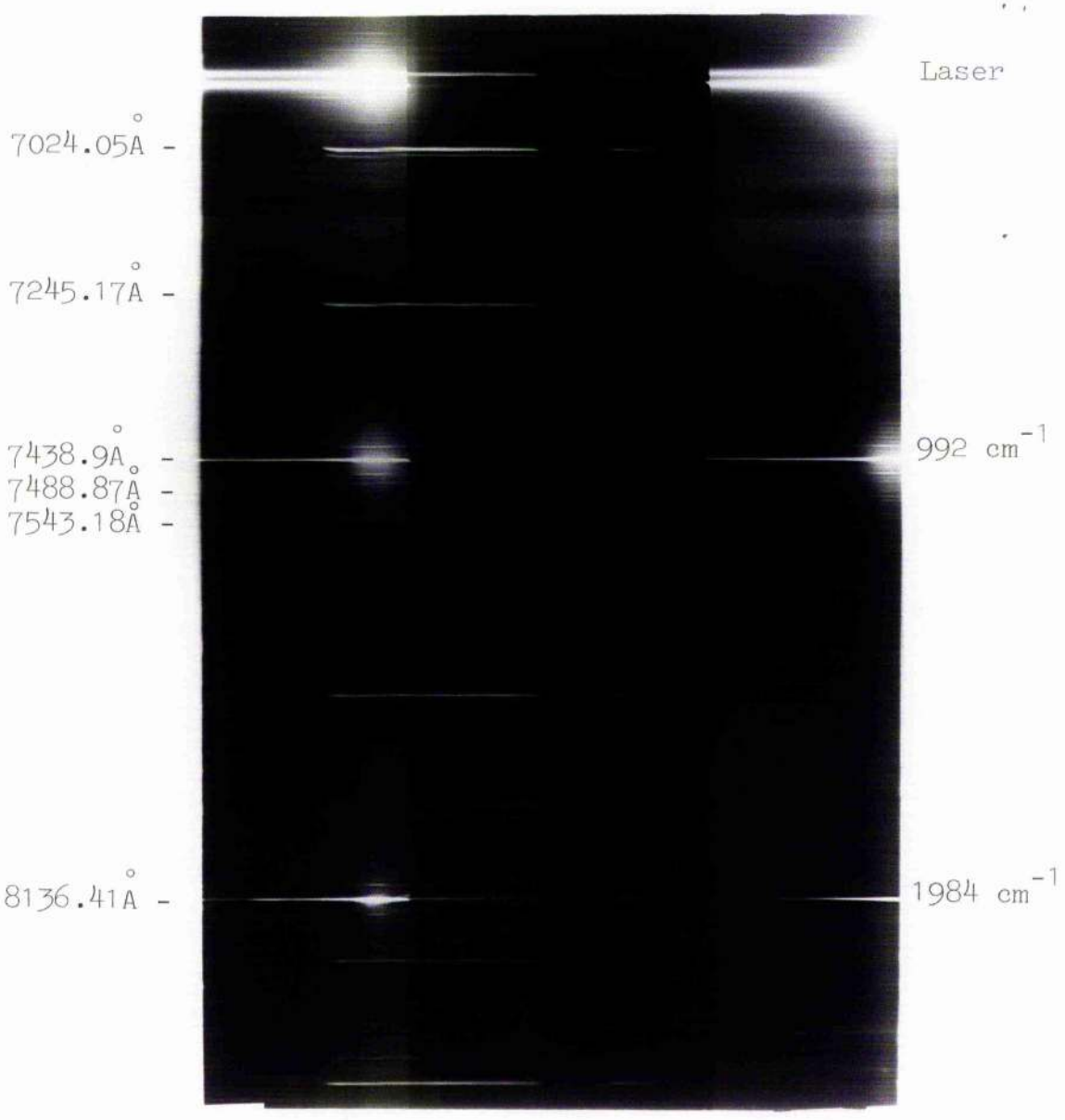
Laser
7024.05Å
7245.17Å
7438.9Å
7488.87Å
7543.18Å
992 cm^{-1}
8136.41Å
1984 cm^{-1}
(b)
(a)

Plate 2

Many orders of Rowland ghosts caused by the periodic error in the ruling of the grating are shown in the intense sections of the Raman lines. Since all the stimulated spectra were well known, recording on photographic plate was thought to be wasteful of time so that a plate holder incorporating a Polaroid camera was constructed and all further spectra were recorded on Polaroid film.

4.6(f) Modification of Spectrometer for Time Resolution

Since it was planned to time resolve the stimulated Raman spectrum the spectrometer had to be modified. As explained above, the field of view was limited to 1600Å and so a complete spectrum containing both Stokes and anti-Stokes components could not be studied. It was therefore decided to modify the spectrometer as shown in Fig 14. A front surface mirror flat to $\frac{\lambda}{10}$ was mounted and inclined at 45^{o} to the beam direction so that the camera focal plane was rotated to the side of the spectrometer. The mirror has dimensions 20 cms by 10 cms so that the available wavelength range is significantly increased. It is mounted on a rotating table with levelling screws and its position is adjusted so that the new focal plane corresponds, with respect to height and distance, to that of the photographic plane. Since the focal plane lies on the arc of a circle of radius 1 metre the focusing arrangement shown in Fig 14 was constructed with the facility for not only positioning a diffusing screen at the focus but also compensating for the curvature. By means of the screw, S the screen is bent into the arc of a circle. Successive adjustments are made until the calibration spectrum is in focus over the whole field

of view. The unit has a slot behind the screen so that the light intensity can be attenuated if necessary by means of neutral density filters; this is necessary to avoid breakthrough on the photo-cathode of the image converter camera or over-exposure of the film.

4.6(g) Setting-up Procedure

In a darkened room the He-Ne laser was tuned to a single transverse mode and the complete optical train was aligned. The laser was firstly aligned along the optical bench using the same pin-hole as that of the autocollimator (see 4.3) so that the output beam had the same axis as that of the ruby unit.

The spectrometer was adjusted so that the beam was centred on both the entrance slit and the collimator mirror. The lenses were aligned by means of self-conjugate imaging until both focused positions were centred on the entrance slit. The flask was then inserted, the beam was focused into the centre, and the focal region was then imaged into the slit plane of the spectrograph. The laser provided a fixed reference beam so that the components could be removed and replaced without loss of alignment.

The ruby laser was fired at regular intervals to ensure that thermal equilibrium was reached; an appropriate time delay was set on the time delay generator and the optical input attenuator was adjusted so that the unit triggered on the leading edge of the input pulse.

The camera was positioned so that the whole field of view was visible and was focused on the spot of the He-neon laser at 6328Å. The magnification of the camera in this position was $\frac{1}{10}$ so that the

effective spot size was ∿0.1 mm enabling measurements to be made with reasonable accuracy. The position of the grating was adjusted so that the ruby laser line at 6943Å was centred on the diffusing screen. This can be done approximately from the known dispersion of 16.3Å/mm and the mm scale placed above the screen. The laser line was attenuated to prevent breakthrough on the photo-cathode. The first pictures were taken at 1 μsec streak duration and were over exposed because of the intensity of the first Stokes line in benzene. This was also attenuated with a neutral density filter. The camera was then operated at the maximum streak speed of 100 mm/μsec and results taken were of the form shown in Plate 3.

4.7(a) Results - Streak Records

The results are shown in Table 2 with typical streak records shown at 1.0 μsec and 0.5 μsec total streak time shown in Plate 3. The slow streak displays the typical multi-pulse output and the first pulse generated is just visible at the top of the picture. The features to note in the fast streak are the time resolution and the "necking" of the laser pulse during Raman generation. The Table indicates that the time delay from initiation of Stokes lines to second harmonic Stokes lines can be less than that for second harmonic Stokes to Stokes cut-off and this suggests some asymmetry in threshold.

4.7(b) Distortion of the Laser Output Pulse During Raman Generation

In order to investigate the constriction observed in the laser streaks it was decided to study the laser output and Raman pulses with photo-diodes. Two possible causes of the effect are given below;

Benzene

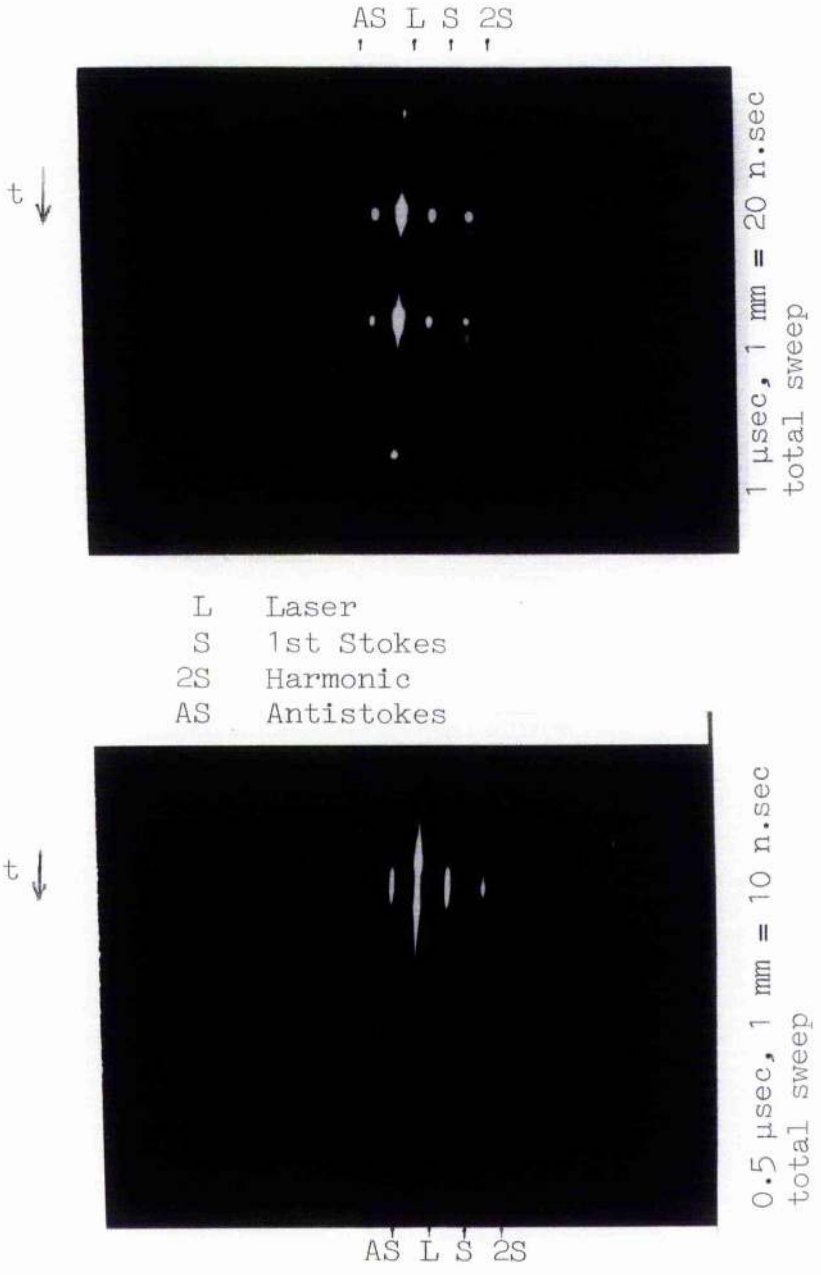

L Laser
S 1st Stokes
2S Harmonic
AS Antistokes

Plate 3

TABLE 2

LIQUID BENZENE

T.D. S-2S	S-2AS	length of S	length AS	length 2R	T.D. 2S-S
10	∿5	70	60	50	10
5	-	70	65*	60	5
10	∿5	70	60	40	20
5	5	70	65*	60	5
10	5	70	65*	50	10

Where S - fundamental Stokes line

2S - second harmonic Stokes line

AS - anti-Stokes line

T.D. - time delay

* - no sharp threshold observed measurement uncertain.

(a) self-focusing leading to a beam constriction, and

(b) an intensity reduction of the laser radiation because of generation of Raman spectra.

Three lengths of fibre optics, each one foot long with a diameter of 3 mm were used to feed the signal from the output screen of the spectrograph to three separate photo-diodes (Fig 14). By locking the fibre optic ends into ball races in the diode unit they were free to move freely over the available field. The fibre optics were rigidly locked into mounts which could be orientated in any direction or position. Alignment was readily attained by using the mount as a gun sight until the spot of interest is centred and then inserting and locking the fibre optic. Neutral density filters were used to prevent overloading the diodes.

The laser output pulse and the fundamental Stokes line of benzene were examined by displaying the photo-diode signals with Tektronix 555 double beam CRO. The CRO was triggered by the laser signal and operated with a common time base at 100 nsec/cm. The CRO was operated "single shot" and the two trace spots were superimposed as accurately as possible. Pictures were taken on Polaroid 10,000 A.S.A. and the results are shown in Fig 15(a).

The pictures clearly showed distortion of the laser pulse with a sharp Raman pulse displaced relative to the dip in the laser trace. Since the co-axial leads from both diode outputs to the CRO were of the same length it was suspected that the displacement was due to an internal delay in the oscilloscope. To check this,

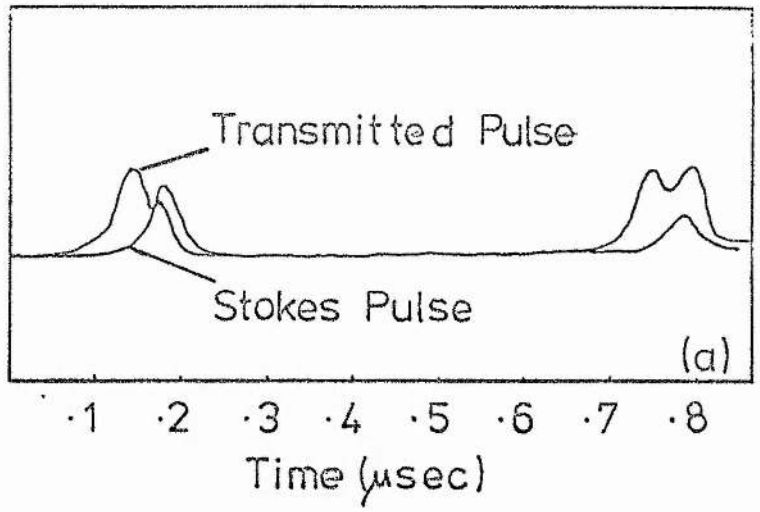

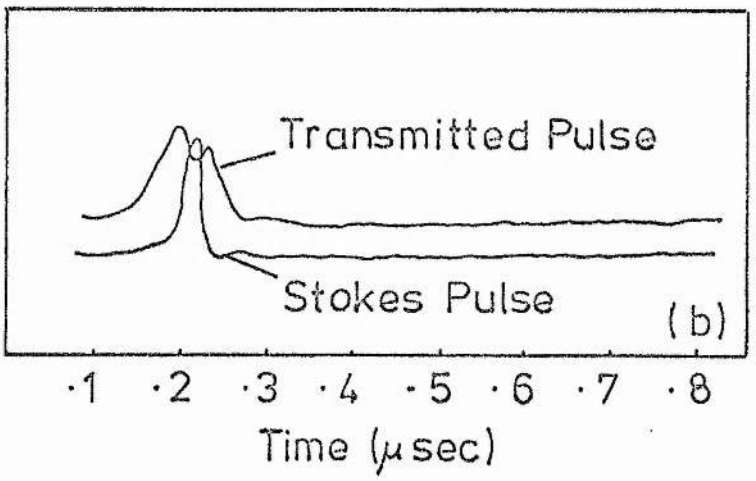

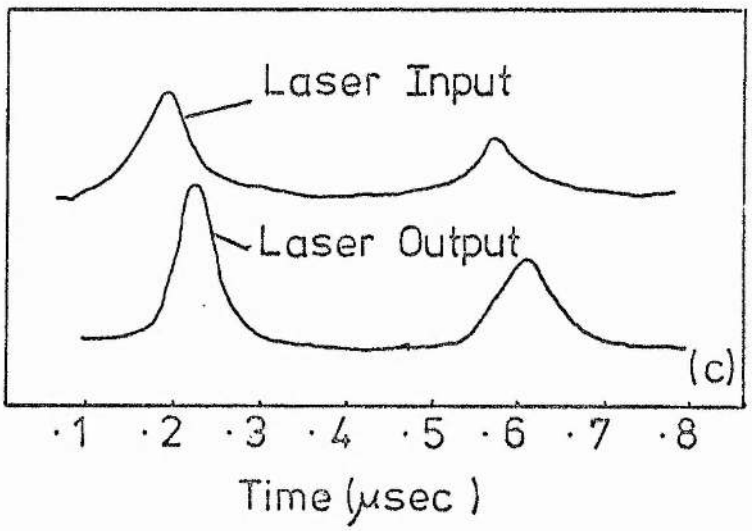

Fig 15 (a,b,c) Correlation between Distortion of Laser Pulse and Generation of Stimulated Raman Spectra.

a signal from a 30 MHz oscillator was fed into the CRO and a similar displacement was found. The shift was corrected by off-setting the second trace with respect to the first so that the two traces coincided. Fig 15(b) shows the laser and Raman outputs after this correction and it is clear that the peak of the Raman coincides with the maximum absorption from the laser. A further control experiment was performed to check that the distortion was not being caused by the diode by removing the flask. The results of this are shown in Fig 15(c) in which it is clear that no distortion exists.

From the traces of the input pulse and the output pulses when no Raman is produced it is possible to estimate the power loss. The loss in Fig 15(b) is 65%. This readily explains the "hole burning" effect on the laser pulse. The input pulse was monitored with a Tektronix 545B oscilloscope.

From these pictures it is clear that the laser output pulse is attenuated when stimulated Raman spectra are generated and the attenuation increases with increasing imput pulse amplitude. It was decided therefore to investigate the correlation between the laser input pulse and output pulses with the Raman Stokes line. The laser input pulses were monitored with the 545B whilst the Raman Stokes and laser output pulses were monitored with 555 oscilloscope. Both oscilloscopes were run at 100 nsec/cm and the sensitivities and positions of the fibre optics were adjusted so that at low pulse amplitude the laser input and output pulses were approximately equal. By this method, the loss of laser intensity could be determined. A typical

result is shown in Fig 16 where a saturation of the laser output is clearly shown at the onset of stimulated Raman. (See Table 3).

4.8 Conclusions

The main features of the stimulated Raman effect in benzene for this particular geometry can be summarised from the above results.

1. The lines are not generated simultaneously on a nanosecond time scale but appear to have the sequence fundamental Stokes, anti-Stokes and second harmonic Stokes.

2. The streak records show a constriction in the laser pulse during the generation of stimulated Raman spectra which is correlated with the pulse distortion observed on the laser output pulse during generation of stimulated Raman spectra. No distortion is observed when threshold is not exceeded.

3. The pulse distortion effect appears to start at the onset of stimulation of Raman spectra and the peak of the first Stokes pulse occurs at the maximum attenuation of the laser pulse. The investigation of all three pulses shows the same absorption effects about the threshold for stimulated Raman and clearly shows the gain on the Stokes pulse.

4.9 Discussion

The results for pulse distortion are similar to those obtained by Maier and Kaiser[30] who, working with carbon disulphide, found a large reflected pulse. A similar effect had previously been found by Giordmaine and Howe[31] who, finding a large attenuation of the pump

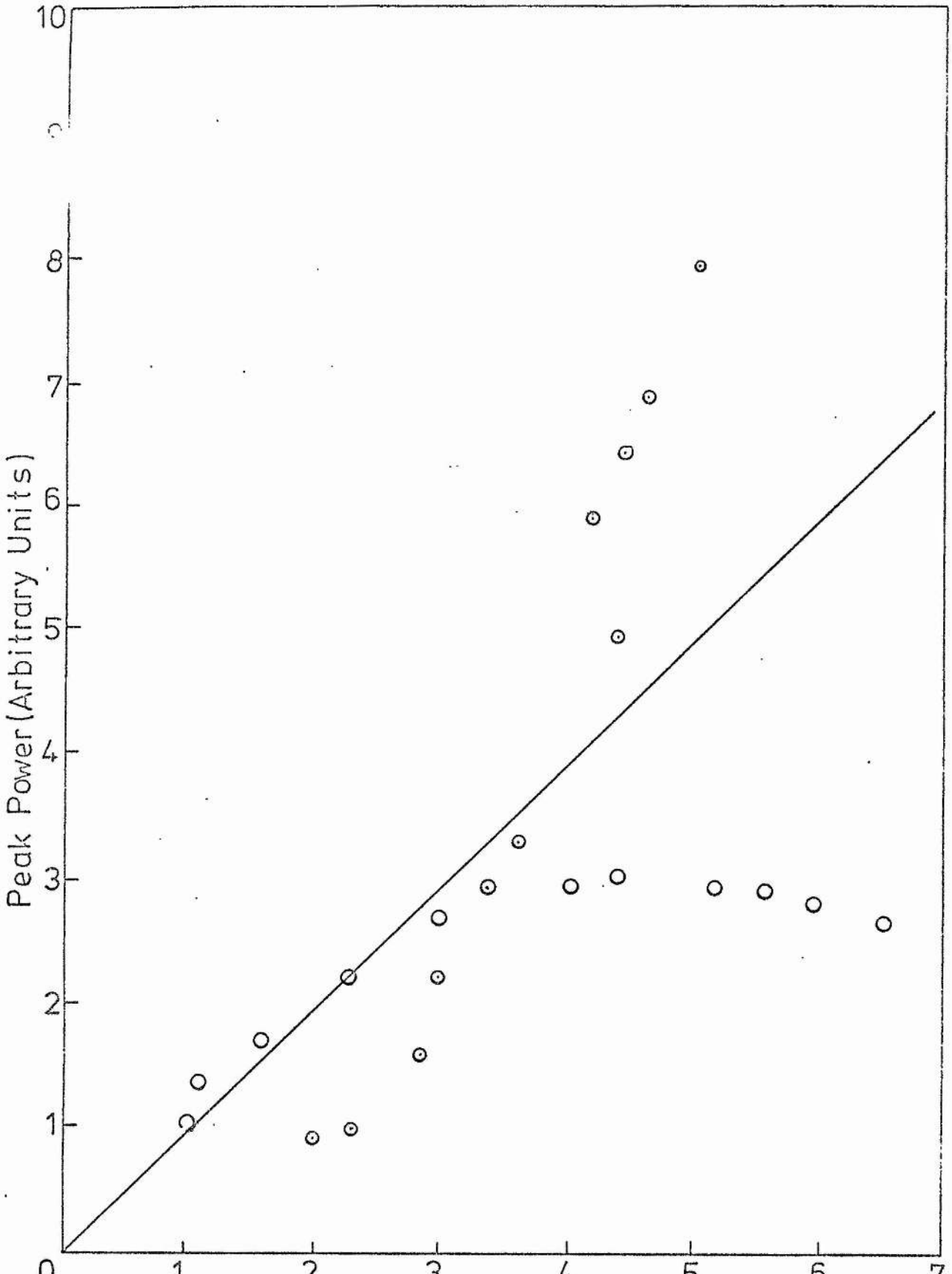

Fig16

Saturation of Transmitted Laser Radiation with Onset of Stimulated Raman Generation

o Transmitted Laser Radiation, ⊙ Stokes Radiation

TABLE 3

LASER INPUT	LASER OUTPUT	LASER ν INPUT	STOKES OUTPUT
ARBITRARY UNITS			
1.1	1.3	2.0	0.9
1.5	1.7	2.3	1.0
1.6	1.7	2.8	1.6
3.0	2.8	3.0	2.3
3.4	3.0	3.4	3.0
3.6	3.0	3.6	3.4
4.0	3.0	4.2	6.2
4.0	3.0	4.4	4.4
5.2	3.0	4.6	7.0
5.9	2.9	5.0	8.0
6.2	2.9	5.2	10.0
6.5	2.8	5.3	11.0

pulse, explained their results on the basis of multiphoton absorption. It was found for CS_2, however, that an intense backward scattered stimulated Brillouin pulse (see 5.11) was generated at a certain power level. Their results of transmitted power, reflected power and input power are shown in Fig 17.

The transmitted pulse reaches a saturation level, then increases slowly with increasing input power whilst the reflected beam increases rapidly. The sum of the input and output powers was shown to add up to 100%. For their experiments a peak reflectivity of 80% was recorded with a 10 cm length cell at powers up to 1 MW. Self-focused filaments were observed in the reflected wave and the generation of the Brillouin pulse was explained on the basis of self-focusing at the exit window of the Raman cell. The intensities of the forward and backward Stokes pulses were found to be only 1% of the total power indicating that the pulse distortion is caused only by the reflected pulse. In a further sophisticated experiment Maier found a very intense backward scattered Stokes pulse in CS_2 with a time duration of 30 μμsec i.e., 1 cm long at the threshold of stimulated Raman. The instantaneous pulse power was found to be twice that of the incident laser power. No pulses of this type were observed in the forward direction. The pulses were explained on the basis of a backward travelling Stokes wave which had access to the stored energy throughout the whole of the medium whilst the absence of forward Stokes pulses was explained on the basis of pulse saturation since the input pulse has the same velocity, and energy can only be extracted from the same

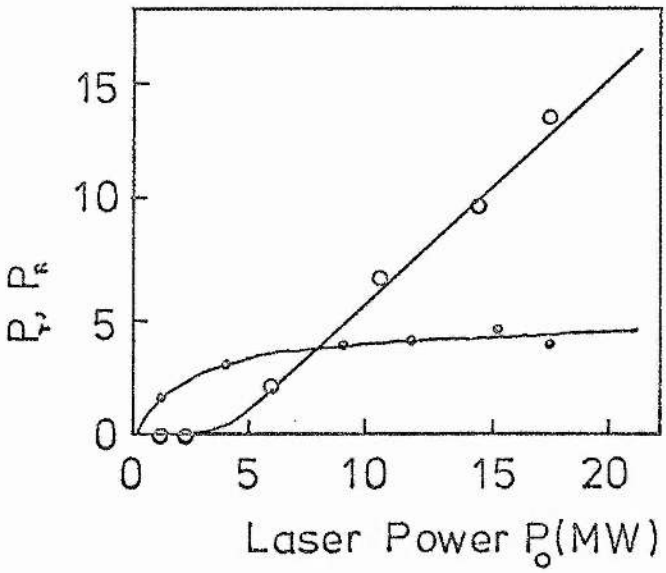

Fig17 Reflected and transmitted laser power in Carbon Disulphide as a function of laser input power

- o Reflected power
- • Transmitted power

volume. The picosecond pulses deplete the pump pulse significantly which defocuses the beam and causes the nanosecond spiking observed by other workers[55].

The results found for benzene are therefore similar to those found for CS_2 in which the beam self-focuses to generate intense backward scattered Brillouin and Raman Stokes pulses which cause a saturation of the transmitted laser pulse. The generation of Brillouin radiation was thought to inhibit further picosecond Stokes pulses. The onset of pulse distortion appears to correspond to the threshold at which self-focusing takes place, so that a measurement of the laser output pulse heights at which this occurs for a range of liquids should be in the inverse ratio of their self-focusing coefficients. A very simple experimental method is therefore obtained to investigate the rate of rise dependence of theshold. From the Table presented in Chapter 3 four liquids were selected, namely benzene, carbon disulphide , nitrobenzene and chlorobenzene.

From the time-resolution results, it appears that the spectrum does develop in a time-dependent way but, because of the comparatively slow streak speeds available, it was not possible to make accurate measurements since the time delays involved are of the order of 10 nanoseconds. It is clearly shown in Fig 16 that the first Stokes line increases linearly with the input pulse height at threshold so that the time delay between Stokes and second Stokes on an iterative basis should be a function of rate of rise of the input pulse.

The liquids chosen have a reasonable range of self-focusing coefficients and stimulated Raman gain coefficients, so that investigation of the dynamics of harmonic generation should provide a means of determining the relative contributions of these parameters to the process.

In order to perform the experiments it was felt that a faster streak unit and oscilloscope were necessary to increase the time resolution and to investigate the correlation between streak photographs and the onset of pulse distortion on the transmitted laser pulse. The experiments performed are discussed in the following Chapter.

B. Spontaneous Raman Spectra

Although spontaneous Raman scattering has been used widely in the study of molecular structures, the results have been limited to a measure of the energy shift because of the limitations of the available exciting sources. With a powerful laser it is now possible to measure not only the shift but also the scattering cross section and line width of a particular transition. The cross section is directly related to the mixed matrix element so that, provided the line width is known, it is possible to determine the stimulated Raman gain coefficients (2.2).

4.10 Raman Scattering Cross Section

The Raman scattering cross section is a constant of proportionality, having the dimensions of area which relates the incident and scattered beams in terms of the scattering of one mode in phase space into another. Experimentally it is measured in terms of energy scattered

per unit band width per unit solid angle so that it can be expressed as

$$\text{cross section} = \frac{\text{power scattered into the } \beta \text{ mode}}{\text{incident power density per } \alpha \text{ mode}}$$

when scattering is from an α mode into a β mode in the direction θ,ϕ. The number of β modes per unit volume per steradian per unit wave number for a given direction of polarisation is given by

$$N = (n^3 \bar{\nu}_\beta^2)/c^2$$

where n is the refractive index of the sample, and if the number of molecules per unit volume is N, then the cross section per molecule is given by

$$d\sigma(N_\beta/N) = d\sigma(\theta,\phi) = \frac{P(\theta,\phi)}{I_o d\Omega N d\bar{\nu}}$$

where I_o is the power density in the α mode, $P(\theta,\phi)$ is the power scattered into $d\Omega$ about (θ,ϕ), and $d\bar{\nu}$ is the spread in wave number. Since the line width of the laser (typically 4-5 GHz for argon) is much less than the Raman line width (typically 90 GHz) I_o can be taken as the total incident power density[32].

An estimate of the stimulated Raman gain coefficient can be made from a measurement of the peak value of $(d\sigma/d\Omega)$ whilst the total differential cross section is obtained by integrating over the Raman line width. The total cross section is obtained by integrating $(d\sigma/d\Omega)$ over all space.

4.11 Proposed Experimental System

The proposed experiment was to measure the peak value of the differential cross section at constant input intensity and with an undisturbed collection geometry. It was not proposed to make absolute

measurements but to compare results relative to some standard liquid. Since benzene had been studied by several workers[33,34,35] and was known to have a relatively high cross section, it was chosen as the reference. Previous investigations on benzene had produced results which were suspect because of either (a) the use of a pulsed light source making power measurements difficult, or (b) the use of narrow band filters to isolate the line under investigation with the problem of the detection of unwanted Raman lines. It was decided therefore to construct a photo-electric Raman spectrometer using a high power continuous wave gas laser and a grating monochromator. To measure the peak value of $(d\sigma/d\Omega)$, it is unnecessary to use slit widths narrower than the width of the lines of interest, because Dalton[36] has shown that the relative values of the peak intensity of the lines obtained with slits very much larger than the line width is directly proportional to the energy in the line.

4.12 Raman Spectrometer for Spontaneous Emission

4.12(a) The Argon Laser

The main experimental difficulty in the construction of the spectrometer was found to be the lack of a commercial high power laser system. The argon laser, with a high power output in the blue-green at 4880Å and 5145Å, was most suitable for this investigation as the sensitivity of most photomultipliers is peaked in this region and the ν^4 proportionality of Raman scattering gave a gain of 2.9 over the alternative He-Ne system operating at 6328Å. It was decided to construct

a high power CW argon laser (shown in Plate 3a). A discussion of the excitation mechanism by which an argon laser operates has been given by Miller et al[37].

4.12(b) Design Criteria

The design of the laser presented problems not previously encountered with the He-Ne laser in that the typical current density required for laser action was 500 amp cm^{-2}. These current densities were obtained by using a capillary discharge and a DC supply producing a discharge current of 10-20 amps at 200 volts. At such high currents the power to be dissipated along the capillary is 4 kilowatts. The capillary was therefore constructed of quartz and was water cooled.

The published graphs of power output/cm as a function of current Fig 18(a) indicated that a 2-3 mm capillary with currents of up to 20 amps should produce a multi-line multimode output of 200 milliwatts[38] under ideal conditions. The optimum pressure in all cases was found to be 0.45 torr. The strong current dependence of the output is shown in Fig 18(b) in which the relationship between power output P and current I is approximately $P \propto I^n$, where n varies between 6 and 2 from just above threshold to the high current region. It was noted that the output was more dependent on current than length so that it was unnecessary to construct a long capillary. Investigation of the power output as a function of an axial magnetic field showed that the power output could be increased by a factor of 5 for a tube of 3 mm bore, Fig 19.

From the above it was decided to construct a laser with a bore of

Argon Laser and Vacuum System

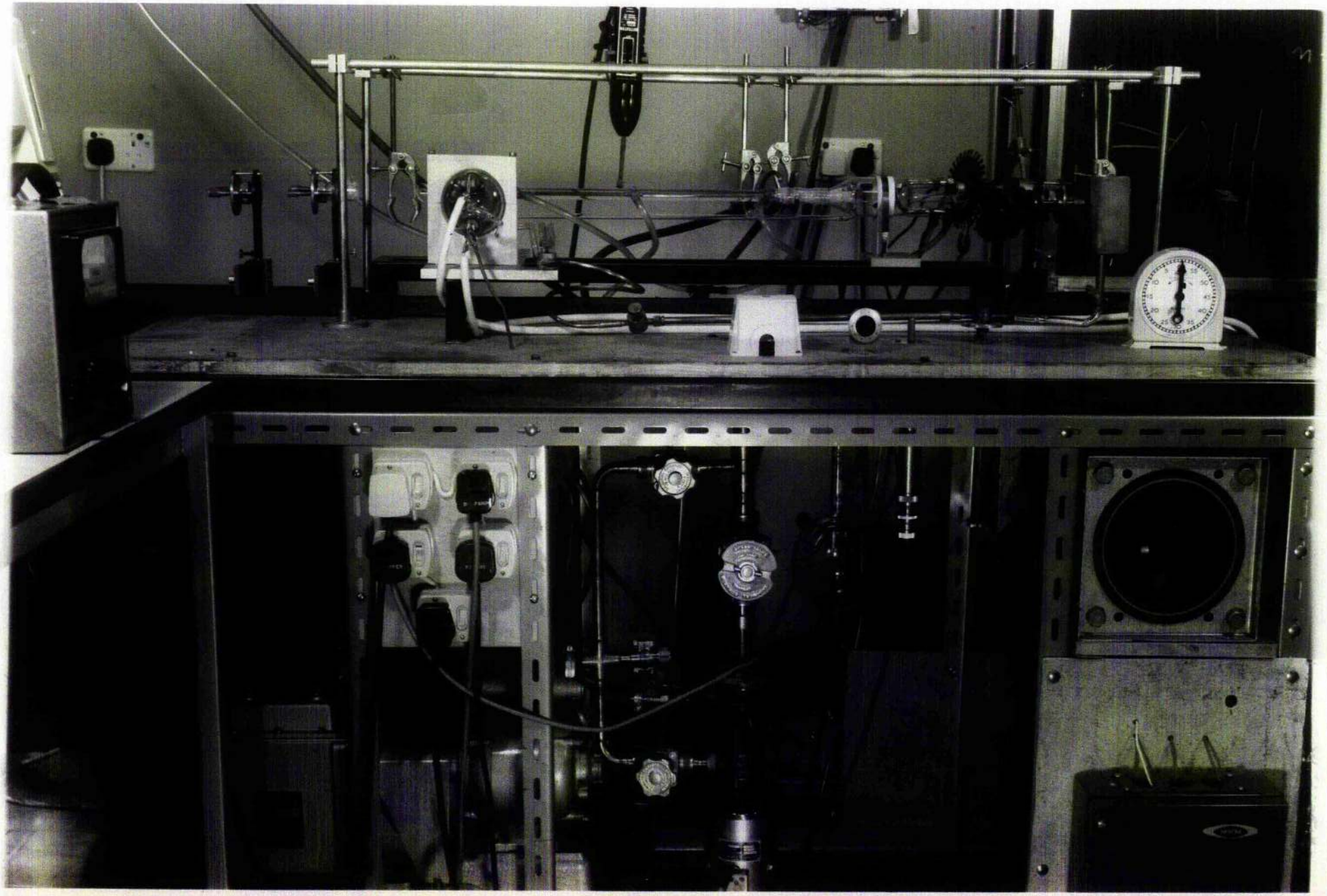

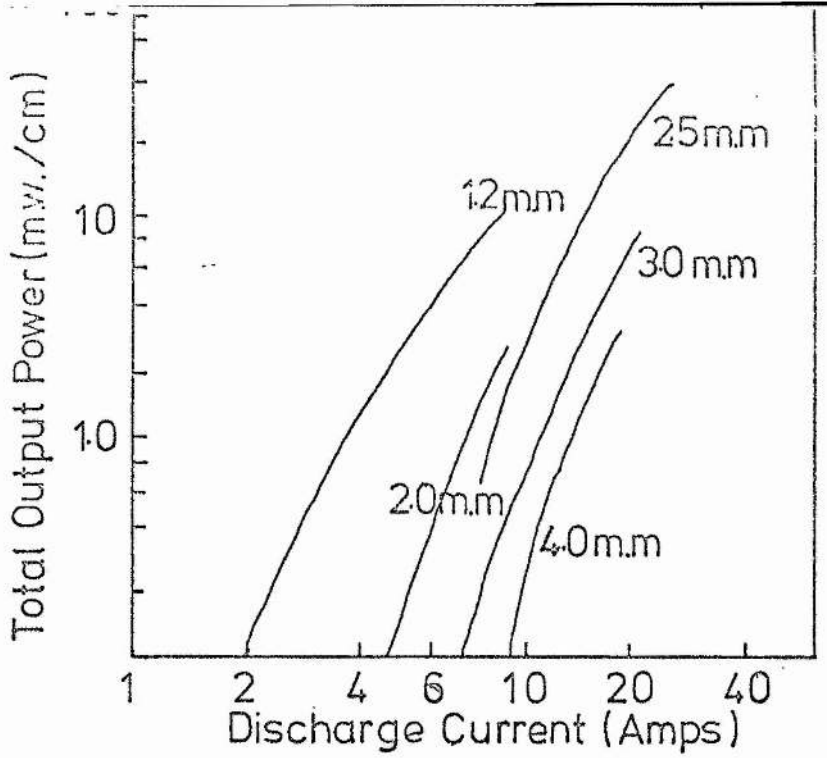

Fig 18(a)

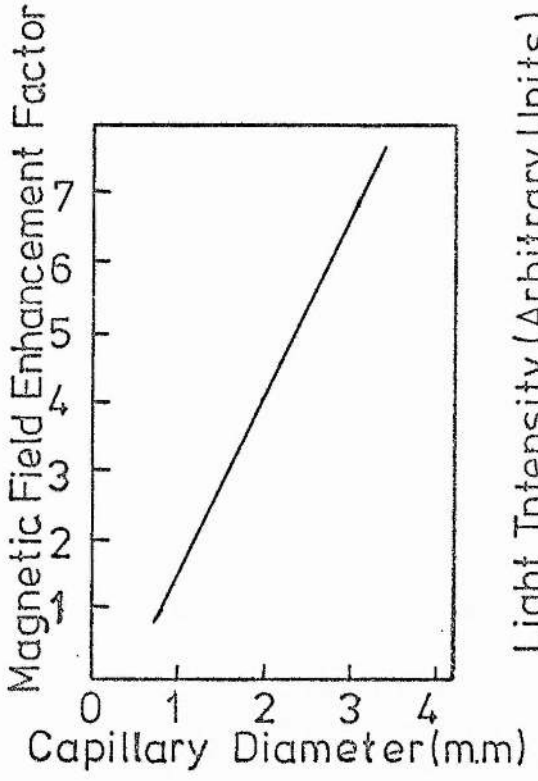

Fig 19

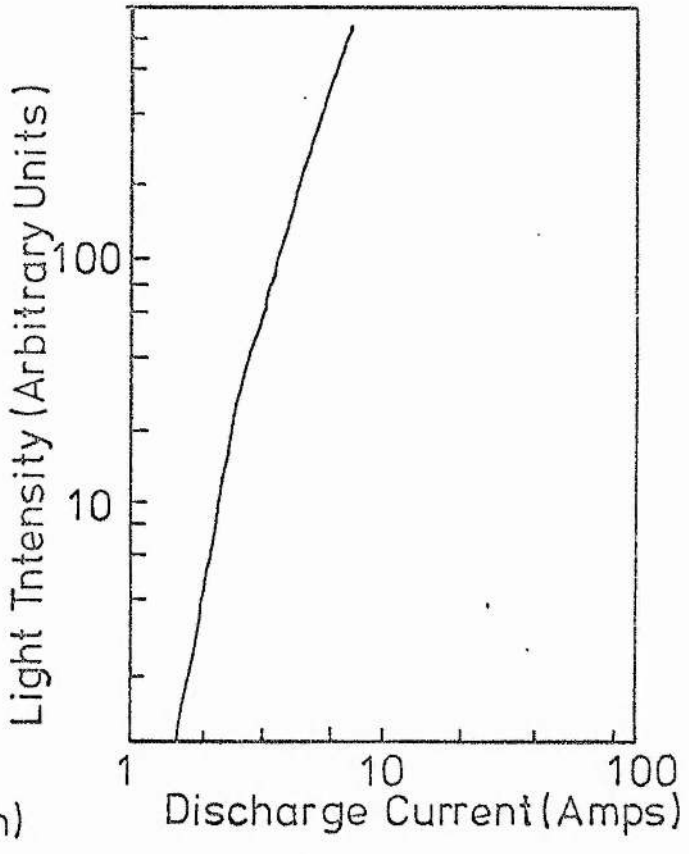

Fig 18(b)

Fig 18(a,b) Output Power of Argon lasers as a function of discharge current for a range of capillary diameters

Fig 19 Magnetic field enhancement factor as a function of capillary diameter

3 mm and a power supply delivering up to 20 amps DC. The tube was designed so that a magnetic field could be used if the higher powers became necessary. To avoid the problem of limited life due to "clean-up" it was decided not to seal the tube after filling but to have it permanently attached to a vacuum system so that the pressure could be adjusted when necessary.

4.12(c) Tube Design

After consultation with S.E.R.L. (Baldock) and the available literature, the tube design shown in Fig 20 was evolved. The tube had several notable features which improved the overall performance.

1. To prevent the fracture of graded seals, found by other workers quartz was used not only for the active section but also the inserts used to protect the seals from the hot discharge.

2. Great difficulty was experienced in obtaining a cathode to provide the required current. Eventually a Mullard cathode was used with an expectation of 10 amp maximum. However it was found to be capable of maintaining discharge currents up to 40 amps and had the added advantage that it could be reprocessed after contamination.

3. The anode was a water-cooled copper spiral.

4. The cataphoresis spiral (4.12(d)) was wound round the cathode so that a magnetic field could readily be incorporated.

5. The tube was sealed with a diaphragm valve so that it would be isolated from the vacuum system.

6. The windows were quartz flats sealed to the tube ends with araldite.

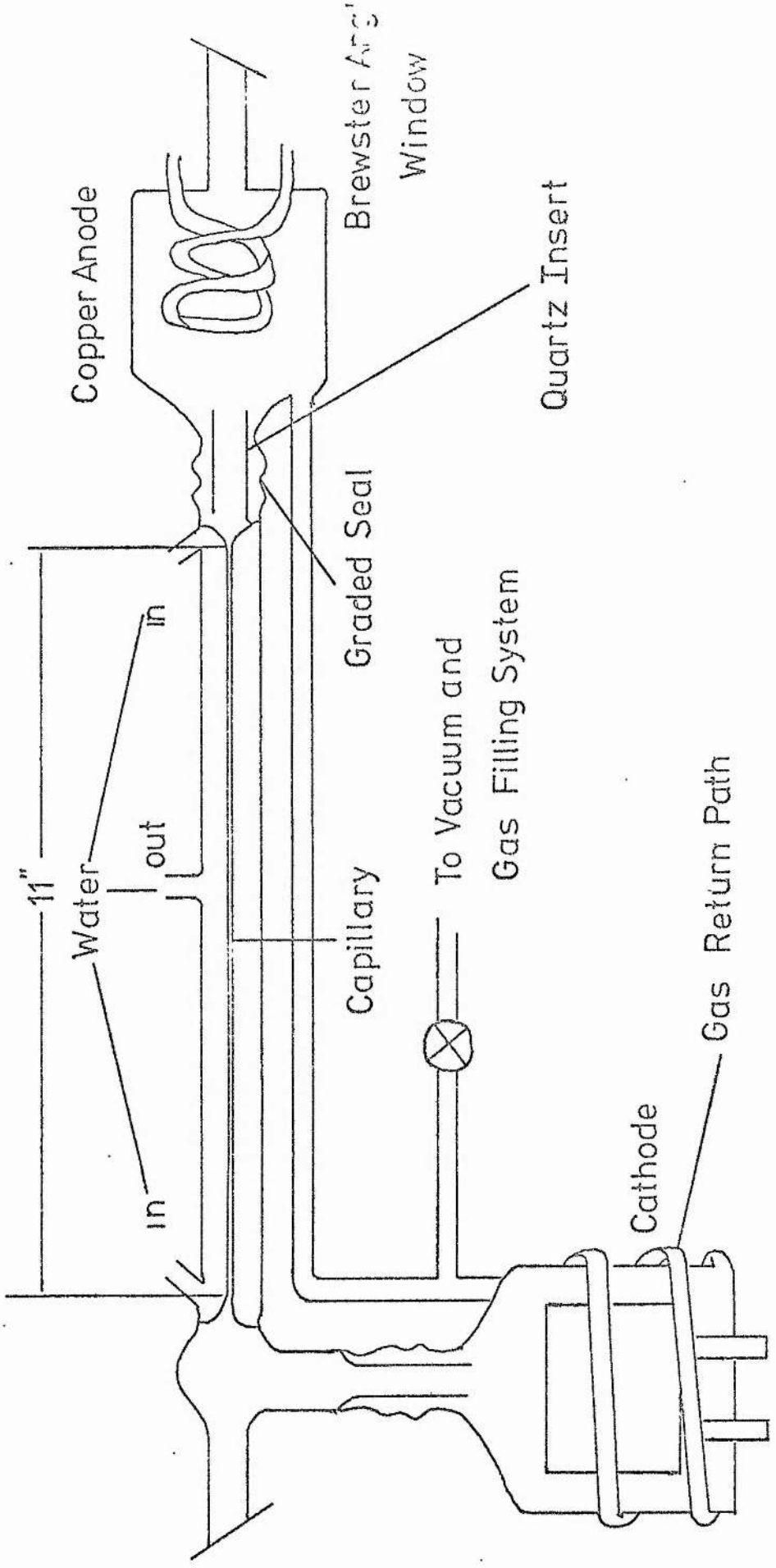

Fig 20 Schematic of Discharge Tube

4.12(d) Gas Return Path

The passage of a large direct current through an ionic discharge leads to the development of a pressure gradient along the tube[39]. At low currents gas is pumped from the anode to cathode whilst at high currents the process is reversed. Because of the high currents used a high pressure develops at the anode of the laser which prevents the laser from oscillating. This difficulty is overcome by a gas return bath between anode and cathode to maintain pressure equilibrium. The tube is constructed in a spiral so that the overall length is very much greater than the discharge length and there is no danger of the discharge taking the wrong path. In the tube used the discharge length was 0.2 of the spiral length.

4.12(e) Power Supply

The power supply had to be capable of producing 20 amps at a voltage high enough to initiate the discharge. A 3-phase full wave bridge rectifier met these requirements. The bridge delivered 60 amps at 600 volts with a 7% ripply at 300 Hz. As shown in the analysis below this ripple can produce a large variation of output due to the high current dependence of argon lasers. Let the mean current be I_o, and let there be a fluctuating component, ΔI. We then have

$$P \propto (I_o + \Delta I)^n ,$$

$$P \propto I_o^n \{1 + n(\Delta I/I_o)\} ,$$

for $\Delta I/I_o << 1$.

The fractional fluctuation in the output power can therefore be expressed

in terms of the current fluctuation, thus we have

$$\Delta P/P_o = (n\Delta I)/I_o \ .$$

A typical current-voltage characteristic for the tube is shown in Fig 21. At certain pressures, the discharge can have a negative characteristic so the current must be limited by a series resistor. If the supply voltage, V_o contains a ripple component, V_R then for a discharge voltage V_D (does not change much with current) the current through the tube is given by

$$I = (V_o + V_R - V_D)/R$$

where R is the limiting resistance. This may be written in the form

$$I = I_o + \Delta I = (V_o - V_D)/R + V_R/R \ .$$

The fractional fluctuation of the output power is therefore given by

$$\Delta P/P_o = nV_R/(V_o - V_D) \ .$$

Since V_D is typically 0.5 V_o the expression can be simplified further to give $\Delta P/P_o = 2n(V_R/V_o)$,

which shows that a ripple of 7% could lead to an output modulation of 80% at threshold where n = 6. The supply ripple was therefore reduced to a value of $\sim$0.5% using the L-C circuit shown in Fig 22.so that under high current conditions (14 amp) where n = 2 the ripple was less than 2%.

4.12(f) Vacuum and Gas Filling System

The requirements of the vacuum system were that a good ultimate vacuum be obtained so that the tube could be processed and filled with argon to 0.45 torr. A schematic of the system evolved is shown in Fig 23.

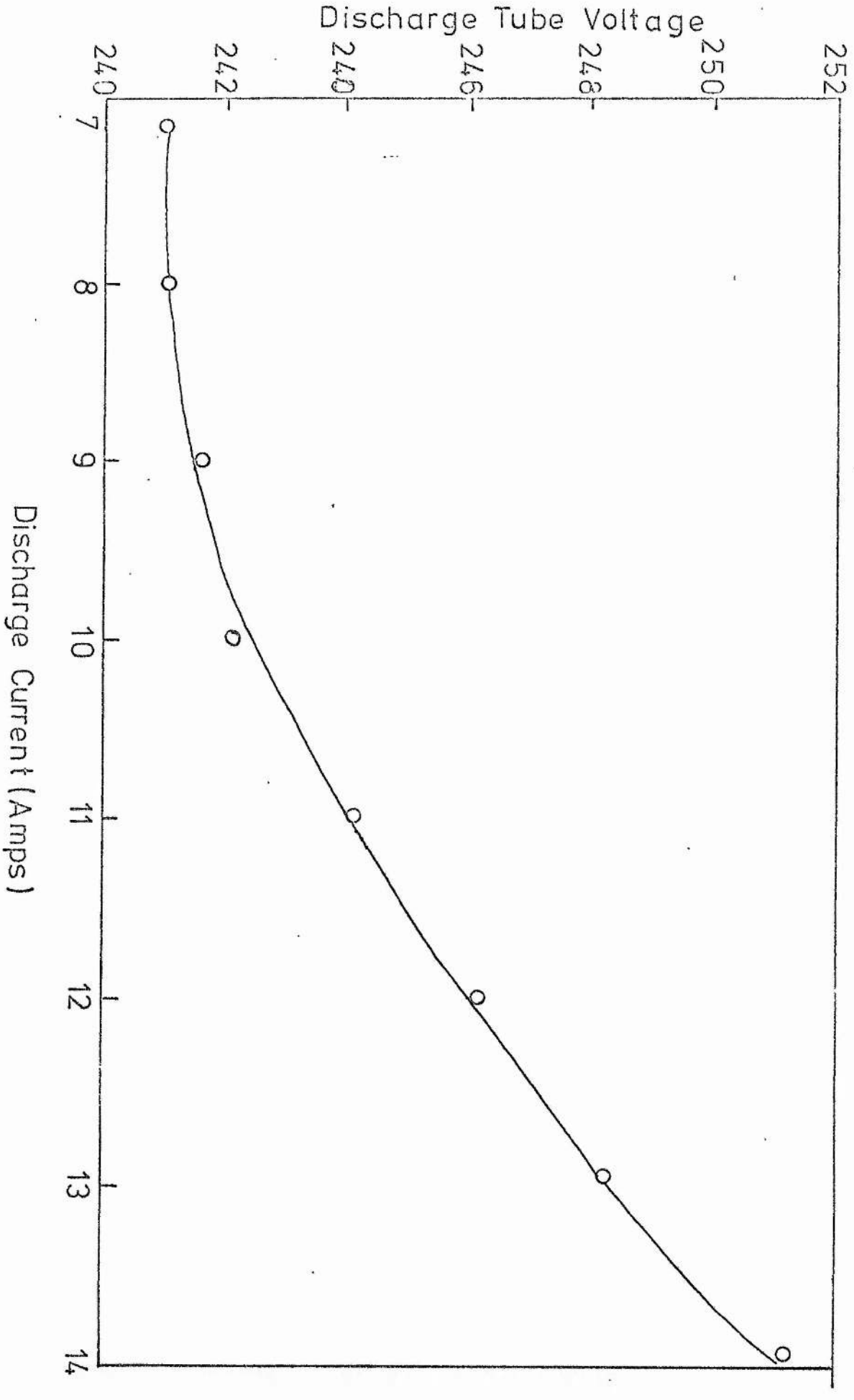

Fig 21 I-V Characteristic of Argon Discharge Tube

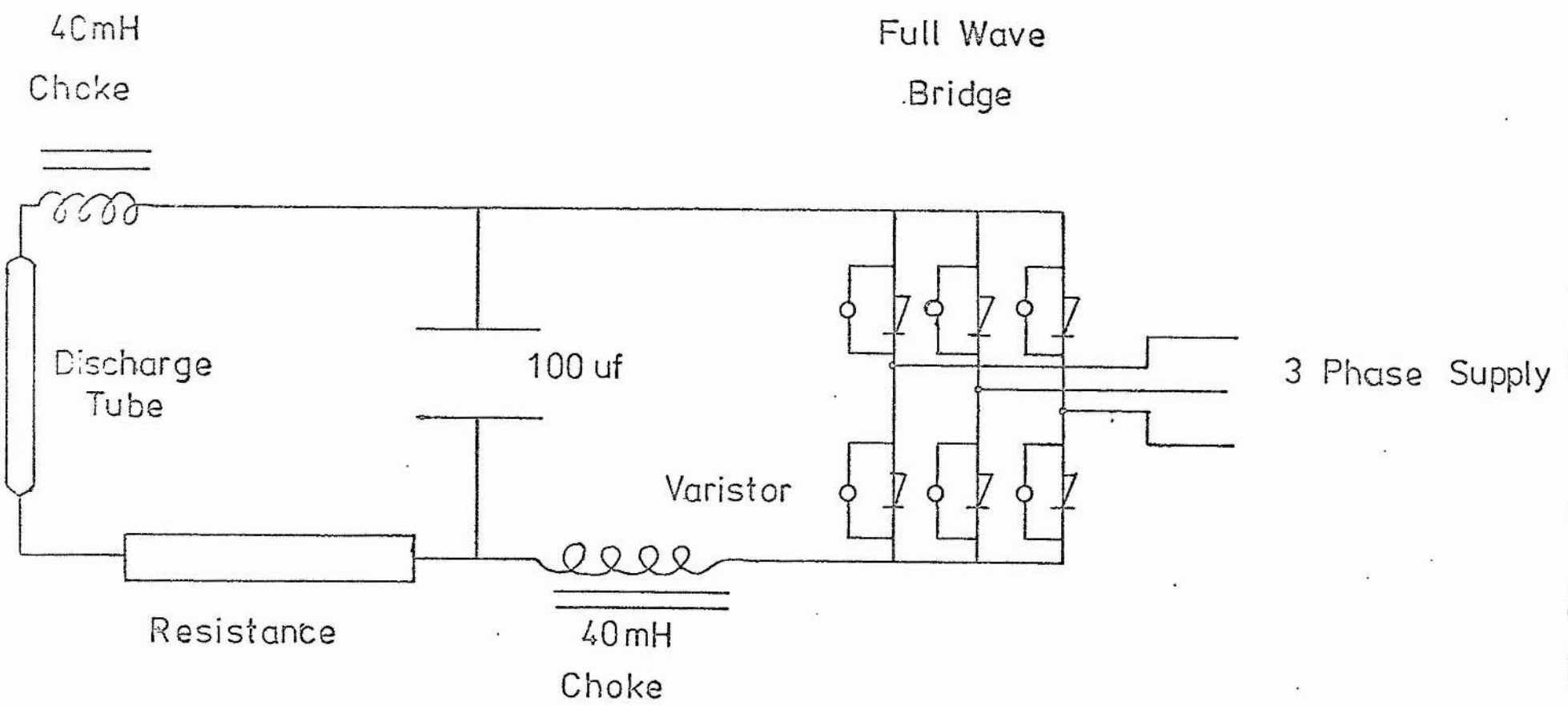

Fig 22 Power Supply

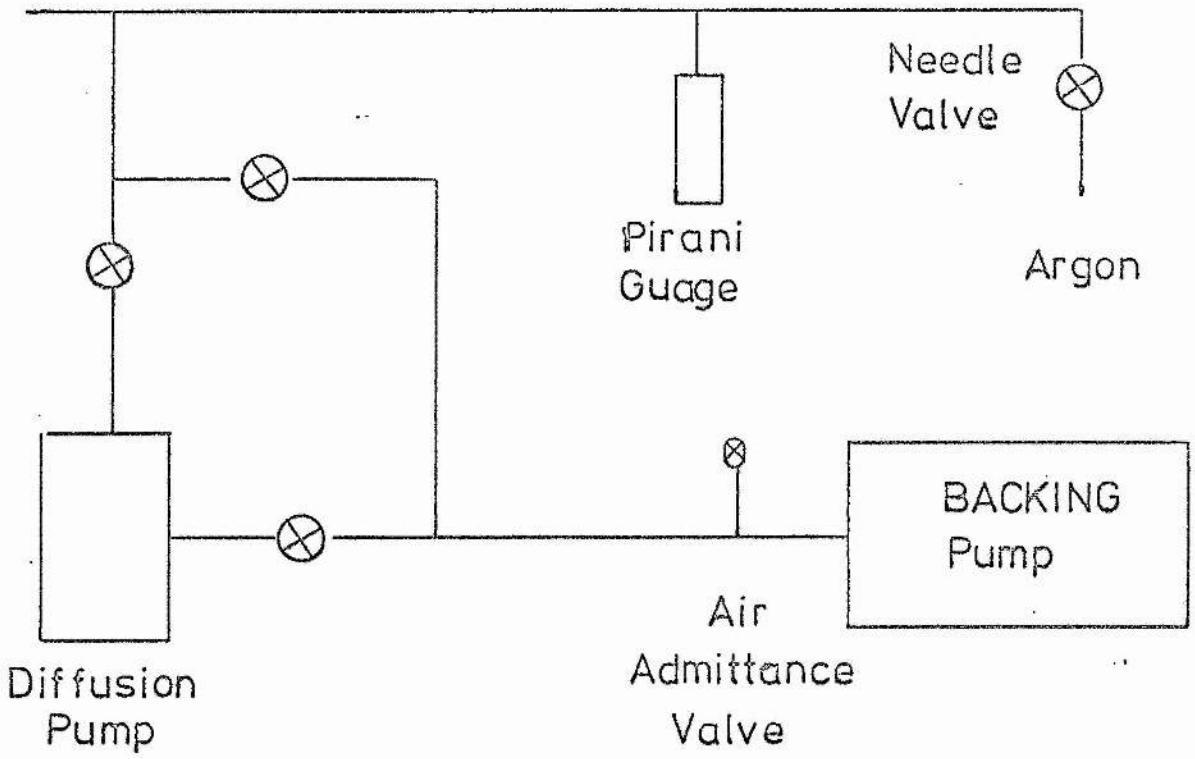

Fig 23 Vacuum and Gas Filling System

4.12(g) Laser Cavity

The laser tube was contained in a simple confocal cavity using dielectric mirrors of 1.5 metres radius of curvature and reflectivities of 100% and 97% respectively. The mounts were clamped to the girder shown in Plate 3a. With the inclusion of an intra-cavity Brewster angle prism[40], 60 milliwatts single line operation at 4880Å was produced.

4.13 Detection and Recording of Raman Spectra

The complete system is shown in the schematic of Fig 24.

A Princeton Applied Research system consisting of a low noise pre-amplifier matched into a phase sensitive lock-in amplifier was purchased for signal detection. The overall gain was 10^8 and the bandwidth could be reduced to 0.012 Hz.

The problem with the photo-detection of Raman scattered light is that the weak signal must be extracted from the noise background generated by the laser and the photomultiplier. Phase sensitive detectors[41] are devices which operate with an extremely low noise bandwidth and whose function is to selectively amplify a narrow frequency band from the spectrum at the signal channel. This frequency band is selected by a reference frequency and the resulting signal is cosine of the phase angle between the reference and signal channels. In the present case the reference frequency was generated by chopping the laser beam inside the cavity with a chopper driven by a synchronous motor and converting this into a voltage by means of a simple photo-transistor circuit so that the signal and the reference channels have

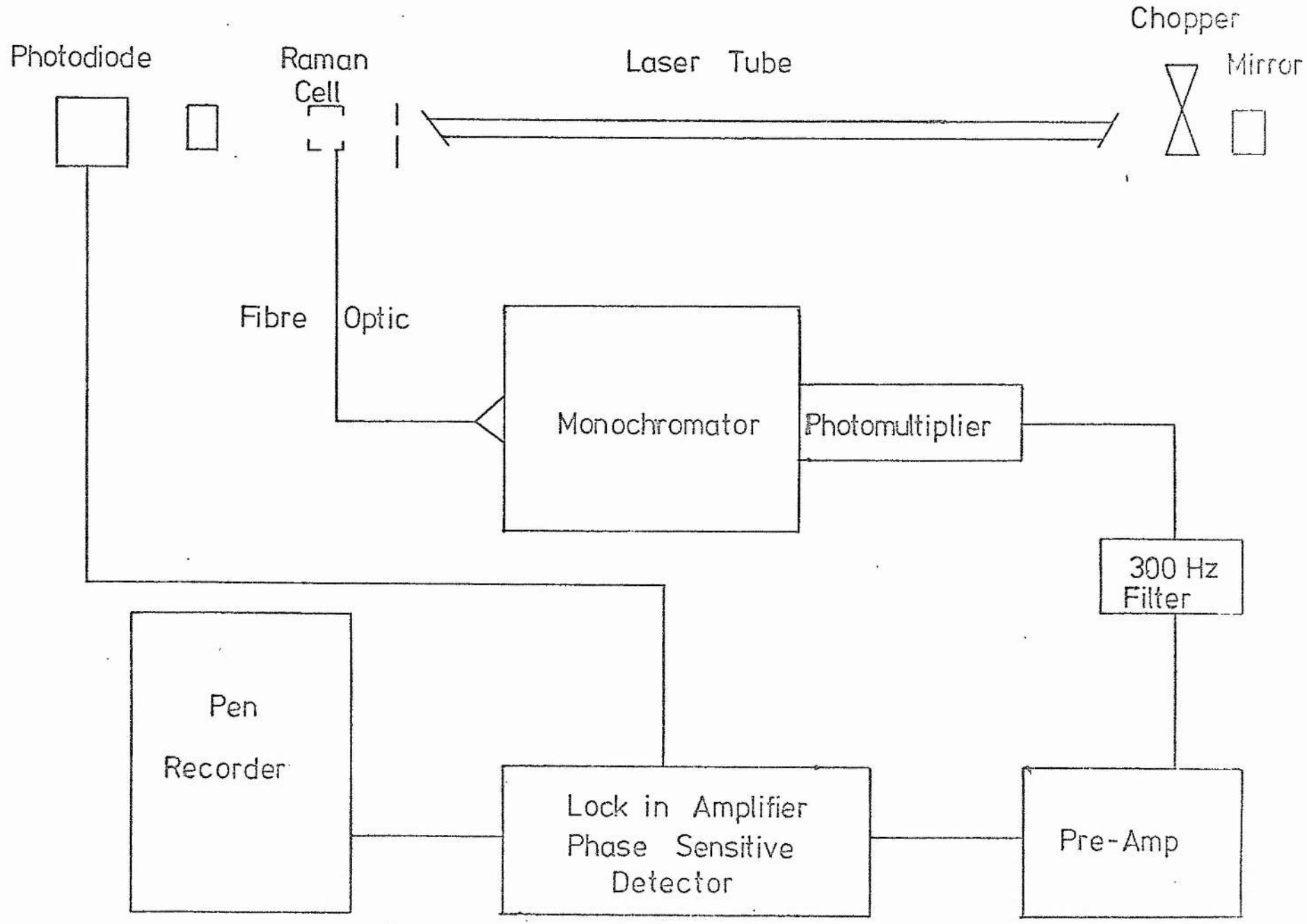

Fig 24 Schematic of Raman Spectrometer

the same frequency but differ in phase. The signal from the photo-multiplier, E.M.I. 9558B is then phase-locked by means of a phase shifter.

4.14 Monochromator and Pen-Recorder System

The Zeiss (Jena) monochromator/pen-recorder system has the following significant features. The dispersive element is a 650 line/mm reflection diffraction grating blazed at 5700Å with an area of 60 x 70 mm. Since the focal length of the collimating entrance slit mirror is 400 mm the instrument aperture is f/6. The bandwidth occupied by the slit dictates the ultimate resolution and so is of great importance in measuring line widths. The bandwidth for a 0.1 mm slit is 1.6 cm^{-1}; since the slit width is variable from 0 to 1.5 mm with a lowest registration mark of 0.05 mm the maximum resolving power attainable is about 0.8 cm^{-1}. The reported[42] line width for the Benzene 992 cm^{-1} line was 3 cm^{-1} so that line widths were measurable but with a correction for the slit function.

The instrument has a projected scale which is linear in wavelength and is scanned by rotating the grating with the pen-recorder drive. By a system of cog wheels the chart speed and drive speed can be independently varied enabling the rate of scan to be matched to the integration time constant of the detection system.

4.15 Scattering Geometries

The two broad classifications of scattering geometry are the intra-cavity and extra-cavity systems. Examples of both methods were assessed.

4.15(a) Intra-Cavity System

The ratio of the power inside the laser cavity to the power outside the laser cavity is given by $P_i/P_o = (1-R)^{-1}$ where P_i and P_o are the power inside and outside respectively with R being the mirror reflectivity, so that an intra-cavity system has obvious advantages. With mirrors of reflectivity $R \sim 1$, the radiation density in the intra-cavity cell could be high provided the insertion losses were minimised.

Insertion loss is a function of the optical quality of the cell and the alignment. The cell holder used is shown in Fig 25(a) and permits alignment in the same way as the cavity mirrors are aligned and with the same accuracy. The cells were quartz of optical quality (U.V. absorption cells). It was found that with the cell normal to the direction of propagation that the output power was low but if the cell was slowly rotated about a vertical axis the system went through a series of maxima and minima. The behaviour at the normal position was thought due to the fact that the system was effectively a multiple cavity and that destructive interference was taking place. The oscillatory behaviour as the cell was rotated was explained on the basis of a cavity resonance satisfying the equation.

$$2nd \cos\theta = m\lambda_R$$

where λ_R is the wavelength of a cavity resonance; n is the refractive index of the cell; m is an integer; d the cell thickness and θ the angle of orientation of the cell with respect to the normal position. Under this resonance condition and with mirrors of reflectivity

100% (nominal), the insertion losses were minimal.

The cell was aligned to give the maximum Raman scattering intensity by monitoring a strong Raman line in the liquid under study. Light was collected and presented to the monochromator by a round-to-slit fibre optic cable. The alignment between the entrance slit of the monochromator and the slit fibre optic was achieved using the system shown in Fig 25(b); with this system spectra were readily attained, Figs 26, 27, 28.

On operating at higher resolutions with narrow slits it was found that the fibre optic system gave results significantly different from those in the published literature[42]. In order to solve this problem an extra-cavity system was set up.

4.15(b) Extra-Cavity System

Apart from the possible disadvantage of a lower radiation density, the extra-cavity method has the advantages of easy alignment and a relaxation of the laser stability requirement. The apparatus for this study is shown in Fig 29. The unit permits the variation of polarisation direction by means of a half-wave plate so that polar plots may be obtained, Figs 30, 31. These polar plots clearly show the classical dipole radiation pattern of the form $A \sin^2\theta + B$ where $B/(A+B)$ is the depolarisation ratio. The measured values of the depolarisation ratios for the benzene and notrobenzene lines investigated are 0.027, 0.1, respectively. The values obtained by Skinner et al[44] for these liquids are 0.02 and 0.15. The power density

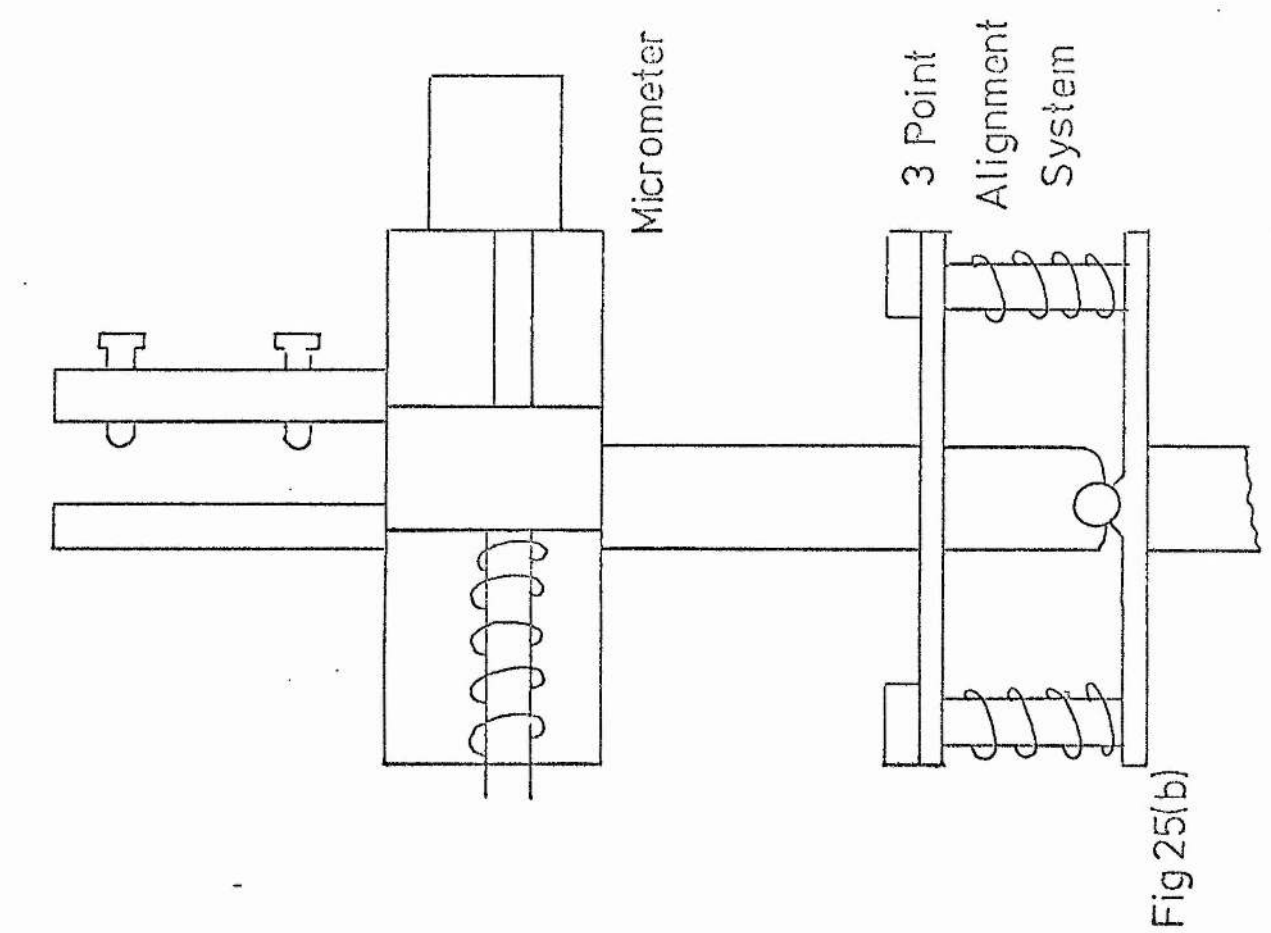

Fig 25(b)

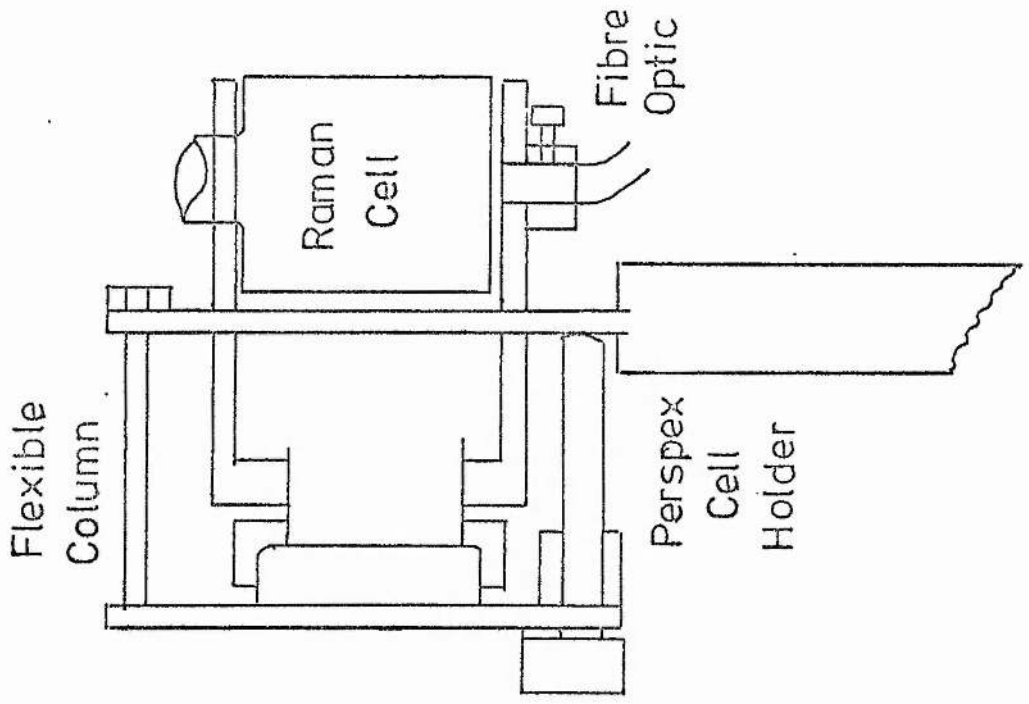

Fig 25(a)

Fig 25(a) The Raman Cell Mount

(b) The Slit Fibre Optic Mount

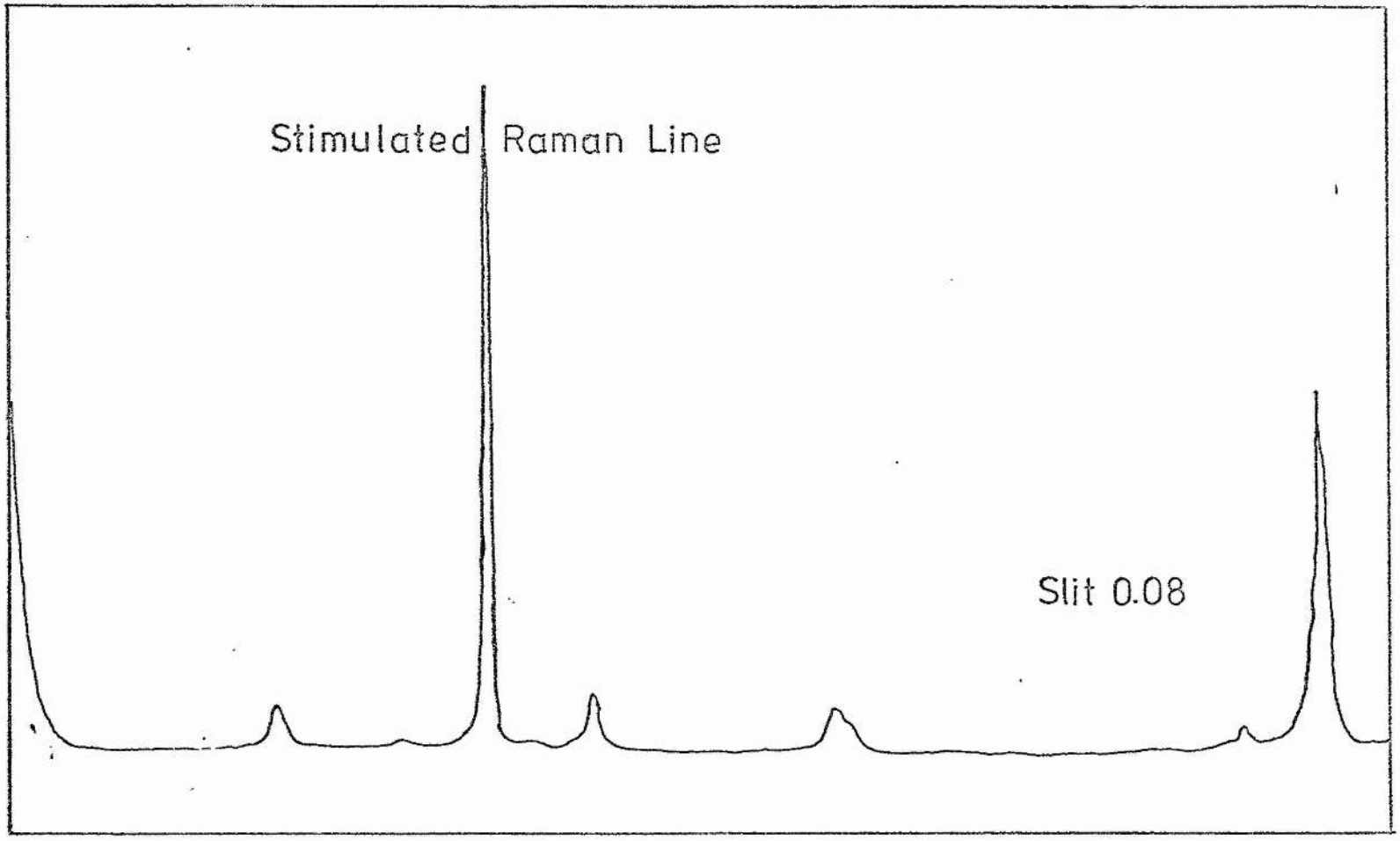

Fig 26 The Spontaneous Raman Spectrum of Benzene

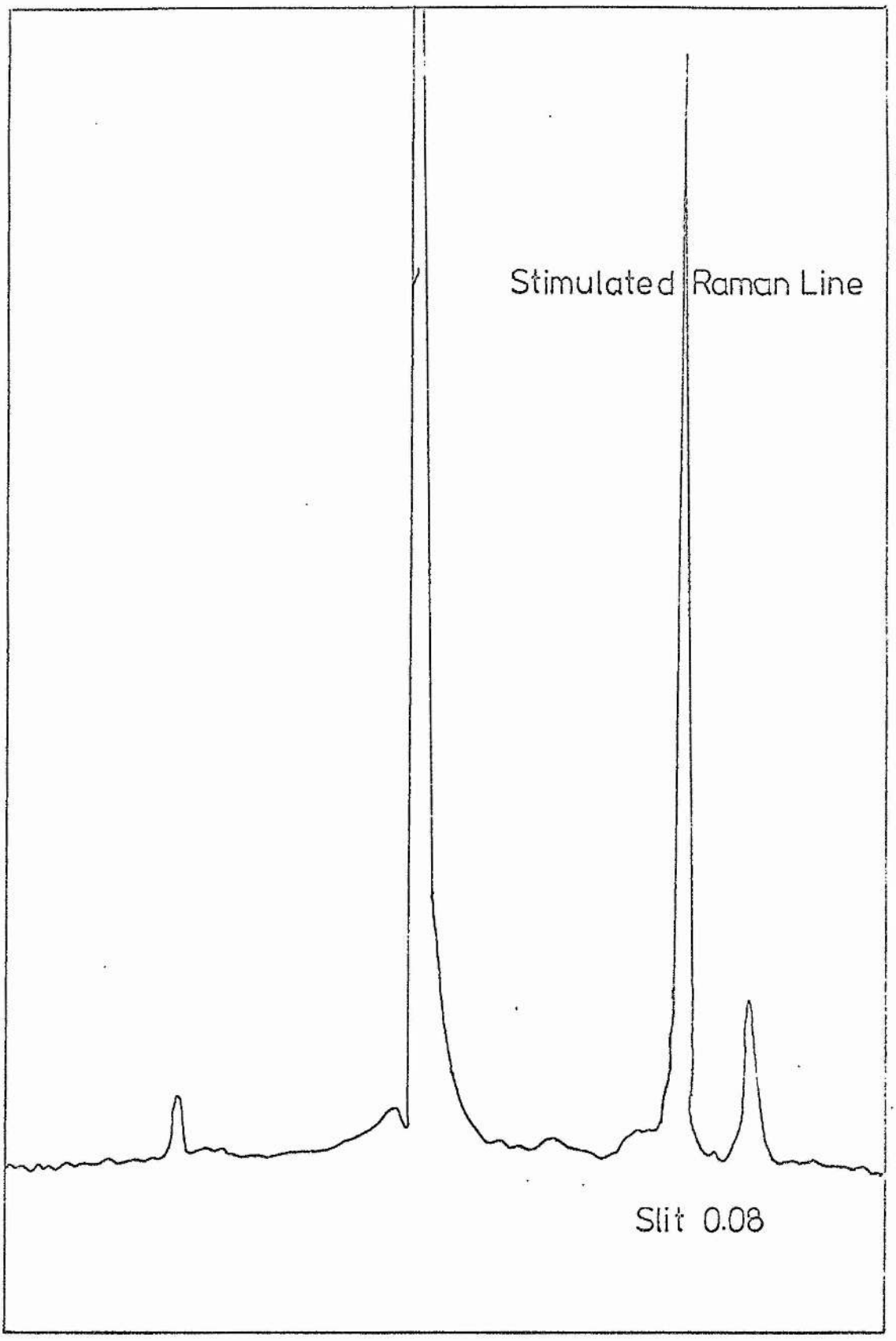

Fig 27 The Spontaneous Raman Spectrum of Carbon Disulphide

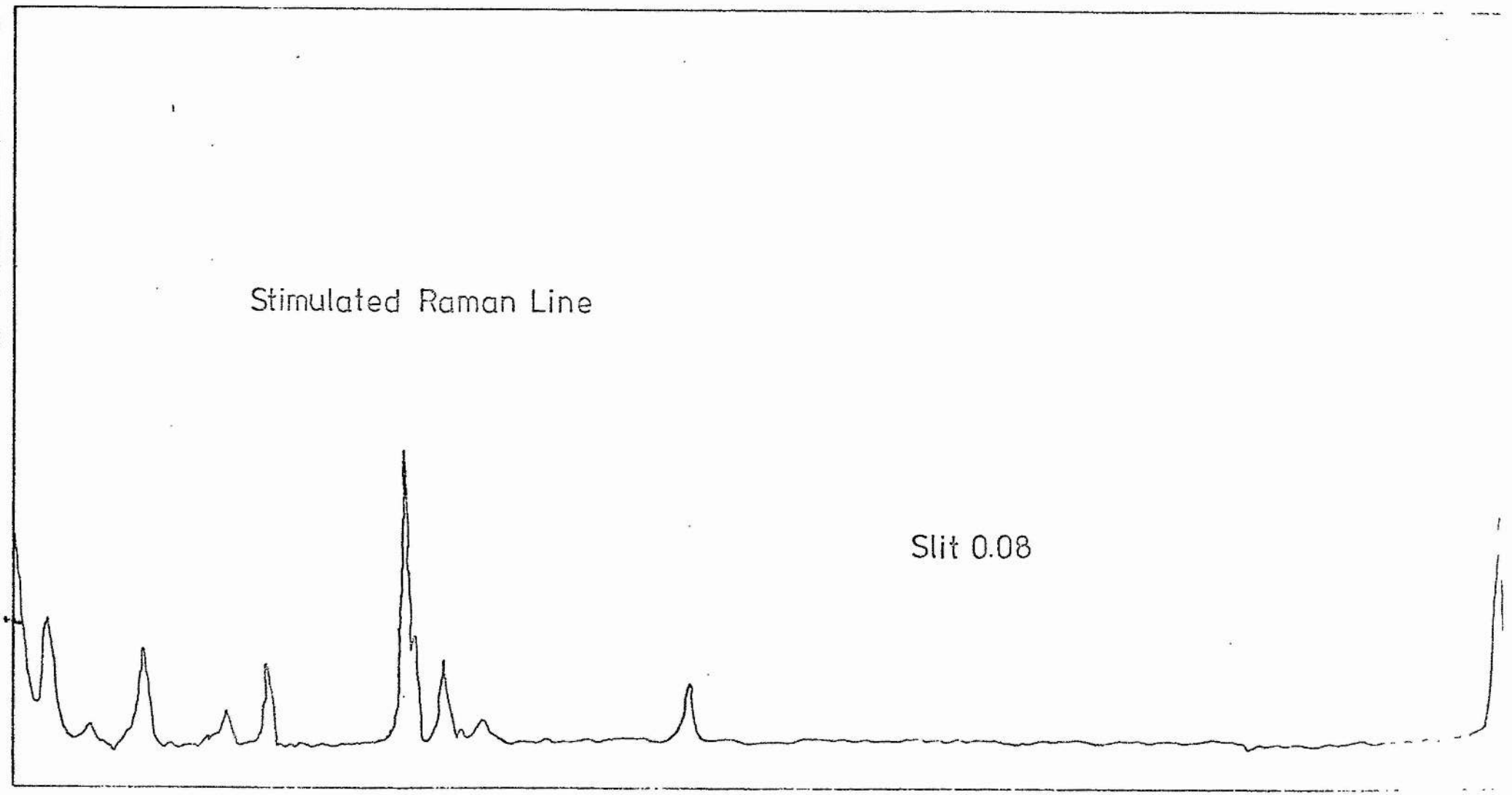

Fig 28 The Spontaneous Raman Spectrum of Chlorobenzene

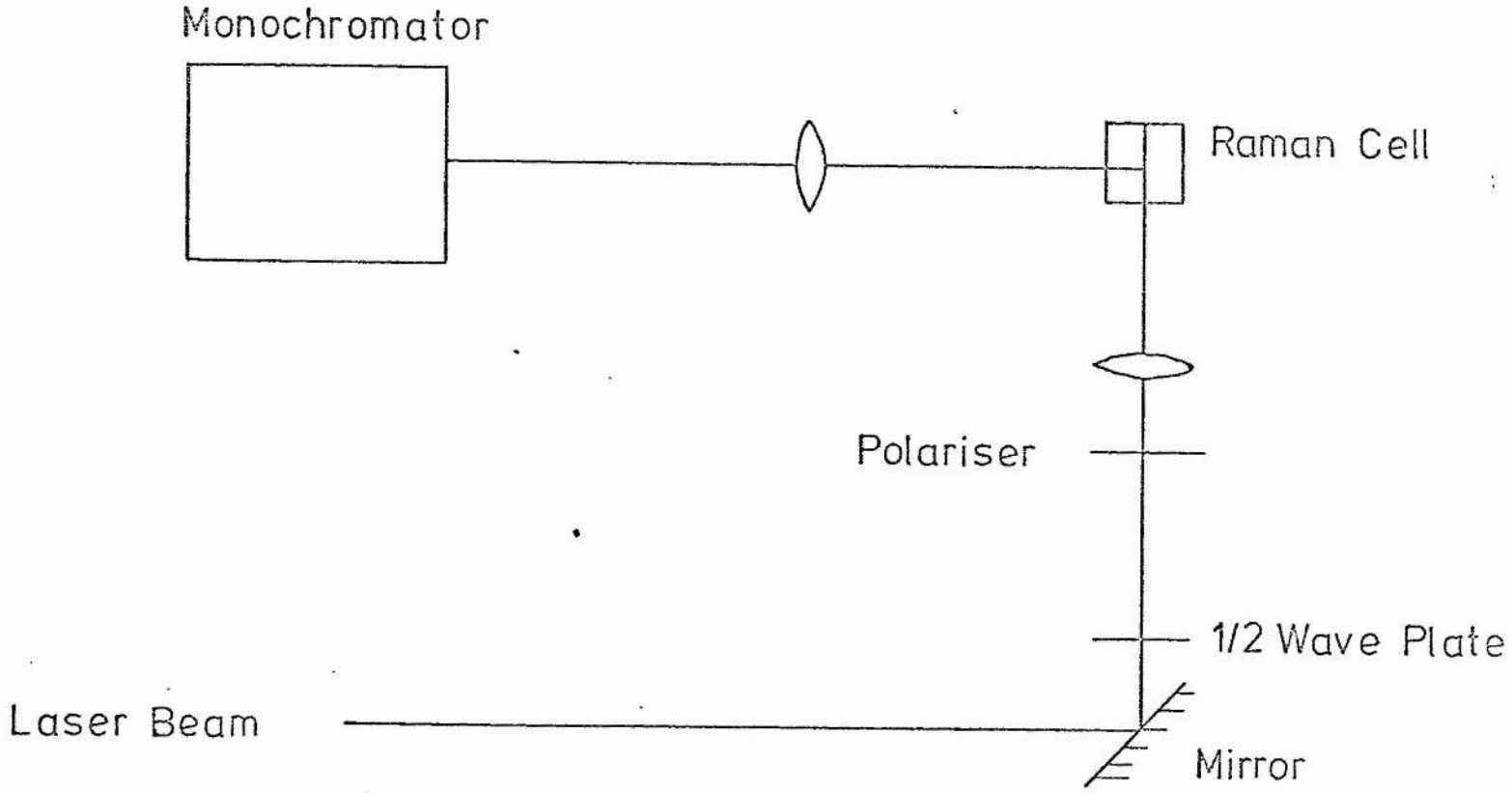

Fig29 The Extra-Cavity Raman System

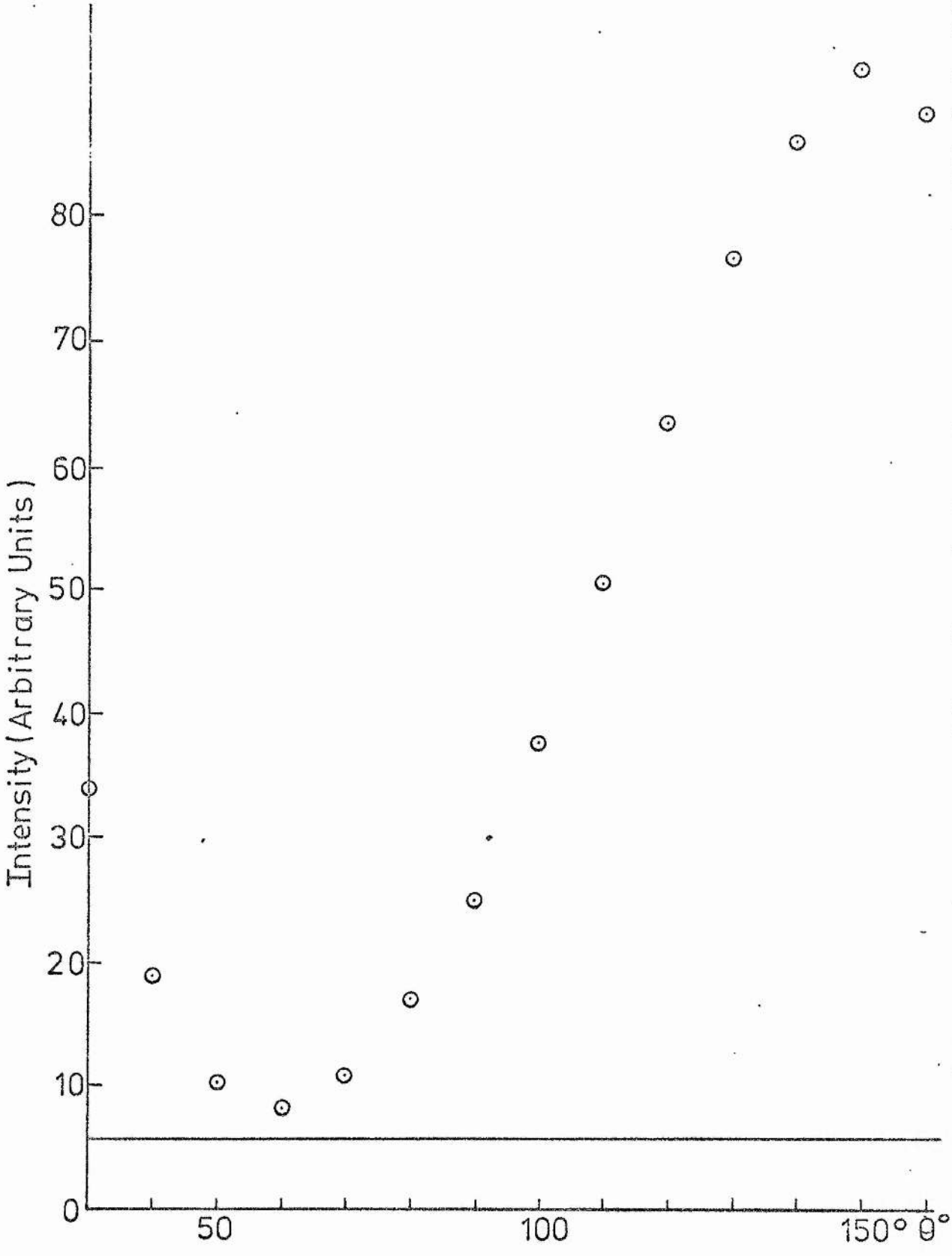

Fig 30 Polar Plot of 992 cm Raman Line in Benzene where θ is the angle of rotation of the Polariser

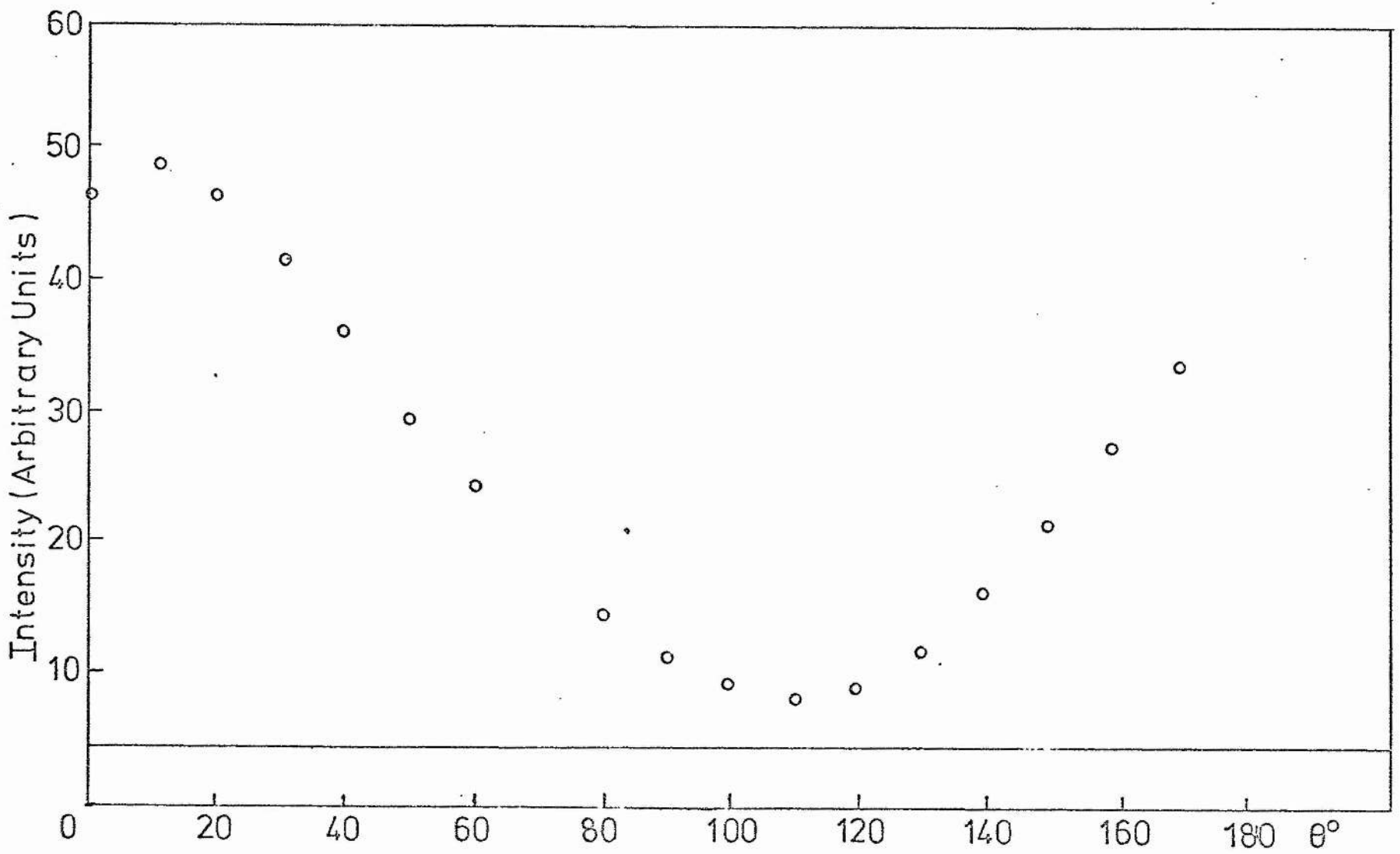

Fig 31 Polar Plot of 1345cm^{-1} Raman Line in Nitrobenzene where θ is the angle of rotation of Polariser

is increased by focusing the laser beam. At the focus, the diffraction limited cylinder has dimensions given by[43]

$$\ell = 3(\lambda/D)^2 f, \quad d = \lambda(f/D),$$

where D is the diameter of the laser beam and f is the focal length of the lens. The diffraction limited focus is imaged at the entrance slit of the monochromator so that the scattered light just fills the grating.

The line width of the nitrobenzene vibration at 1340 cm^{-1} was measured to be 6.6 cm^{-1}. At the smallest slit width available, the line width of the benzene 992 cm^{-1} line was found to be 2.7 cm^{-1}, Fig 32. Since this value is only three times the slit width, a correction should be made from a knowledge of the predicted line shape and the instrumental function. However this correction was not made.

4.16 Assessment

At this point the normal Raman investigation was terminated after the results described above had been obtained. It was realised that the commitment of running two separate systems was too heavy, and that as a study of spontaneous Raman spectra was not the main purpose of the investigation, all future work would be concentrated on the stimulated Raman system. Summarizing the objectives realised, we have

(a) The Raman laser spectrometer was successfully constructed and spectra obtained.

(b) Polar plots using the extra-cavity system were produced showing that the relative values of the peak differential scattering

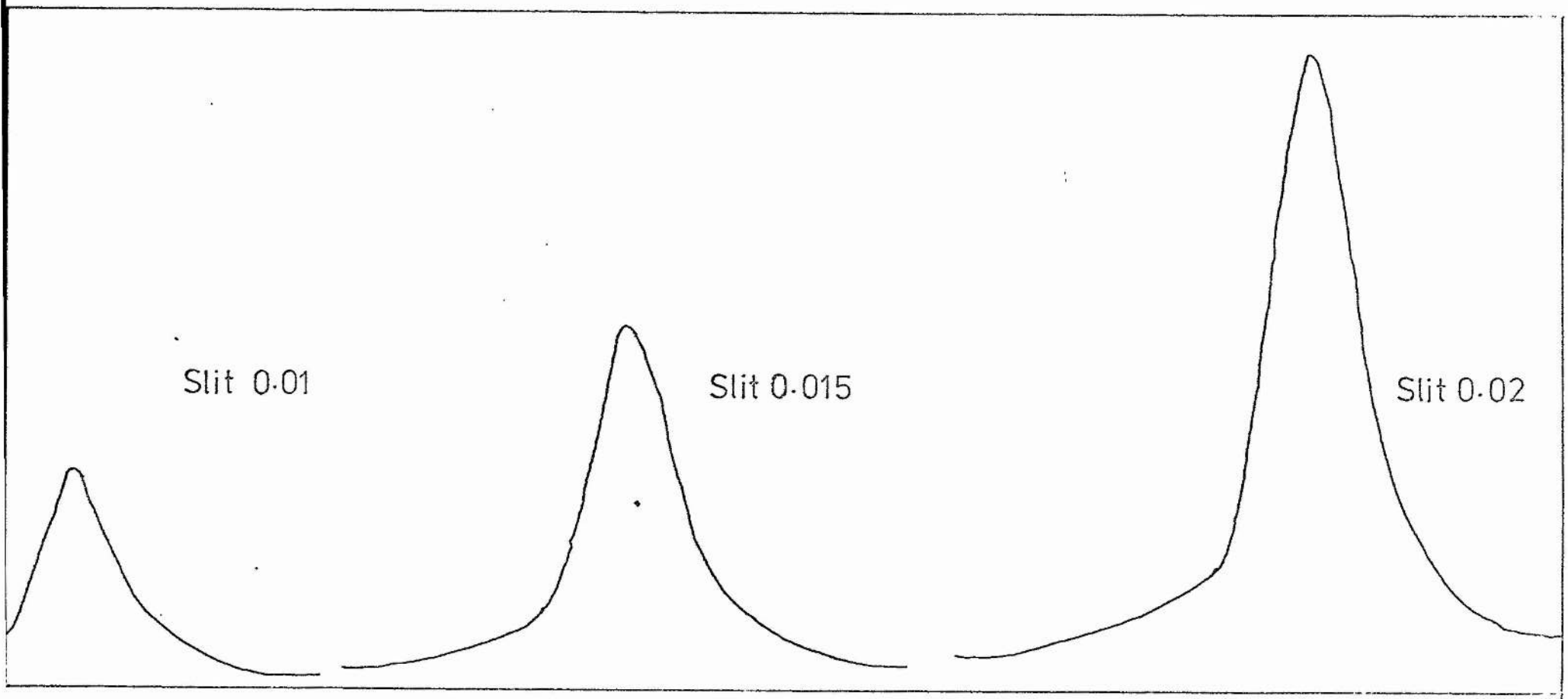

Fig 32 Line width of the 992cm^{-1} shift Raman line in Benzene as a function of slit width

cross section could be calculated after the wavelength sensitivity of the system had been determined.

(c) Preliminary measurements of line width indicated that the system was limited in resolution due to the relative sizes of slit width and line width.

In conclusion, for future work undertaken to measure relative cross sections, a standard source with a known spectral distribution should be used to calibrate the total system with respect to distribution of sensitivity with wavelength since both the grating and the photo-multiplier responses (S20 photo cathode) are strongly wavelength dependent. A grating of greater dispersion should be purchased. Alternatively a scanning Fabry-Perot interferometer would have the required resolution. With these improvements it should be possible to complete the aims of this part of the investigation.

CHAPTER 5

CORRELATION OF TIME RESOLUTION EFFECTS IN STIMULATED RAMAN WITH PULSE DISTORTION OF TRANSMITTED LASER PULSE AND RATE OF RISE OF EXCITING PULSE

5.1 Introduction

On the basis of the preliminary experiments described in Chapter 4 the following investigations were carried out on the liquids chosen.

1. The time resolution of the stimulated spectra were investigated using the image converter camera in the streak mode with a faster streak unit with writing speeds of 0.4, 1, 2, and 4 nanoseconds/mm.

2. The time delay between the generation of Stokes radiation and second harmonic Stokes was investigated as a function of rate of rise of the exciting pulse. Rate of rise was varied by using a number of glass microscope slides as attenuators.

3. Correlation between the total duration of stimulated Raman radiation as seen by the streak camera and the time during which the transmitted pulse was distorted was investigated.

4. The dependence of the distortion of the transmitted laser pulse on rate of rise was studied to determine whether there were effects limited by the response time of the liquid.

5.2 General Experimental Conditions

A sampling plate was positioned at 45° to the axis of the laser beam and the photo-diode system was adjusted to monitor the transmitted laser pulse. The image converter camera was positioned as described

in Chapter 4, Fig14 such that the complete focal plane of the spectrograph was recorded by the camera. The positions of all the components were kept fixed throughout the investigations to be described.

The prism speed of the laser system was set at 15,000 rpm and the voltage on the condenser bank was set at 1.8 KV. Firing at regular intervals produced a primary Q-switched pulse of width about 40 nsec at the half intensity points.

The two oscilloscopes used were operated with a time base of 40 nsec cm^{-1}. The optical inputs to the photocells were suitably attenuated to prevent distortion. In order to obtain clear oscillographs it was necessary to pre-fog the film (3000 ASA Polaroid). The system was set so that up to four separate pulse events could be recorded on a single frame.

The ruby laser line was attenuated so that the camera aperture could be opened up to record all the weaker Raman lines generated and to ensure that the total time generation of any line was recorded. The appropriate aperture and streak speeds were found by trial-and-error for each liquid.

5.3 Experimental Modifications

Since the trigger unit had an optical photo-diode input giving a faster trigger with a maximum time delay of 25 nanoseconds after the radiant intensity reached 25μ watts cm^{-2} it was possible to monitor the first laser pulse generated by triggering on the leading wing of the pulse. Electronic time delay problems (c.f. 4.6(a)) were

therefore easily avoided using the system shown in Fig 33 in which the photodiode was fed with a 3 metre fibre optic.

In order to record the transmitted pulse and the streak spectrum simultaneously, the point spectrum was sampled with a glass plate of photographic quality, inclined at 45^{o} to the beam direction and placed immediately before the diffusing screen of the spectrometer. The resultant spectrum was diffused by another screen and sampled as outlined in 4.7(b).

The transmitted laser pulse was viewed by a Hewlett-Packard oscilloscope type 180A with a writing speed of 10 nsec cm^{-1} and a rise-time of 5 nsec whilst the exciting pulse was monitored with a Hewlett Packard oscilloscope type 195A with a rise time of 7 nsec.

5.4 Experimental Procedure

The apparatus was aligned with the He-Ne laser in exactly the same manner as outlined in 4.6(g). The ruby laser line was centred in the field of view by rotating the diffraction grating.

5.5 Reproducibility Check

In order to compare the results for the range of liquids chosen it was necessary to ensure that the results for a given liquid were reproducible and that the liquids could be interchanged without disturbing the system. The laser was triggered at regular (10 min.) intervals and the output pulse was monitored with the photo-diode in conjunction with the H.P. 180A oscilloscope. The polaroid photographs were measured to determine the onset of pulse distortion from the base line and are shown for a few liquids in Table 4.

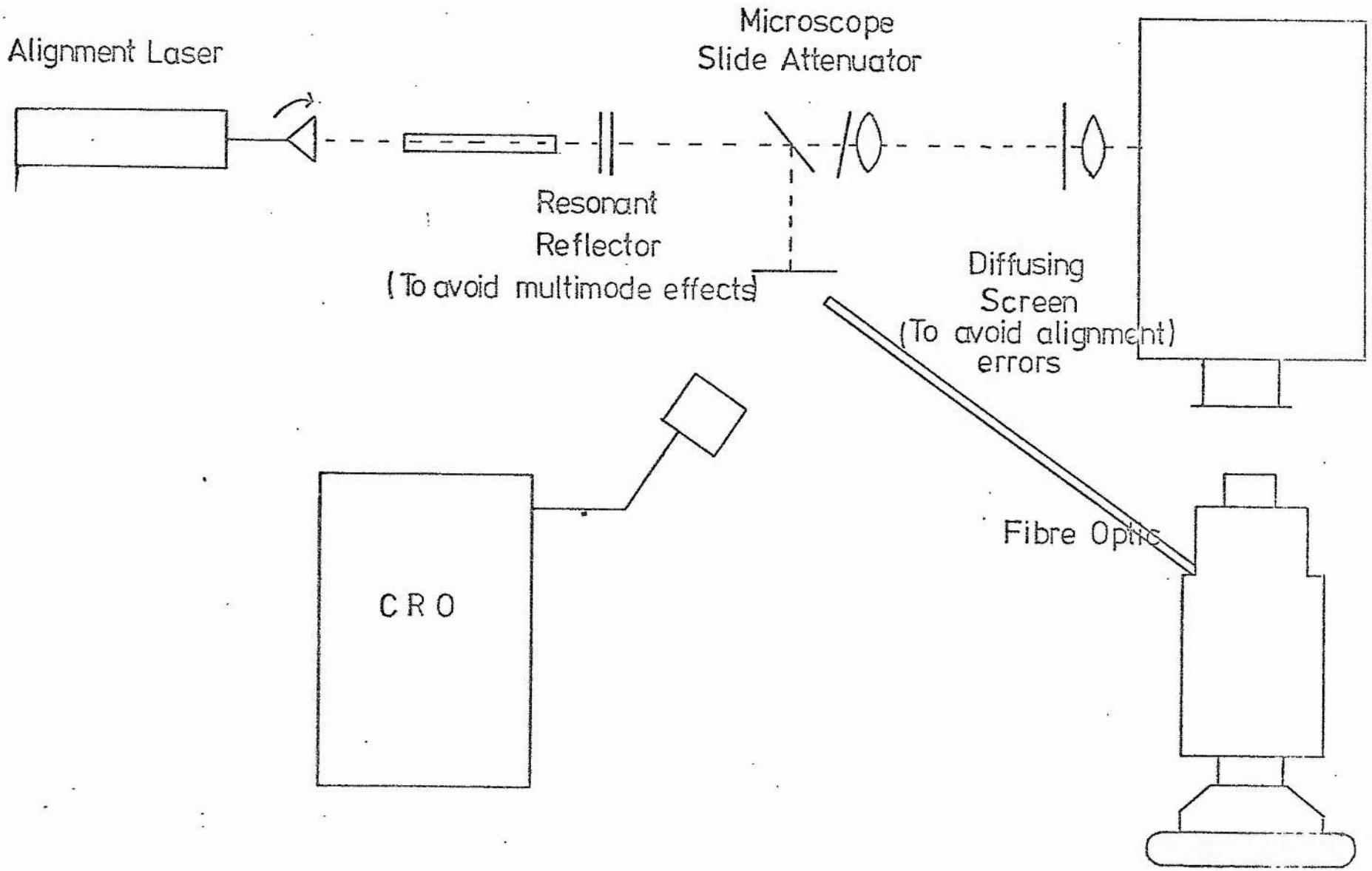

Fig 33 Modified Stimulated Raman Spectrometer

TABLE 4

CHLOROBENZENE	BENZENE	NITROBENZENE	INTERCHANGE*
30.0	23.0	11.5	N-B
32.0	23.5	12.0	11.0,12.5,12.0
31.5	24.0	12.0	B
30.0	25.0	13.0	25.0,25.0,24.0
31.5	28.0	12.5	Cl-B
31.5	26.0	13.0	31.5,31.0,31.5
30.0	23.0		
	26.0		
31.0±1.0	25.0±2	12.2±1.0	

* These results were obtained by switching from one liquid to another in a random sequence to avoid problems due to possible drift in laser power or drift due to deterioration of the liquid samples studied.

It is clear from the Table that the results are consistent within themselves and that interchanging the liquids does not produce significant differences. The system can therefore be used to study and compare results from a range of liquids.

5.6 Determination of Pulse Distortion

To measure the pulse distortion, the polaroid photographs of the CRO traces were magnified (4x) by using an overhead projector. This was done for the input pulse and distorted pulse for all the results. A typical example for benzene is shown in Fig 34 in which each millimetre corresponds to 1 nanosecond.

It is clear that the onset of pulse distortion is rapid and that the system is limited by the response time of the oscilloscope (5 nsec). In order to minimise the error, the threshold for pulse distortion, T_1 was measured at the point indicated where the minimum detectable departure from linearity was observed. Similarly, as the pulse was found to be asymmetric, the "cut-off" threshold, T_2 was measured at the start of the linear region (see Fig 33). The total time duration of distortion, L_D was measured from T_1 to T_2.

5.6(b) Rate of Rise Measurements

The rate of rise of the pulse, M_L, was determined by measuring the gradient of the pulse at the onset of pulse distortion.

Due to the finite rise time of the oscilloscope, the measured

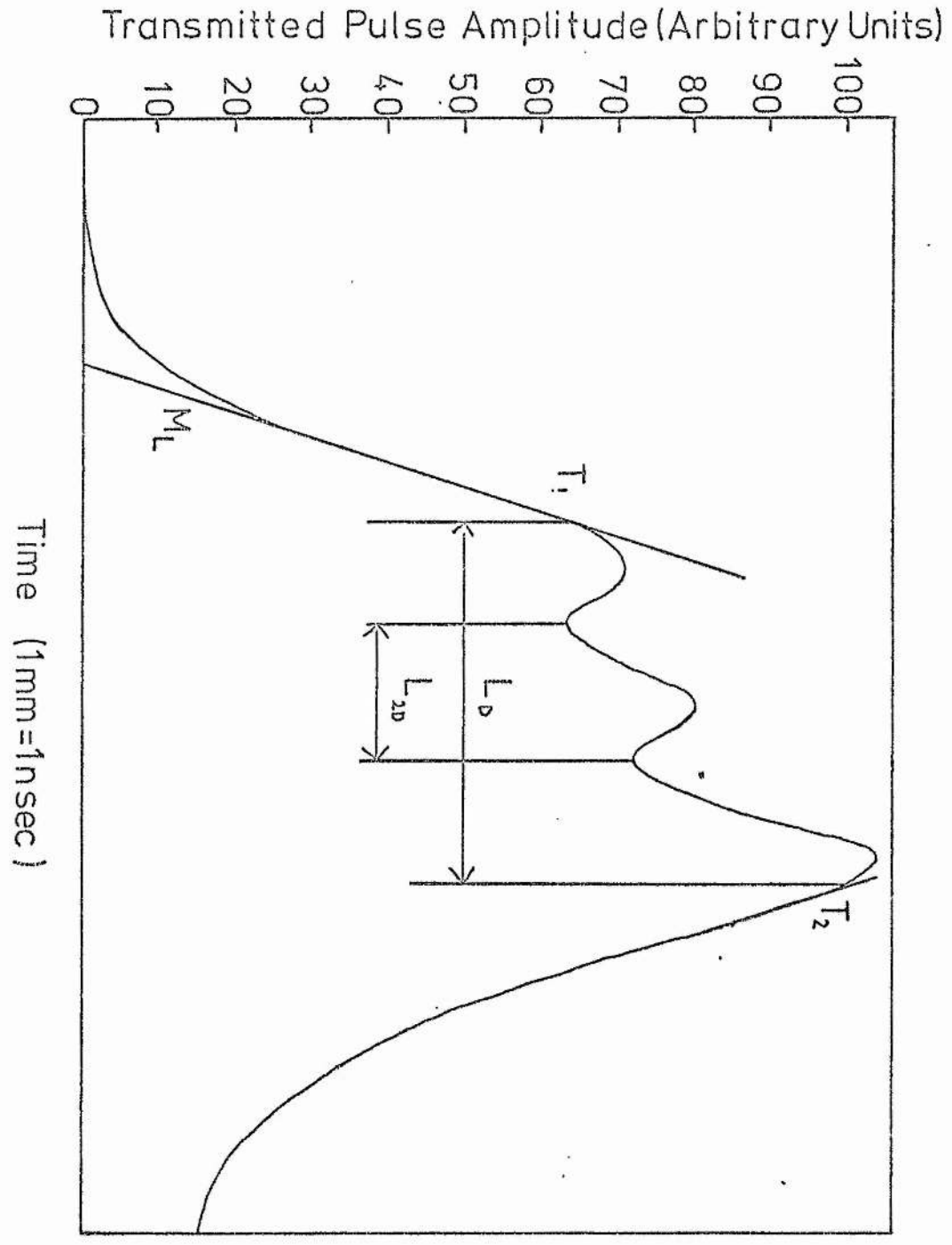

Fig 34 Typical Pulse Distortion Trace for Benzene showing the Distortion Thresholds T_1 and T_2, the Distortion Lengths L_D and L_{2D}, along with the Gradient, M_L.

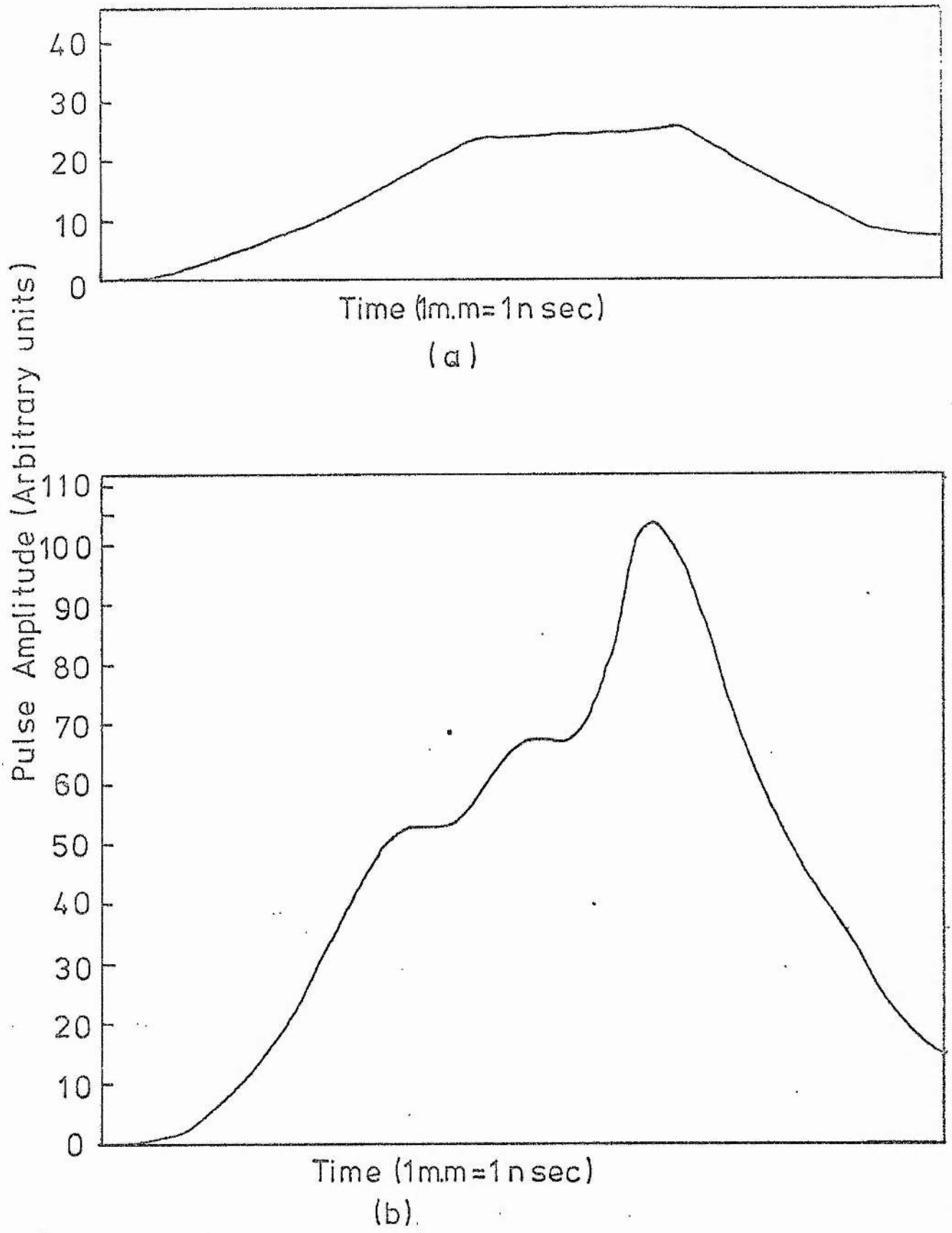

Fig 35 Characteristic distorted laser pulses after Raman generation in Benzene

(a) No harmonic

(b) Harmonic generated

gradient could be in error since the measured rise-time τ_M is given by,

$$\tau_M = (\tau_S^2 + \tau_A^2)^{\frac{1}{2}}$$

where τ_S is the rise-time of the CRO, and τ_A is the actual rise-time. The actual rise time is therefore given by

$$\tau_A = (\tau_M^2 - \tau_S^2)^{\frac{1}{2}} \qquad 5.6.1$$

and the fractional error, E_M is given by

$$E_M = \frac{\tau_M - \tau_A}{\tau_A}$$

In order to eliminate this error all results were corrected by means of equation 5.6.1.

N.B. The rise time is defined as the time taken for the pulse to go from 10 to 90% of the pulse height. The rate of rise was obtained by dividing this height by the corrected time.

5.6(c) Error in Pulse Distortion Threshold

If a maximum error of 2 nsec is assumed in the estimation of the onset of pulse distortion, then the fractional error is given by

$$E(T_1) = 2M_L/T_1$$

where M_L is the rate of rise and T_1 is the measured threshold value. A similar result is obtained for T_2. From the estimated error of 2 nsec in the detection of distortion it is clear that the error in the measurement of L_D is $\pm$ 4 nsec.

5.6(d) Streak Photographs

All the streak photographs were measured with an accuracy of $\pm$ 0.1 giving a maximum error of 0.1S (where S is the streak speed in nsec/mm).

5.6(e) Treatment of Results

The treatment of the results is based on the findings described on Chapter 4 in which it was shown that the onset of pulse distortion of the transmitted pulse corresponds to the threshold for generation of stimulated Raman spectra. Assuming that the onset of pulse distortion also corresponds to the threshold for self-focusing, response time effects in the medium were sought by investigating the influence of the rate of rise of the exciting pulse, M_L, on the distortion threshold, T_1. It was also shown in Chapter 4 that the amplitude of the transmitted pulse is controlled by backward stimulated Raman and Brillouin scattering, therefore if the observed forward stimulated Raman spectrum is controlled by this pulse, correlations should exist between features of the transmitted pulse and the duration of the stimulated Raman lines excited. Correlations were sought by looking for features of the pulse distortion which correspond with the overall duration of the stimulated Stokes and second harmonic Stokes lines. Since the cut-off threshold, T_2 is greater than the initiation threshold, T_1, it was thought that multiphoton absorption (which is proportional to the intensity of the exciting beam) might be occurring so that the influence of I_L on T_2 was investigated. The results shown in Fig 16 indicate that the Stokes intensity increases linearly with input pulse amplitude, so that, on the basis of an iterative generation scheme, the time delay between first and second harmonic Stokes should be a function of the rate of rise of the exciting pulse; in view of this, the influence

of M_L on T_D, S-2S is studied.

5.7 Results - Benzene

5.7(a) Streak Record

The stimulated spectra were taken at a streak speed of 2 nsec/mm to ensure that spectra for the full duration of the pulses were obtained. A typical streak is shown in Plate (4) at a magnification of 3x. It is clear that the spectrum is stimulated with a sequence of Stokes, Anti-Stokes, and second harmonic Stokes lines as was found previously, 4.7. For brevity, we shall call second harmonic Stokes lines simply "second Stokes" in the discussion below.

Threshold, however, has a completely different character at this faster streak speed. Stokes initiation consists of one or two short pulses followed by the main generation after a time delay. Although it is difficult to make accurate measurements of very short pulses frame (1) appears to have an initiation pulse of duration 0.6 nsec. The multi-pulse nature of the Stokes generation is clearly shown in frame (4). In this frame no second Stokes generation is visible.

5.7(b) Characteristics of Pulse Distortion

As with the previous investigation, no pulse distortion was observed in the absence of stimulated Raman generation. The pulse shape when Raman is generated displays a marked distortion followed by a rise in pulse amplitude until "cut-off" is reached. The thresholds T_1, T_2 show marked asymmetry. A characteristic pulse shape for second Stokes generation was found, Fig 34 in which three peaks

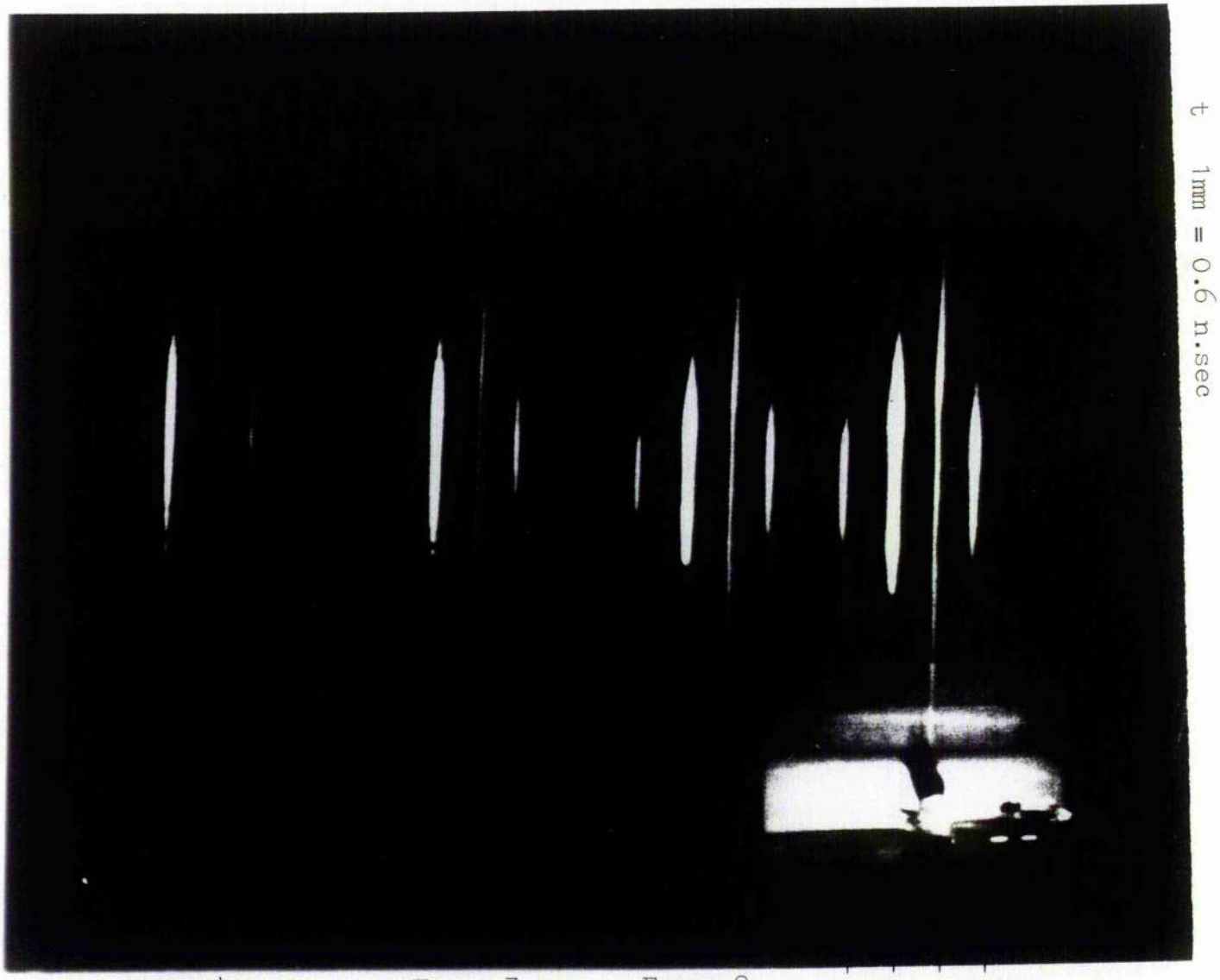
t
1mm = 0.6 n.sec
Frame 4
Frame 3
Frame 2
2S
S
L
AS

Frame 1 AS L S 2S Frame 3 Frame 4

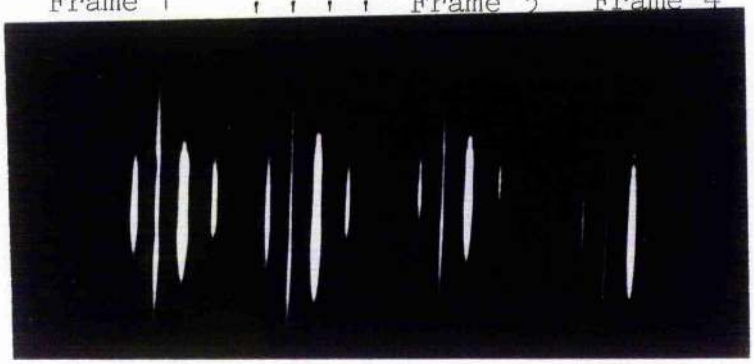

1mm = 2 n.sec

Plate 4a. Benzene

AS L S 2S Frame 2 Frame 3 Frame 4

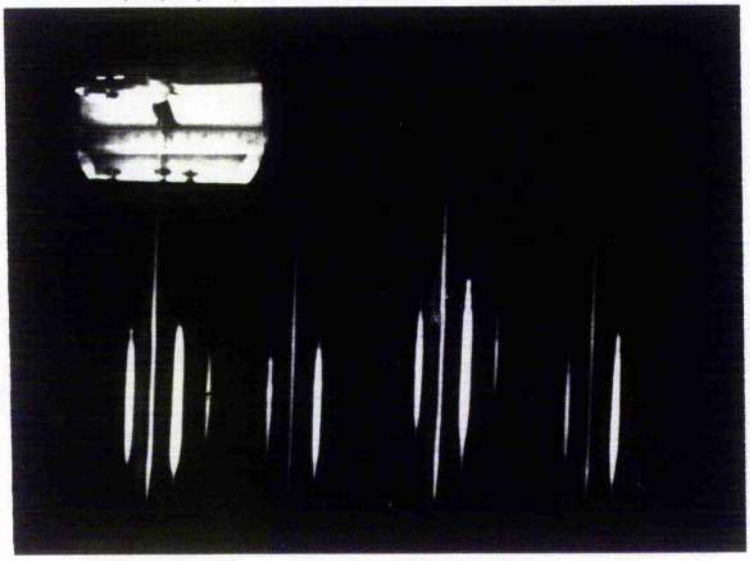

1mm = 1 n.sec

Plate 8. Toluene

2S S L AS 2 3 4

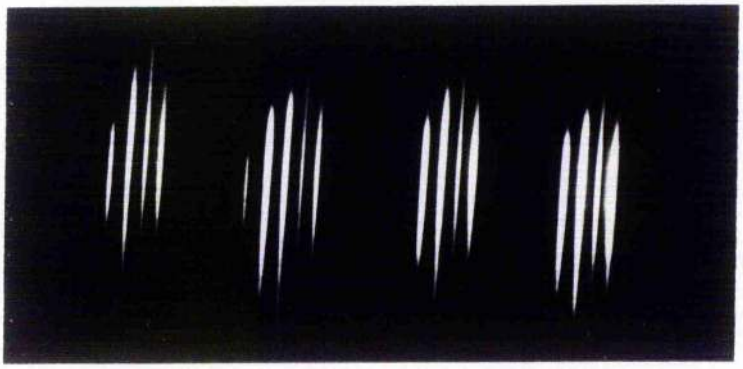

1mm = 2 n.sec

Plate 5. Carbon Disulphide

occurred with the intermediate peak corresponding to harmonic generation. No harmonic generation was observed in the absence of this intermediate pulse.

5.7(c) Correlation of Stokes Generation with Distortion of Transmitted Pulse

To check that the distortion of the laser pulse corresponds to the total duration of stimulated Raman a graph was plotted of the duration of pulse distortion against Stokes duration. The results are shown in Fig 36 in which it is clear that there is a good correlation.

5.7(d) Delay between Stokes and Second Stokes Threshold as a Function of Rate of Rise of Exciting Pulse

Results from this investigation are shown in Fig 37 in which it is seen that the delay decreases with increasing rate of rise of the exciting pulse.

5.7(e) Influence of Rate of Rise of Exciting Pulse on Pulse Distortion Threshold

The graph of T_1 against M_L is shown in Fig 38 in which it is seen that the threshold increases with the rate of rise of the exciting pulse.

5.7(f) Influence of Input Pulse Amplitude on Pulse Distortion Cut-Off

The influence of the input pulse amplitude, I_L, on the cut-off threshold, T_2 is shown in Fig 39 in which it is seen that T_2 increases with I_L.

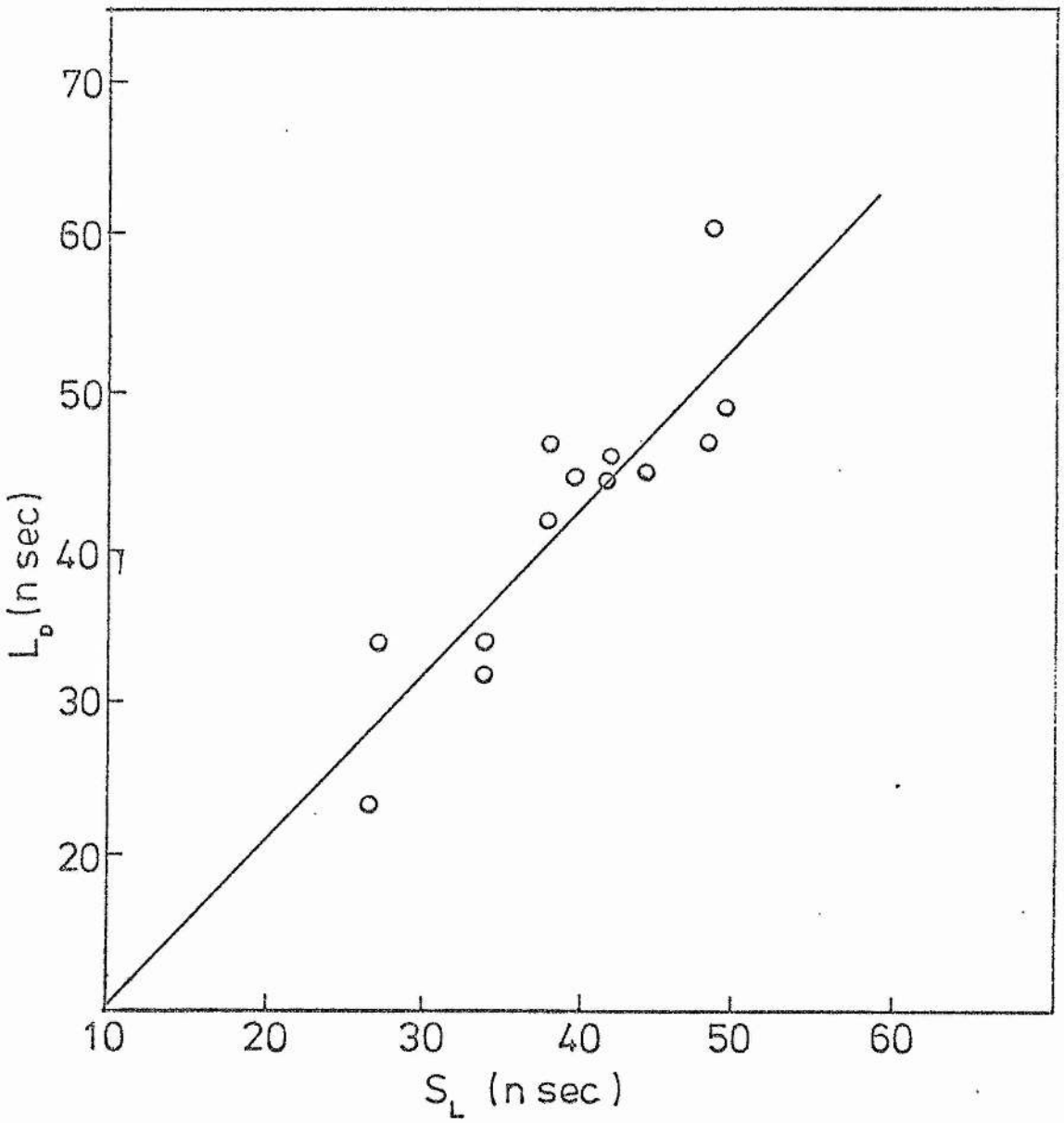

Fig 36 Correlation between Streak Duration of 1st Stokes in Benzene and Pulse Distortion of Transmitted Laser Pulse

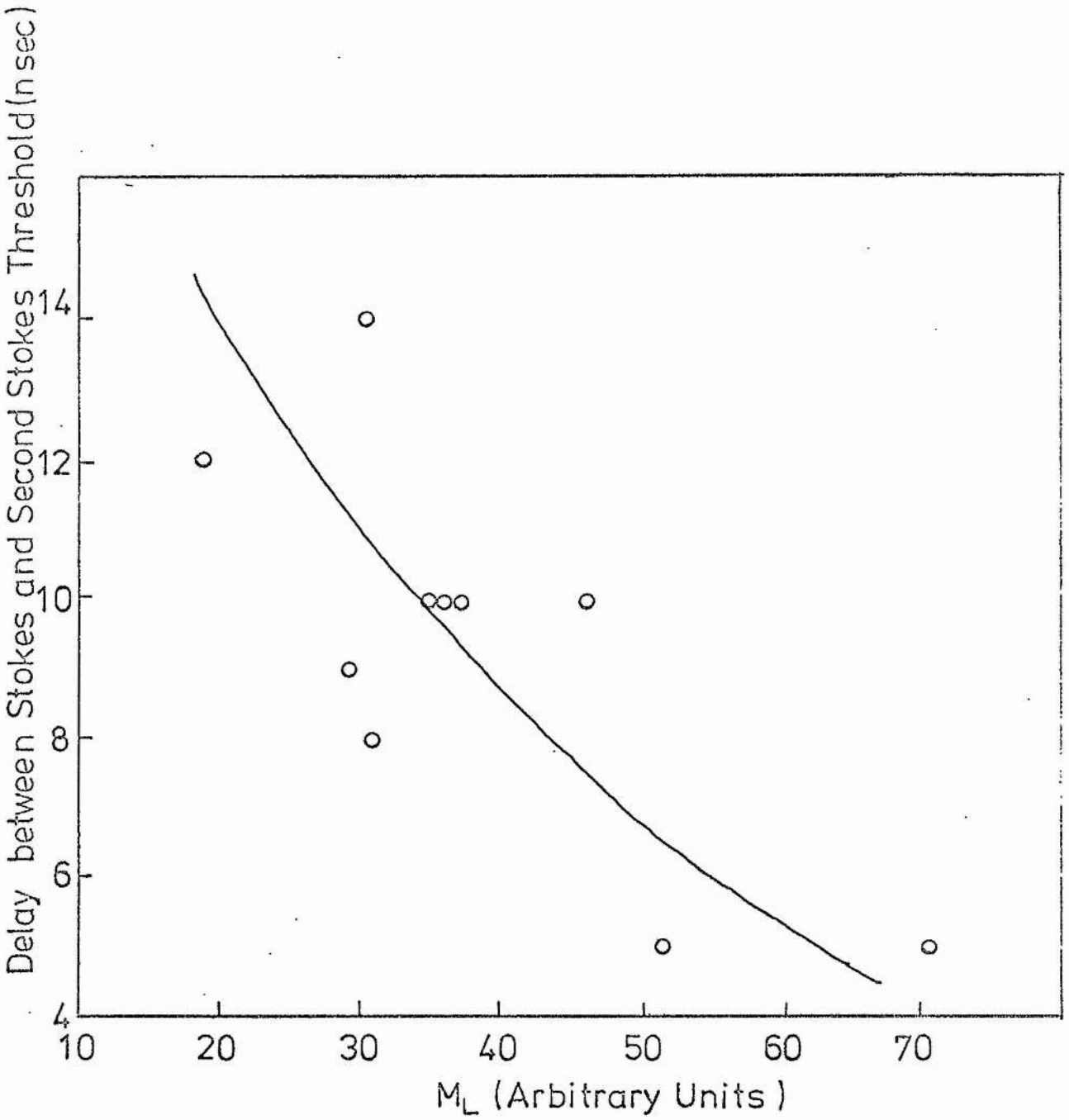

Fig37 Delay between Stokes and Second Stokes Threshold in Benzene as a function of Rate of Rise of Exciting Pulse

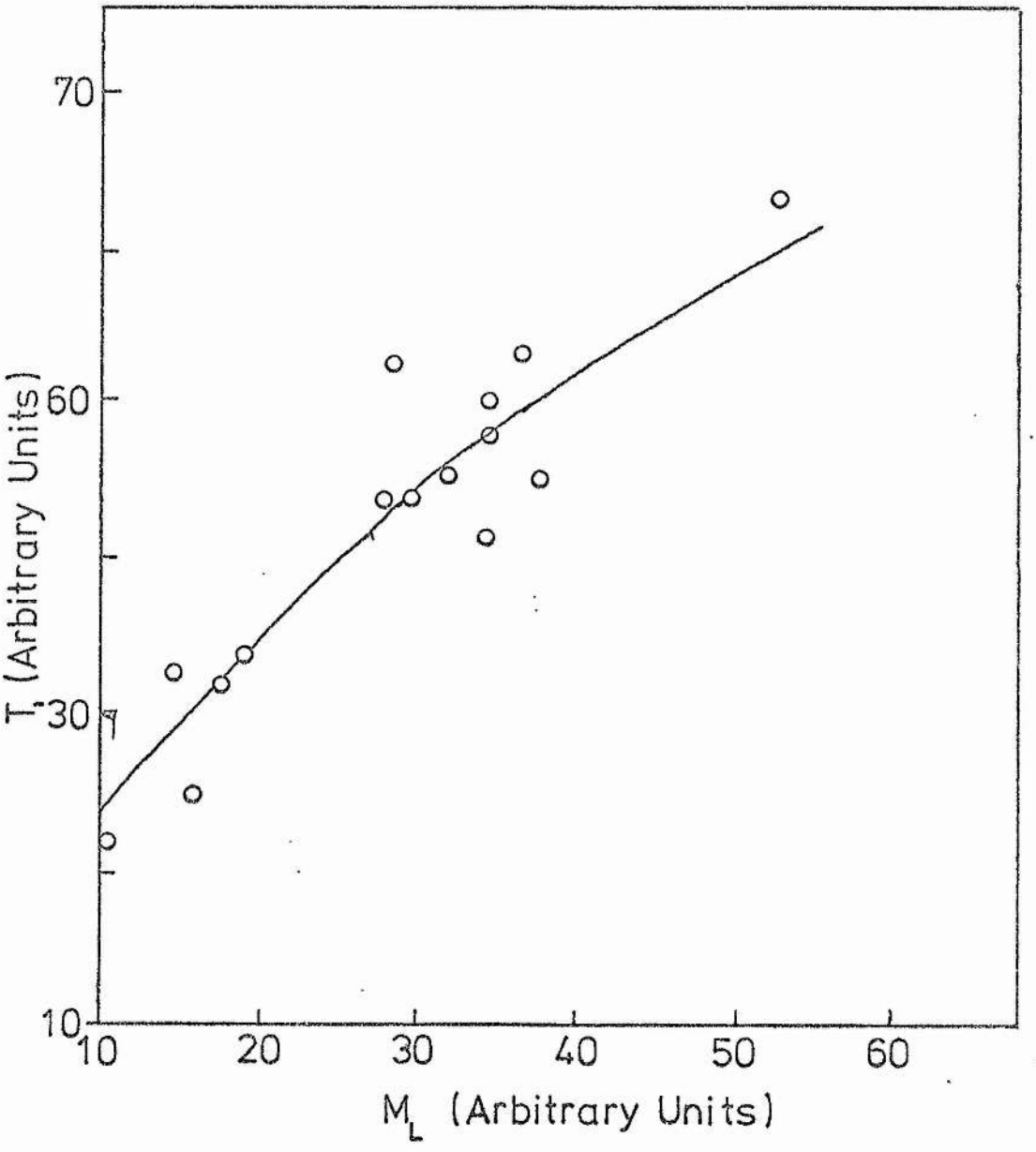

Fig 38 Influence of Rate of Rise of Exciting Pulse on Pulse Distortion Threshold in Benzene

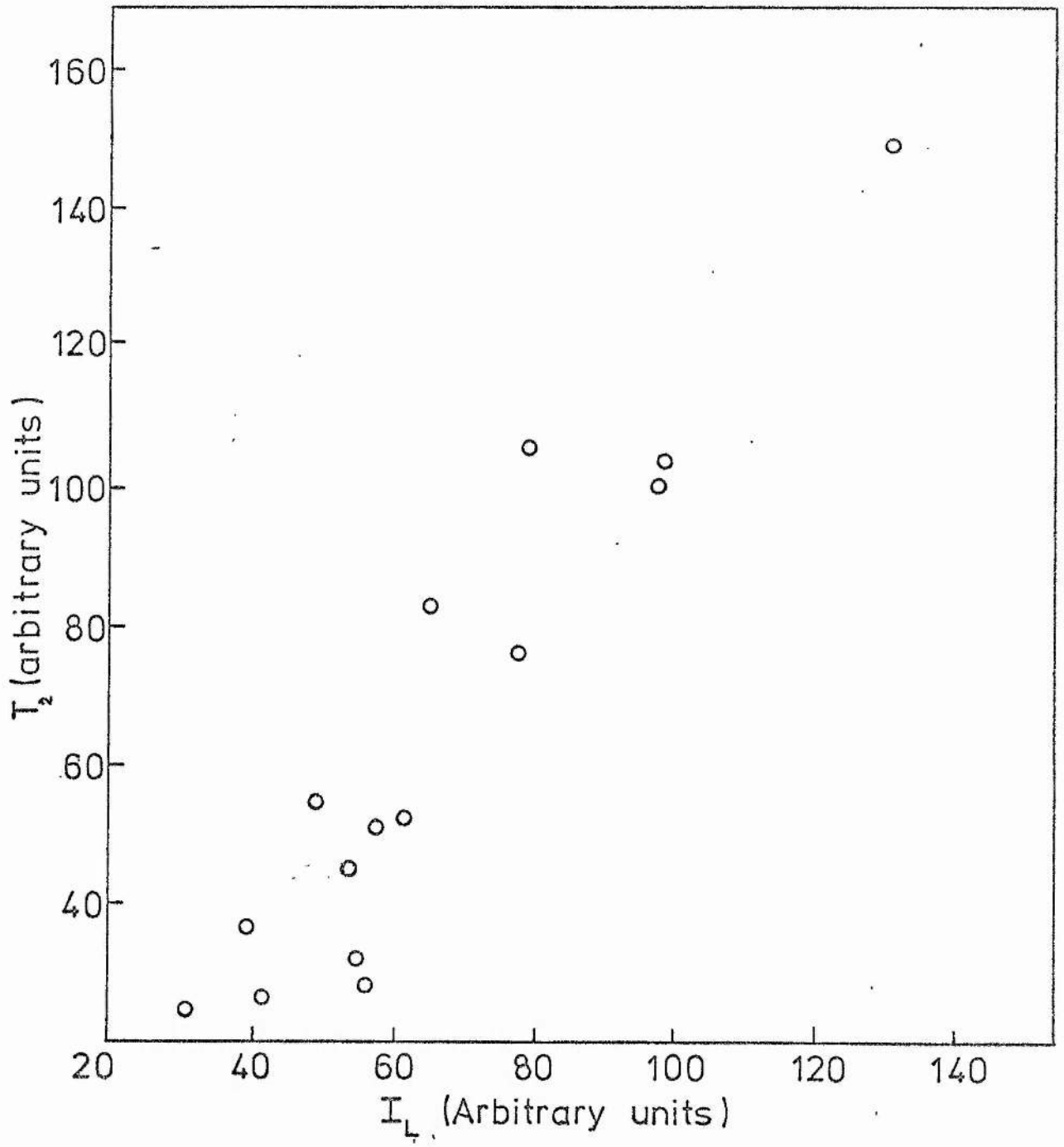

Fig39 Pulse distortion "Cut Off", T_2 in Benzene as a function of the peak laser input pulse amplitude, I_L

5.7(g) Generation of Second Harmonic Stokes Radiation

The appearance of second harmonic Stokes radiation was found to be correlated with the appearance of the intermediate distortion pulse. A graph showing this is given in Fig 40 in which it is clear that the intermediate pulse corresponds to harmonic generation.

5.8 Results - Carbon Disulphide

5.8(a) Streak Record

A typical streak record for carbon disulphide is shown in Plate 5. A streak speed of 2 nsec/mm was used to ensure that the total generation time was observed. A streak speed of 1 nsec/mm was used to enable accurate measurements to be made of the time delays between successively stimulated Raman lines. A similar set of measurements to those for benzene were made.

5.8(b) Characteristics of Pulse Distortion

As with benzene, the distorted transmitted laser pulse had a characteristic form as shown in Fig 41. The clearly defined pulse distortion threshold, T_1 is followed by a central peak leading to the cut-off, T_2 which, in general, is less well defined than in the case of benzene. The central peak is very much larger than that occurring with benzene. Again no distortion was observed in the absence of stimulated Raman generation.

5.8(c) Influence of Rate of Rise of Exciting Pulse on the Delay between Stokes and Second Harmonic Stokes

Results from the investigation of the influence of the rate of

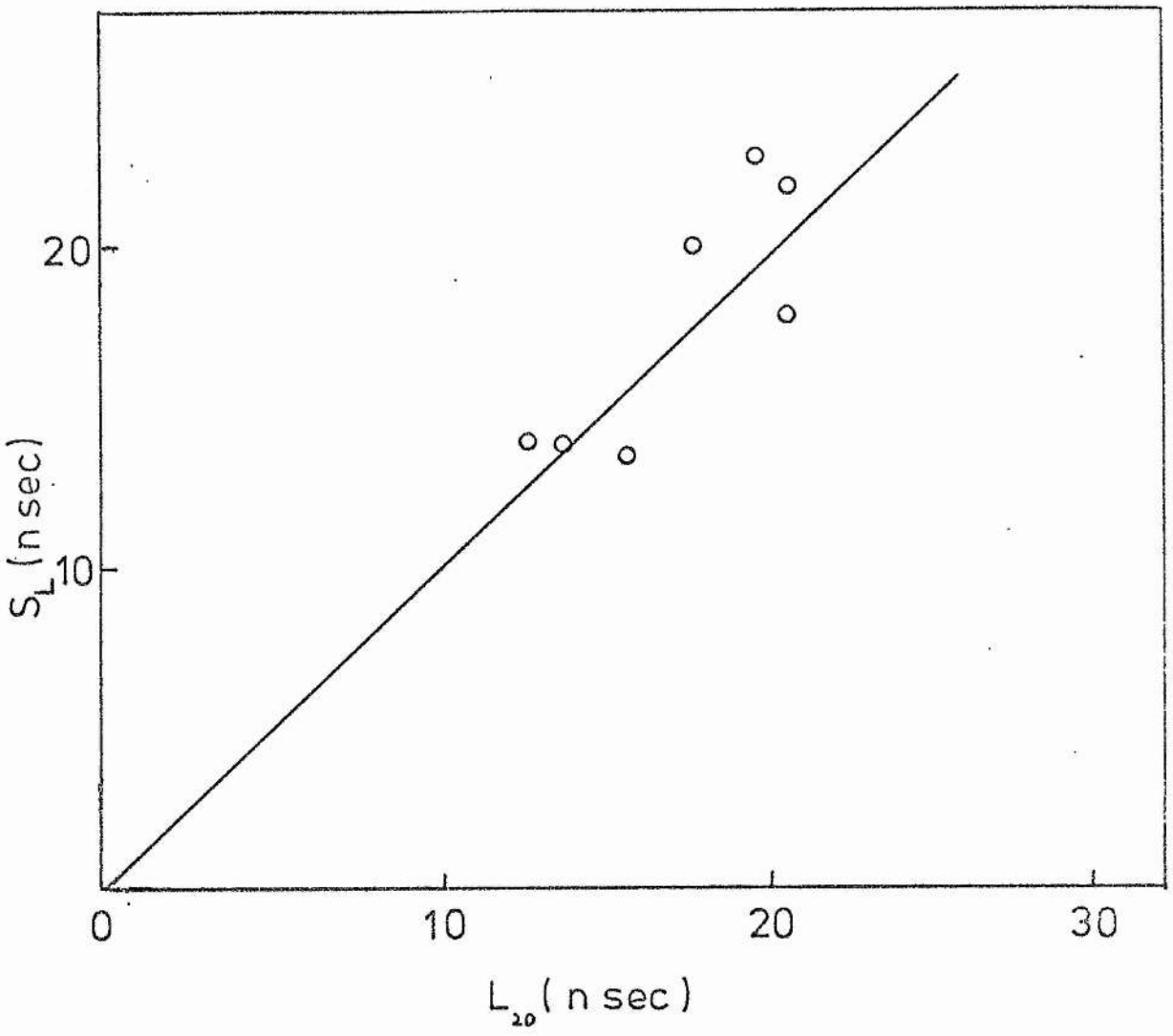

Fig 40 Correlation between the streak duration of second Stokes in Benzene and the duration of the secondary pulse distortion in the transmitted laser pulse

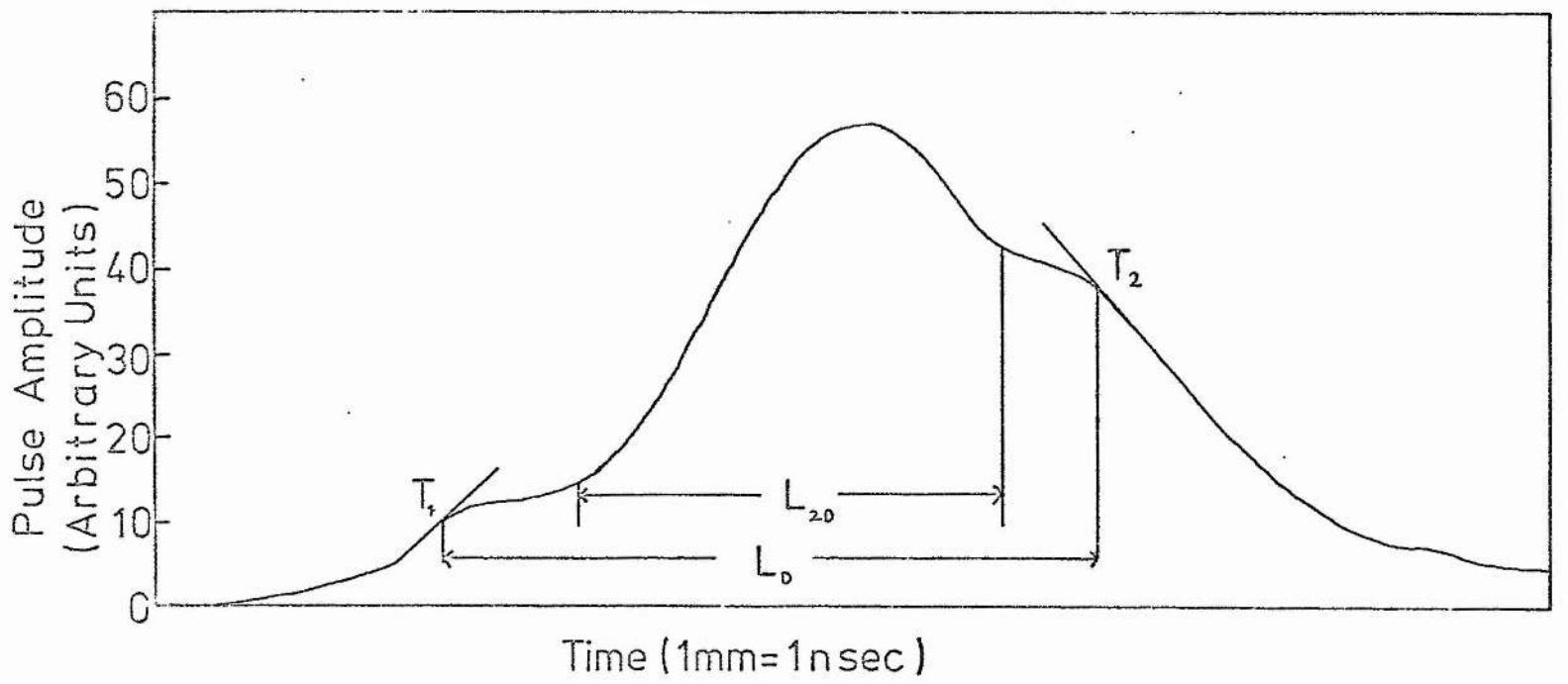

Fig41 Characteristic distorted laser pulse after Raman generation in Carbon Disulphide.

rise of the exciting pulse M_L, on the delay between Stokes and Second Harmonic Stokes, T_D, are shown in Fig 42 in which the experimental scatter is seen to be large.

5.8(d) Stokes Streak Duration and Pulse Distortion Duration

Results from the investigation of the relation between the Stokes streak duration, S_L, and the pulse distortion duration, L_D, are displayed in Fig 43.

5.8(e) Influence of Rate of Rise of Exciting Pulse on Pulse Distortion Threshold.

Results from the investigation of the influence of the rate of rise of the exciting pulse M_L on the threshold at which pulse distortion occurs are displayed in Fig 44(a,b) in which it is not only shown that T_1 increases with M_L but also that T_1 appears to approach a limiting value with $T_{1max} \sim 2T_{1min}$.

5.8(f) Influence of Input Pulse Amplitude on Pulse Distortion Cut-Off

Results from the investigation of the influence of the input pulse amplitude I_L on cut-off level at which pulsed distortion ceases are displayed in Fig 45, suggest that in the case of carbon disulphide T_2 is largely independent of the input pulse amplitude.

5.8(g) Generation of Second Harmonic Stokes Radiation

A graph of the second harmonic duration against the duration of pulse distortion is shown in Fig 46 where the large spread in points is probably due to the uncertainty in the "cut-off" time, T_2. Similar correlation was sought for higher harmonics but none were

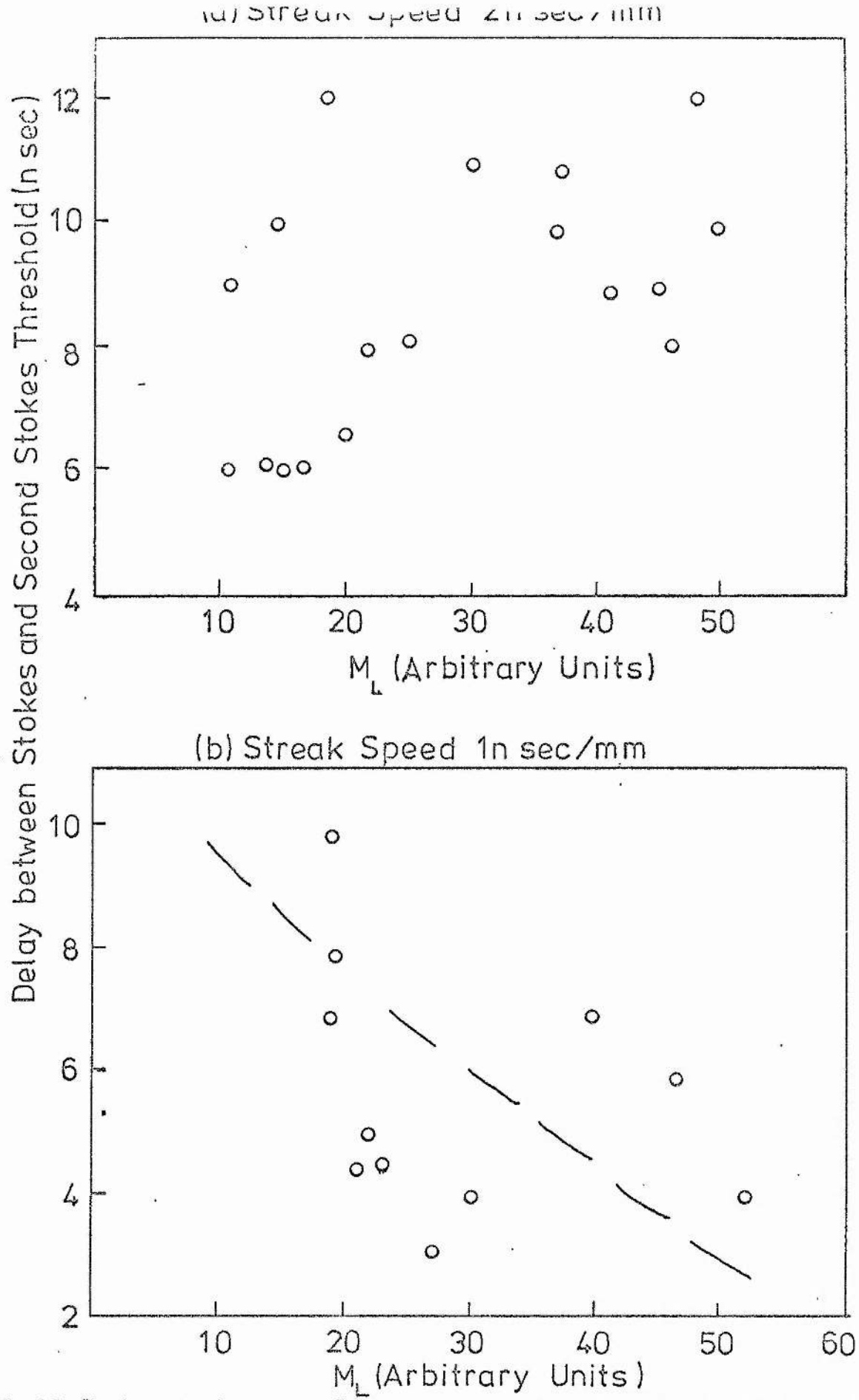

Fig42 Delay between Stokes and Second Stokes Threshold in Carbon Disulphide as a function of Rate of Rise of Exciting Pulse

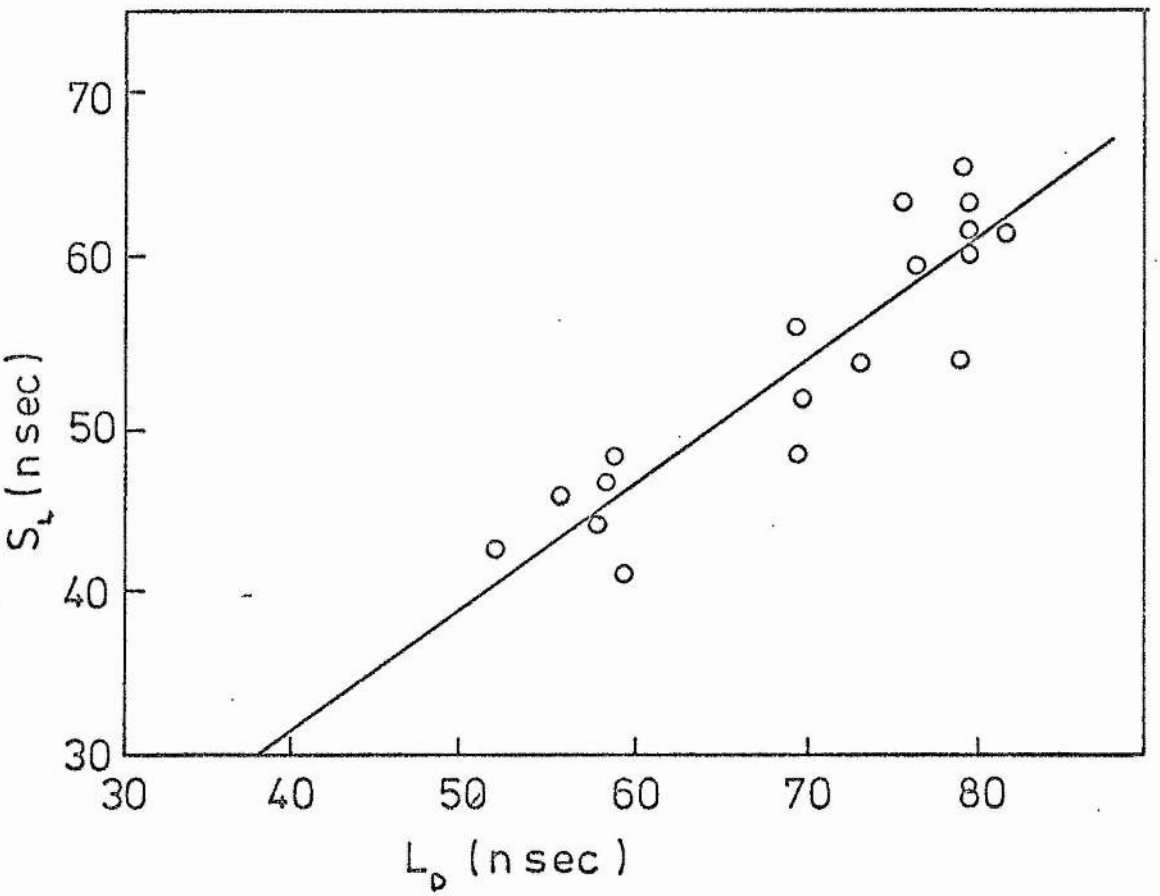

Fig 43 Correlation between the streak duration of 1st Stokes in Carbon Disulphide and pulse distortion in transmitted laser pulse.

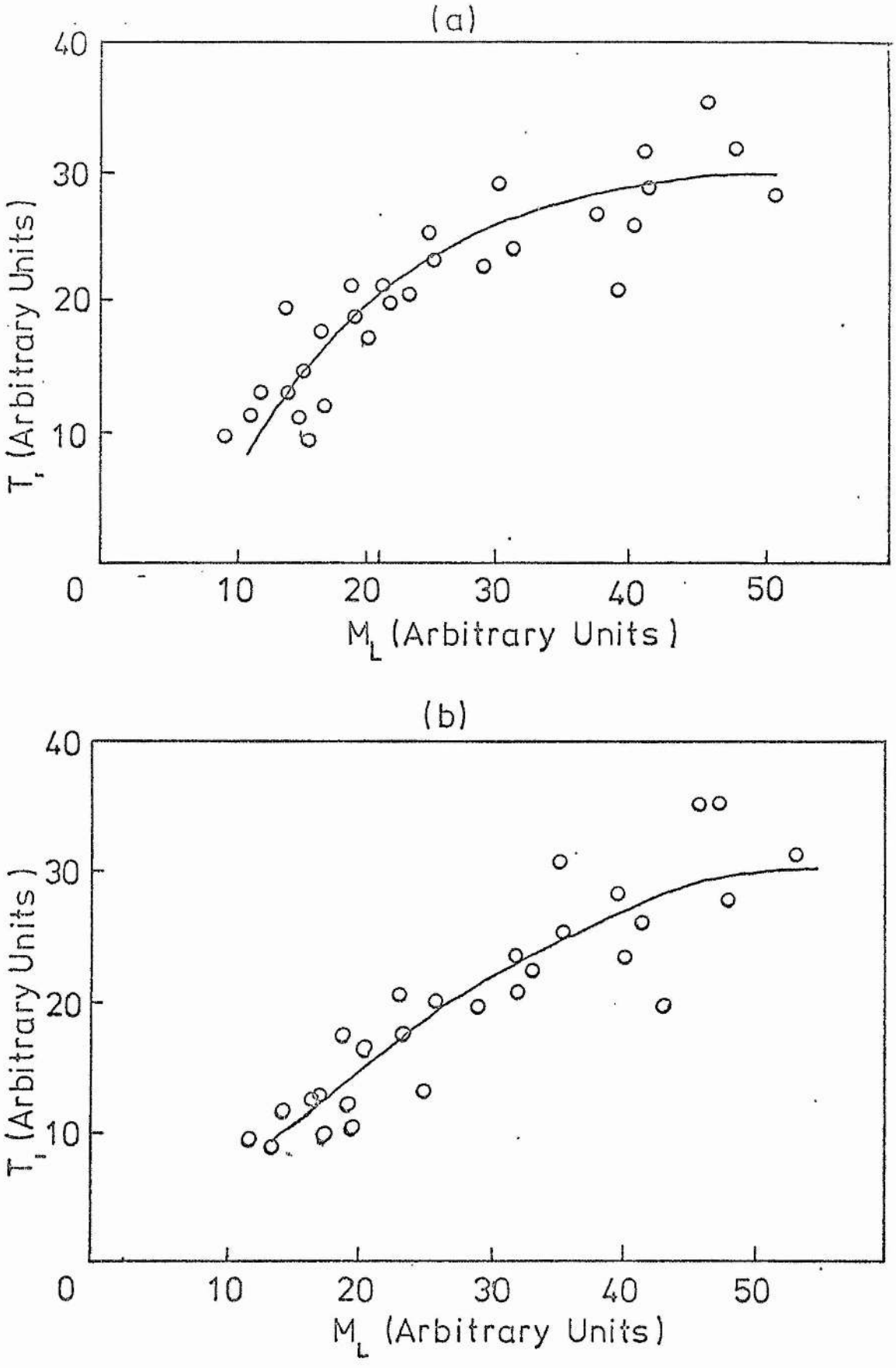

Fig 44 Influence of Rate of Rise of Exciting Pulse on Pulse Distortion Threshold in Carbon Disulphide (a) Uncorrected (b) Corrected

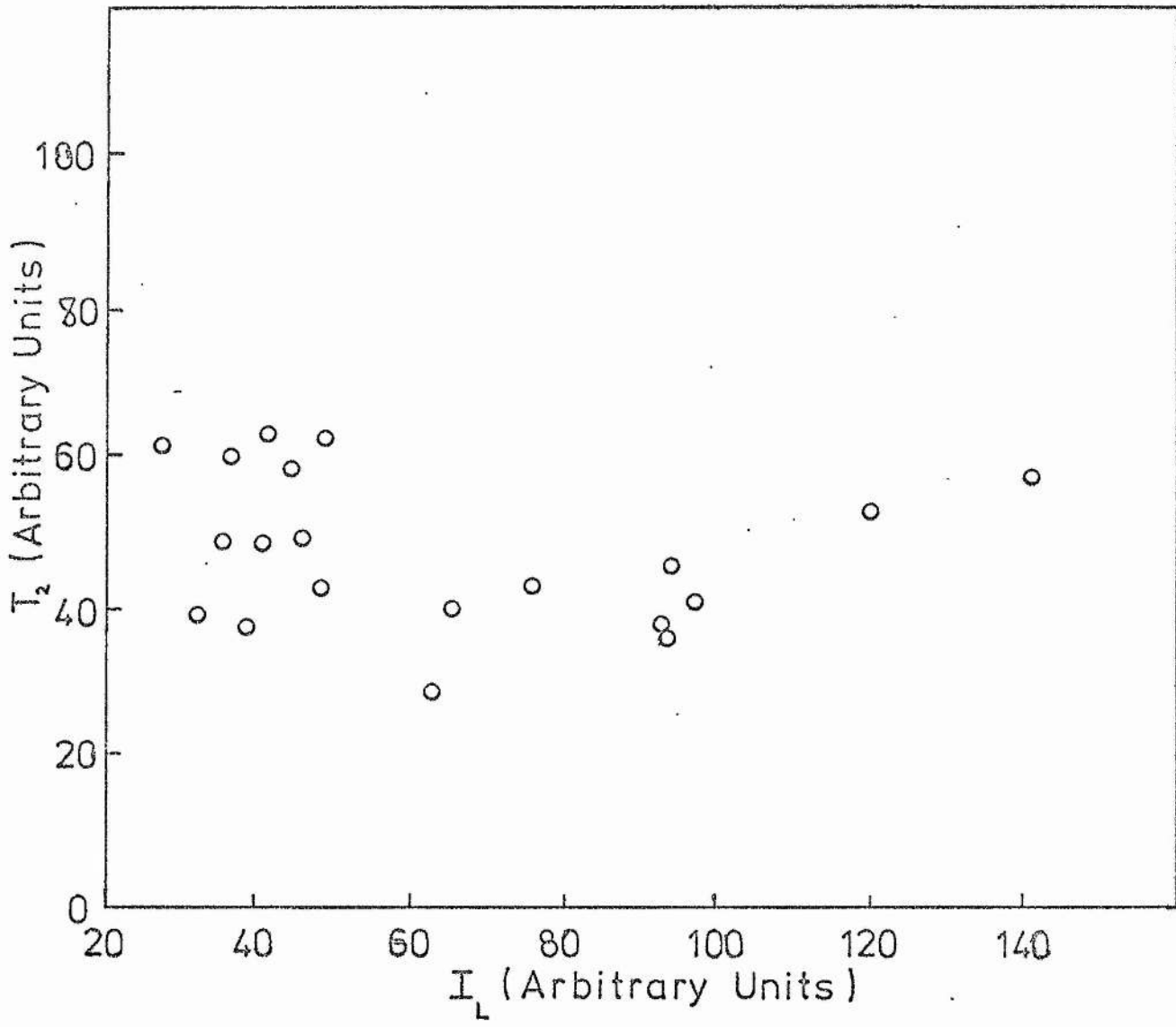

Fig45 Influence of Input Pulse Amplitude on Pulse Distortion Cut-Off in Carbon Disulphide

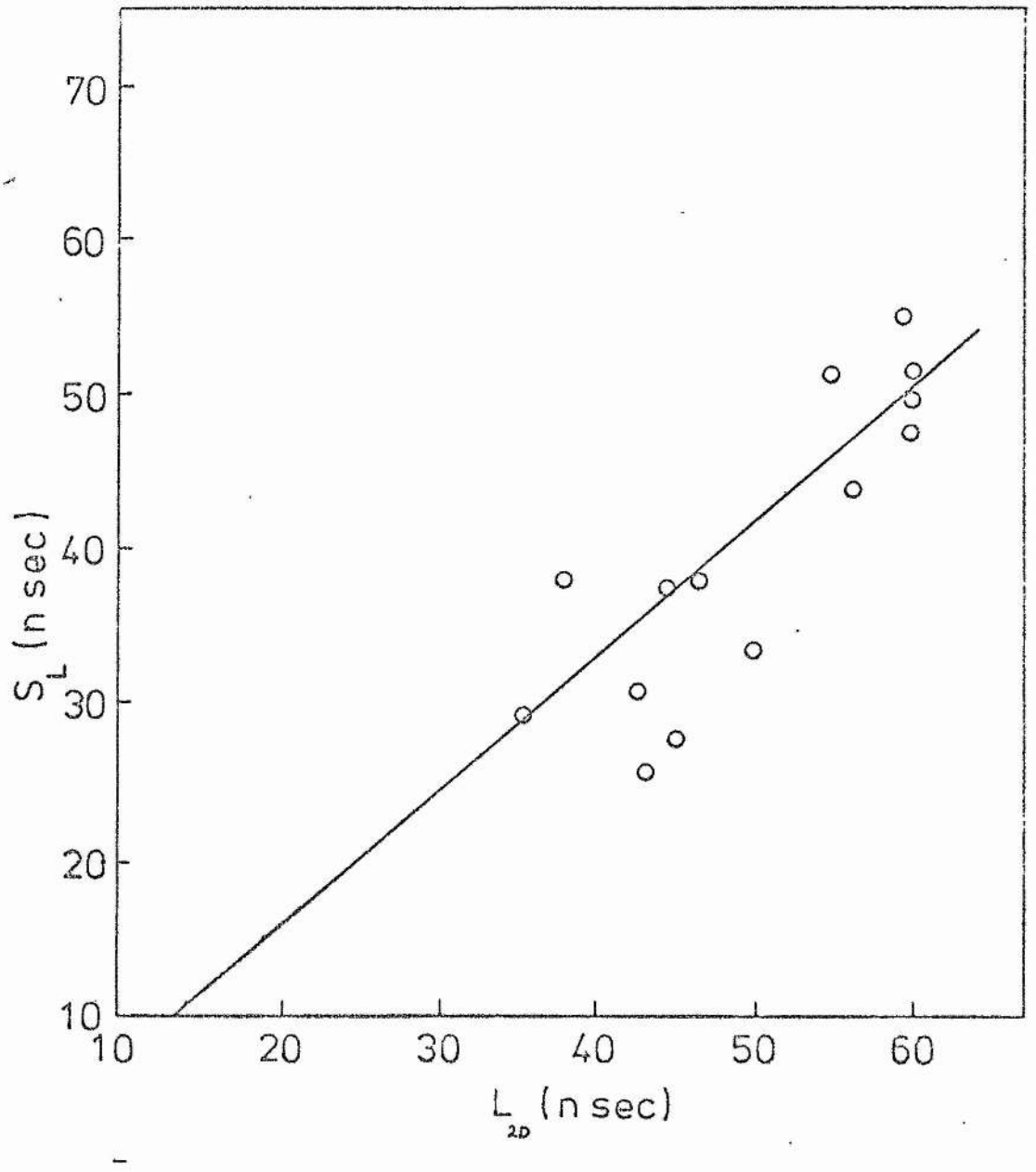

Fig46 Correlation between Streak Duration of Second Stokes in Carbon Disulphide and Secondary Pulse Distortion

found.

5.9 Results - Chlorobenzene

5.9(a) Streak Record

A typical streak record is shown in Plate 6. The harmonic is only generated weakly and there is a notable asymmetry with respect to first Stokes generation. The irregular pulsation at threshold is observed as is the case with all the liquids investigated.

5.9(b) Characteristics of Pulse Distortion

The transmitted pulse had the characteristic form shown in Fig 47. The pulse distortion threshold, T_1 is clearly defined and, as with benzene, shows cut-off T_2 at a different amplitude. The central peak observed in other liquids was not found.

5.9(c) Stokes Streak Duration and Pulse Distortion Duration

Results from the investigation of the relation between the duration of Stokes radiation S_L and the duration of pulse distortion, L_D are displayed in Fig 48. As with the other liquids investigated, S_L and L_D are found to be related.

5.9(d) Influence of Rate of Rise of Exciting Pulse on Pulse Distortion Threshold

Results from the investigation of the rate of rise of the exciting pulse M_L on the pulse distortion threshold T_1 are displayed in Fig 49, and clearly show that T_1 increases with M_L.

5.9(e) Influence of Input Pulse Amplitude on Pulse Distortion Cut-off

The influence of the amplitude of the input pulse I_L on the

Frame 1 Frame 2 Frame 3 Frame 4

t

1mm = 2 n.sec

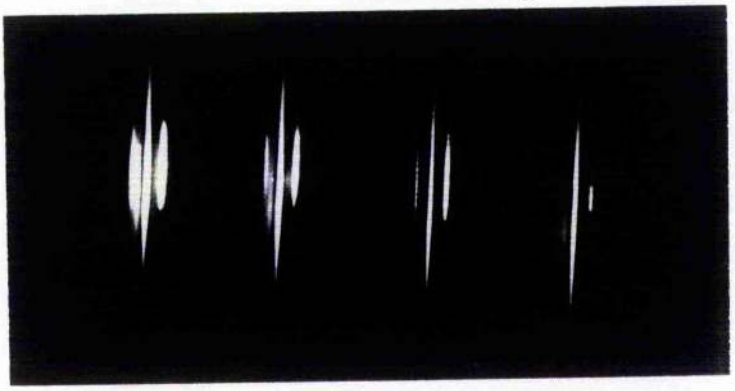

Plate 9. 50%/50% Benzene, Carbon Disulphide

AS L S 2S 2 3 4

t

1mm = 2 n.sec

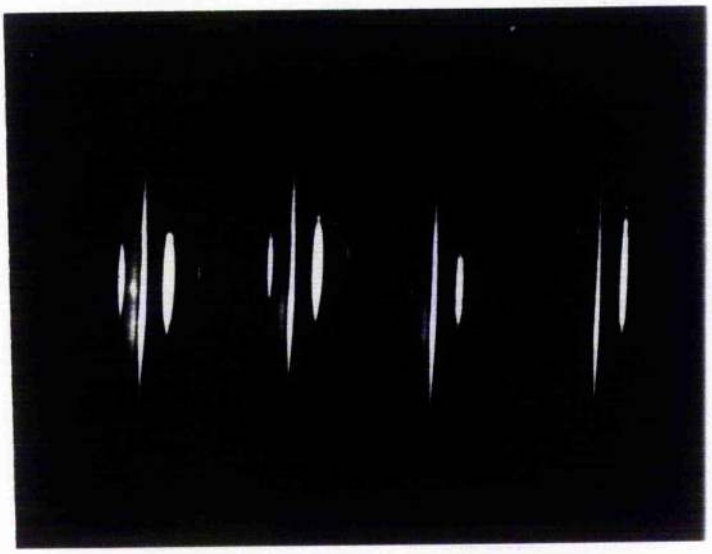

Plate 6. Chlorobenzene

AS L S 2S 2 3

t

1mm = 0.4 n.sec

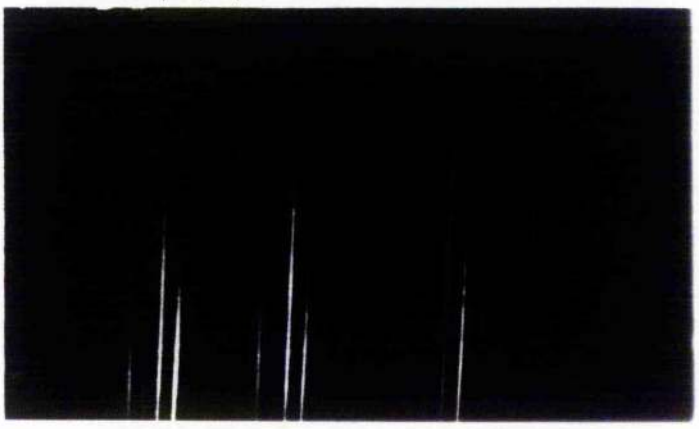

Plate 10. Carbon Disulphide

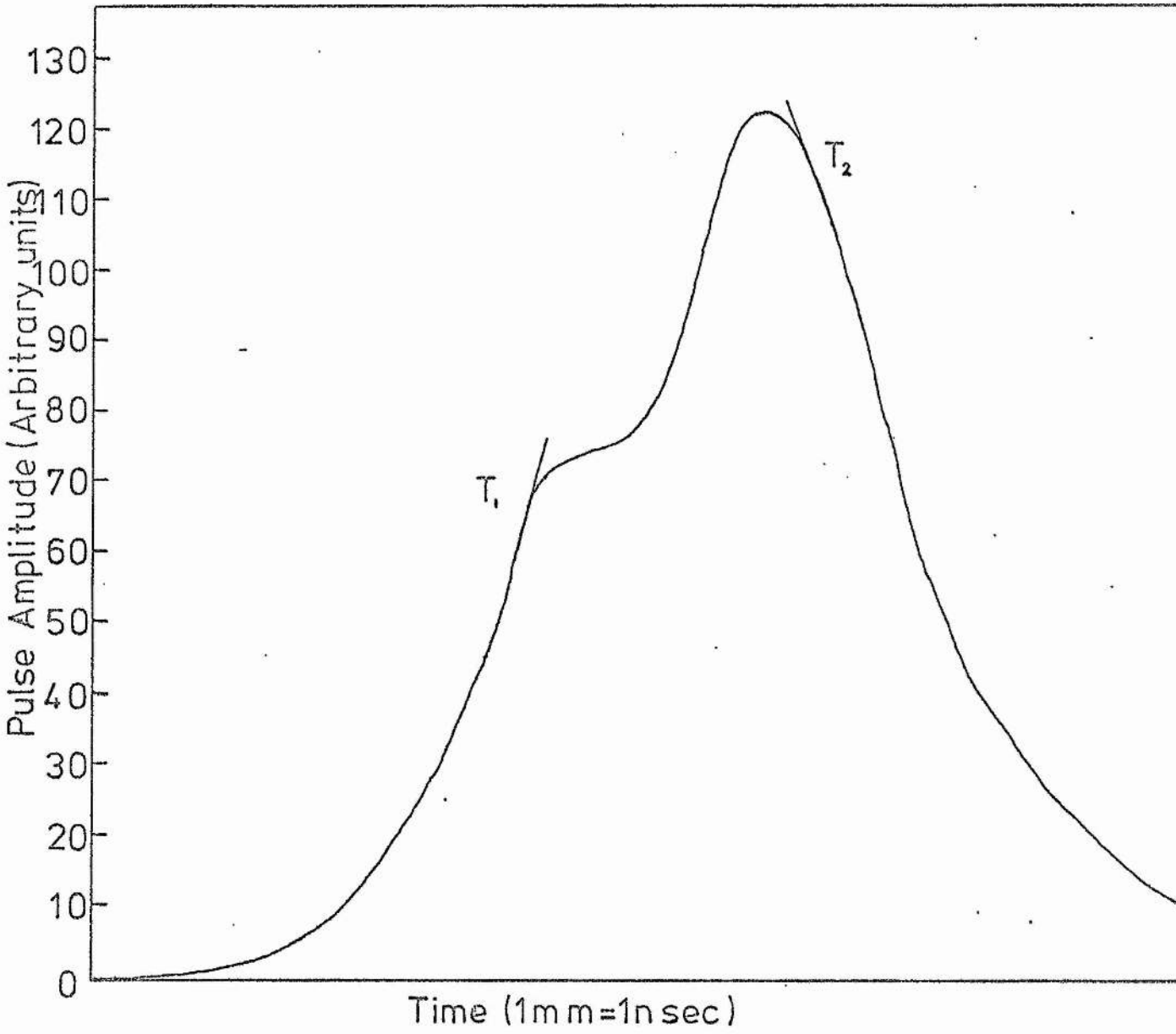

Fig 47 Characteristic distorted laser pulse after Raman generation in Chlorobenzene

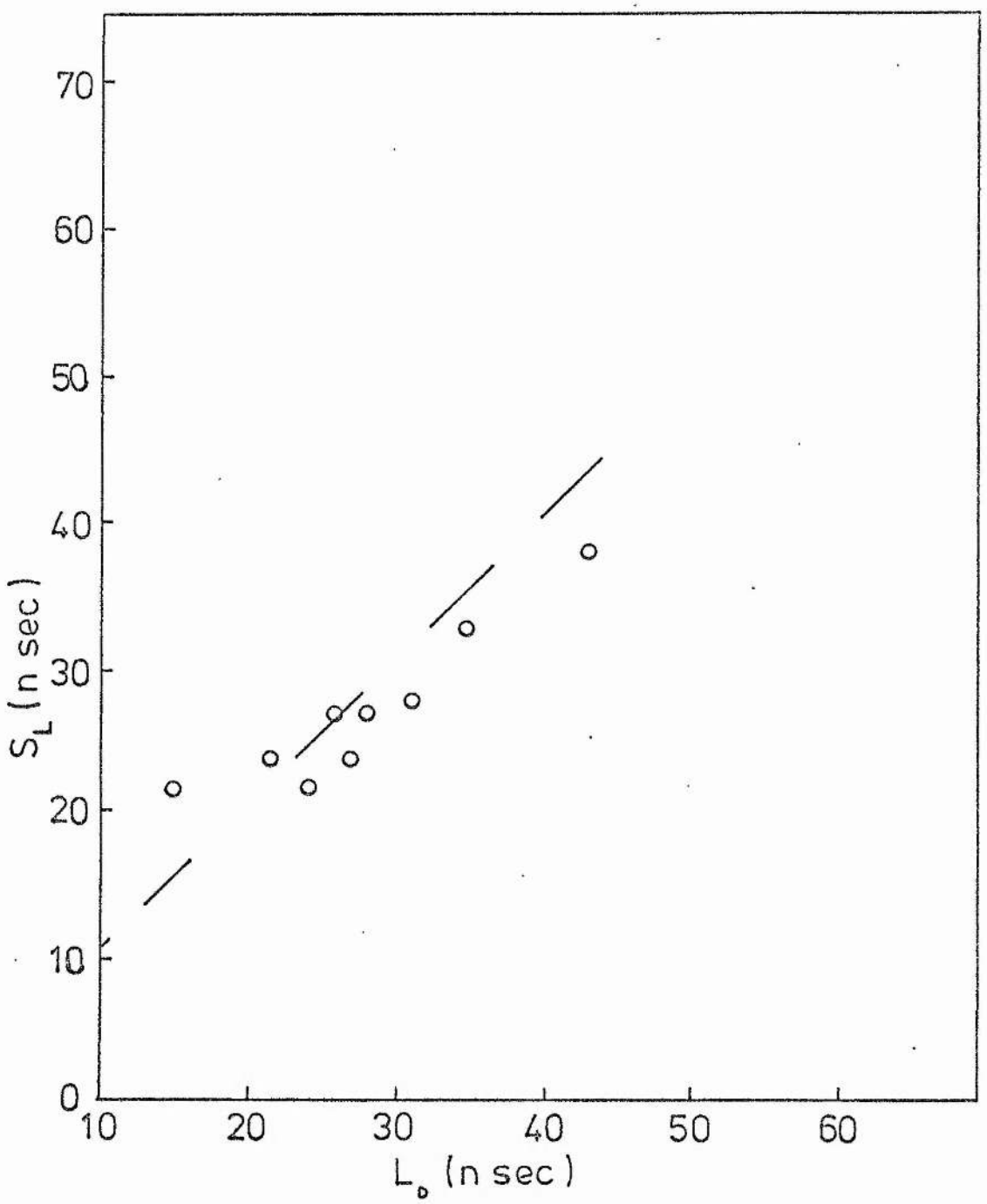

Fig 48 Correlation between Streak Duration of 1st Stokes in Chlorobenzene and Pulse Distortion of Transmitted Laser Pulse

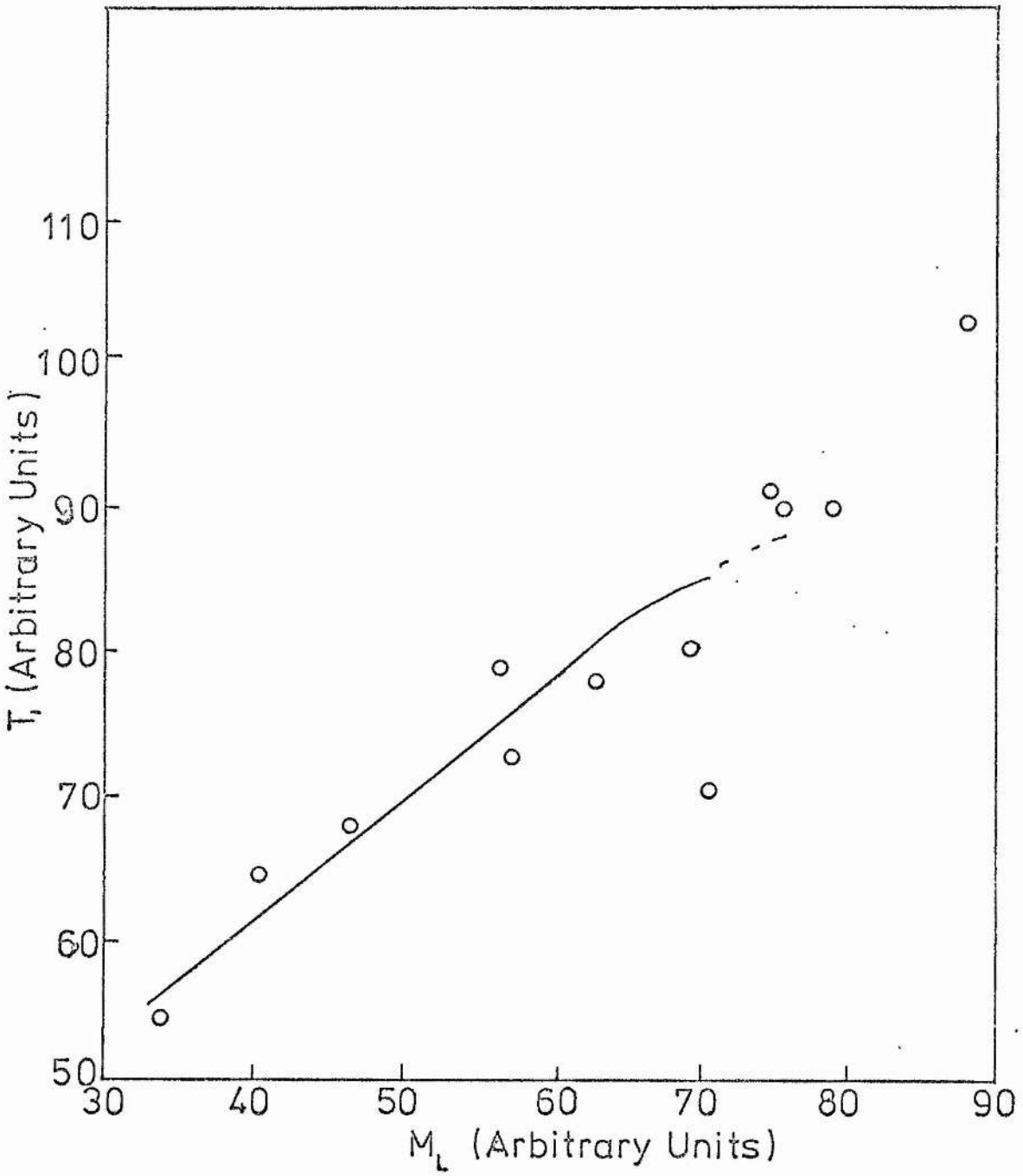

Fig49 Influence of Rate of Rise of Exciting Pulse on Pulse Distortion Threshold in Chlorobenzene

level T_2 at which pulse distortion ceases is shown in Fig 50. In this case the correlation appears to be rather poor.

5.10 Results - Nitrobenzene

5.10(a) Streak Record

A typical streak record is shown in Plate 7. No generation of Stokes harmonics was observed for the range of powers used in this investigation.

5.10(b) Characteristics of Pulse Distortion

Nitrobenzene was found to have an extremely marked pulse distortion threshold T_1. The pulse distortion cut-off was found to be such that $T_2 \gg T_1$. No harmonics were observed and no central pulse was found in the distorted pulse shape. Typical pulses are shown in Fig 51(a,b) for undistilled and freshly distilled samples, respectively. It is seen that the freshly distilled sample produces a more symmetric pulse.

5.10(c) Influence of Rate of Rise of Exciting Pulse on Pulse Distortion Threshold

The influence of M_L on T_1 is shown in Fig 52 in which T_1 clearly increases with M_L.

5.10(d) Stokes Streak Duration and Pulse Distortion Duration

The results of the investigation of the relation between S_L and L_D are displayed in Fig 53.

5.10(e) Influence of Input Pulse Amplitude on Pulse Distortion Cut-off

Results from the investigation of the influence of I_L on T_2, are shown in Fig 54.

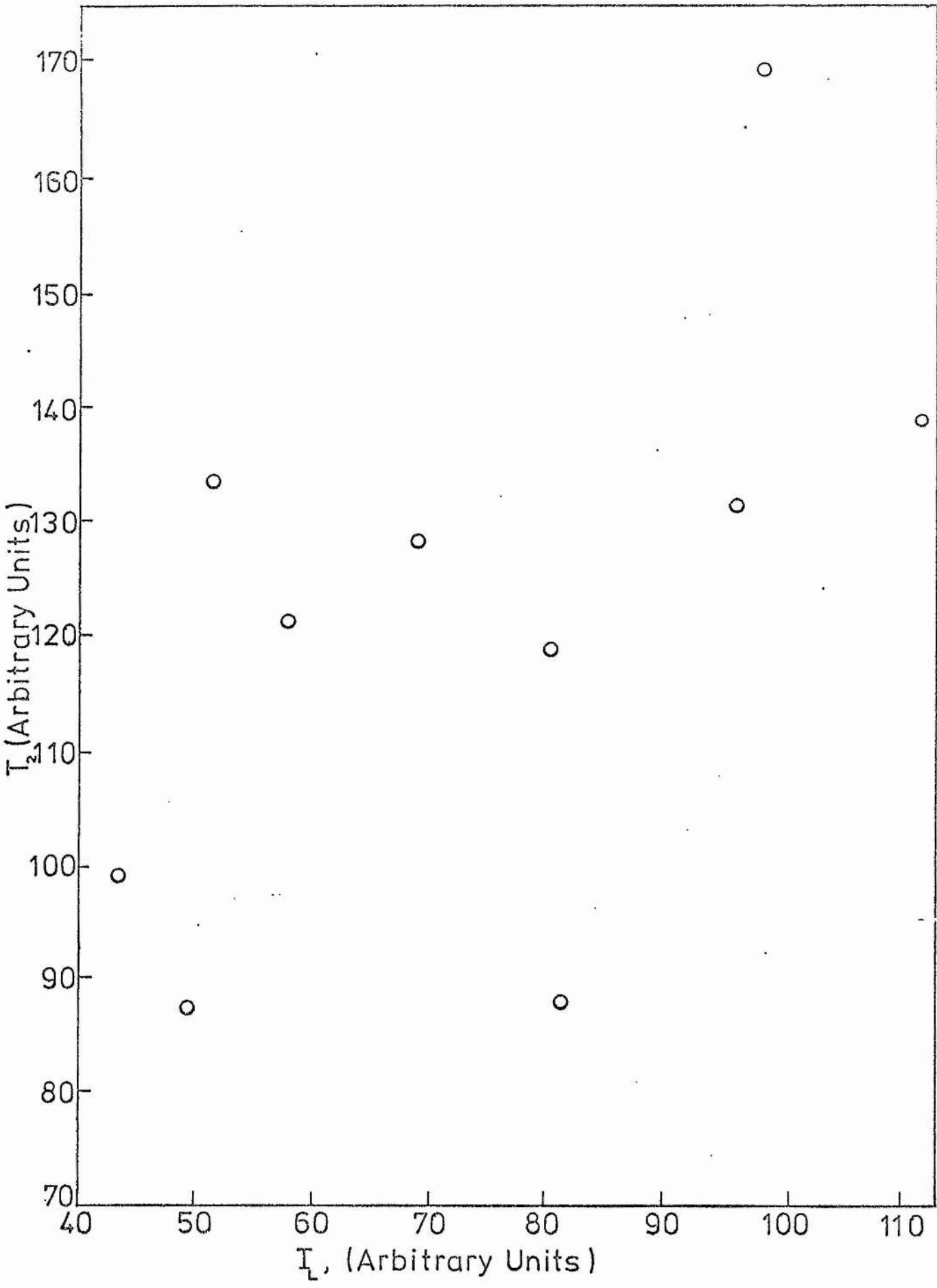

Fig 50 Influence of Input Pulse Amplitude on Cut-Off Threshold in Chlorobenzene

Frame 1 Frame 2 Frame 3 Frame 4

t

1mm = 2 n.sec

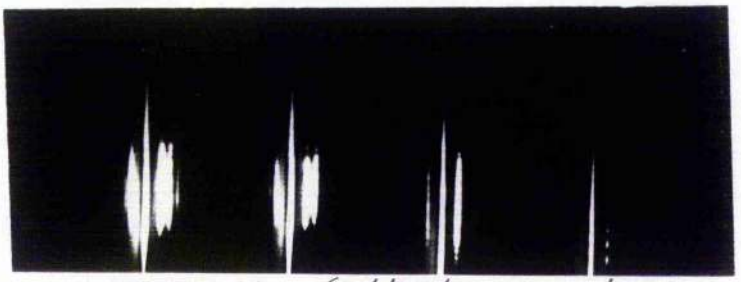

Plate 11. 65%/35% Benzene/Carbon Disulphide

L S 2 3 4

t

1mm = 2 n.sec

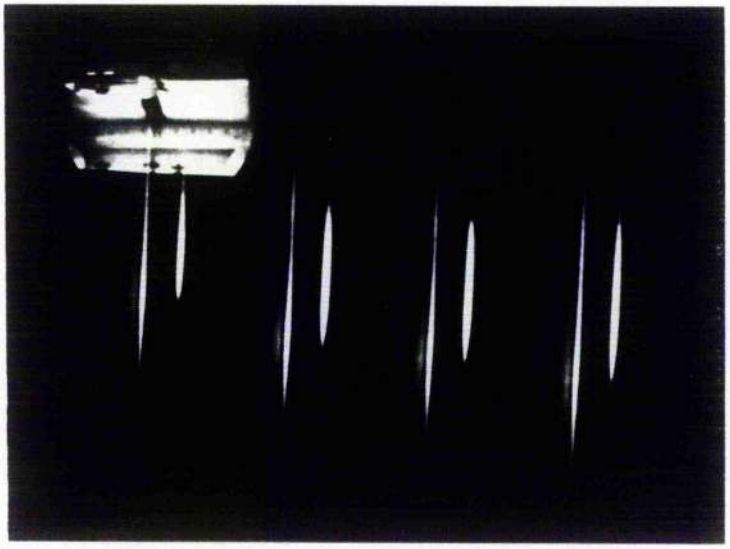

Plate 7. Nitrobenzene

AS L S 2S 2 3 4

t

1mm = 2 n.sec

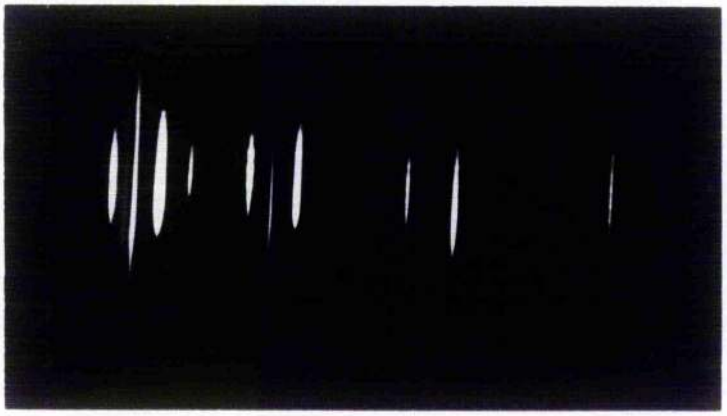

Plate 12. Bromobenzene

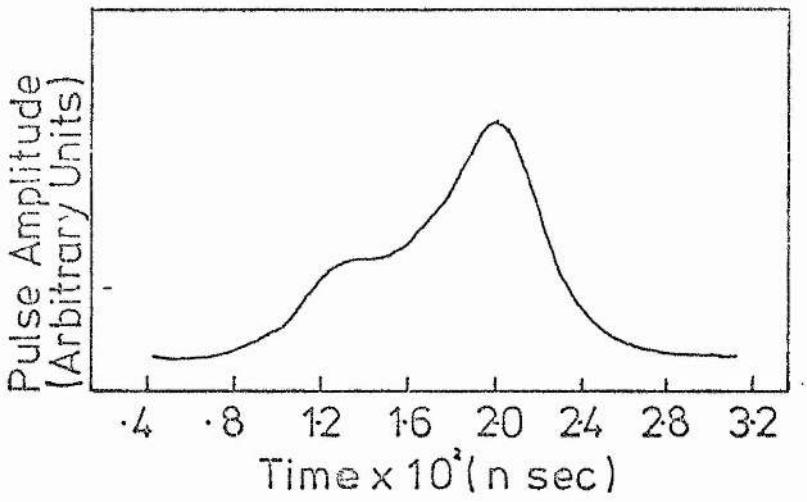

Fig 51(a)

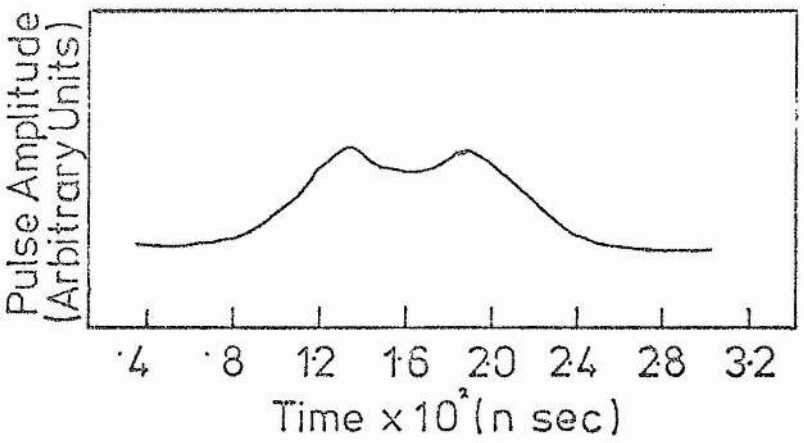

Fig 51(b)

Fig 51 (a,b) The Transmitted Laser Pulse in Nitrobenzene.
(a) Before Distillation
(b) After Distillation

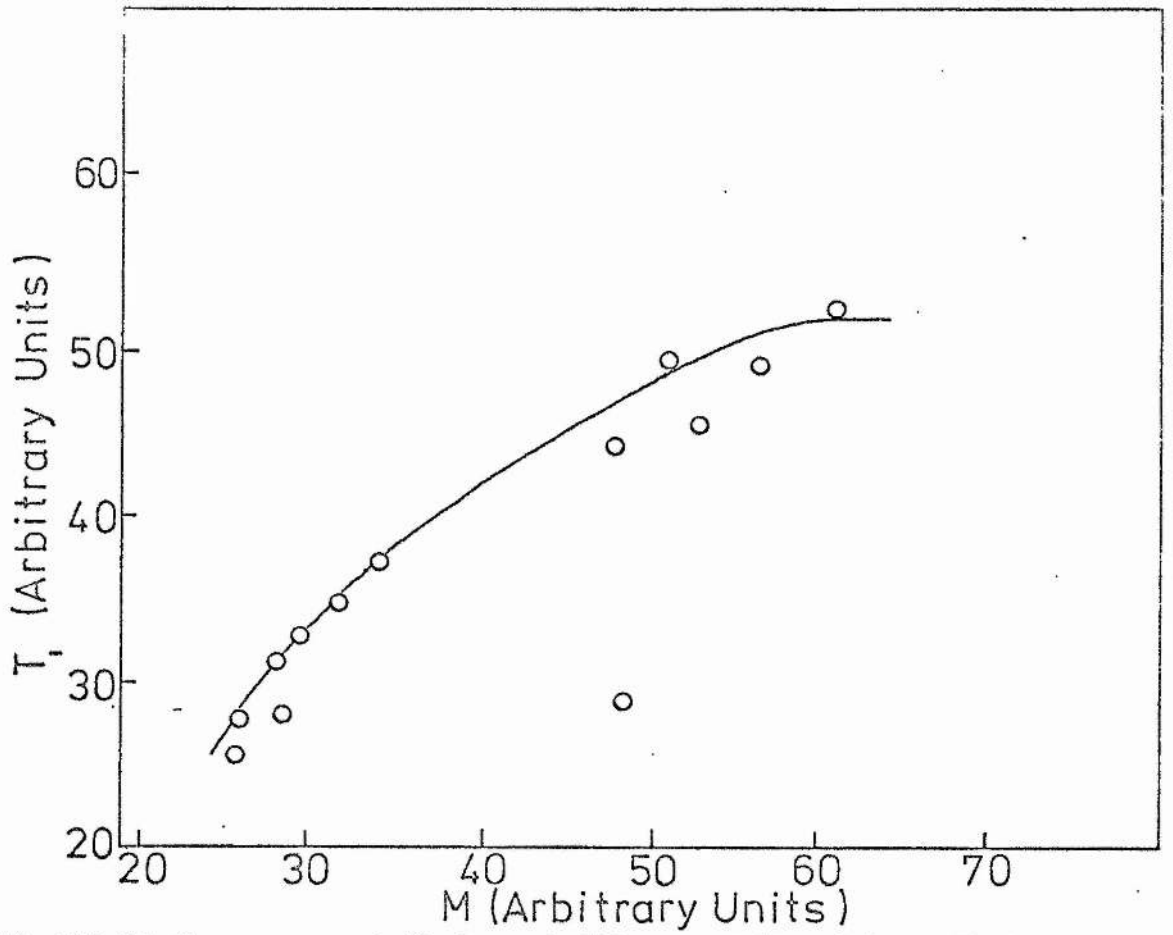

Fig 52 Influence of Rate of Rise of Exciting Pulse on Pulse on Pulse Distortion Threshold of Nitrobenzene

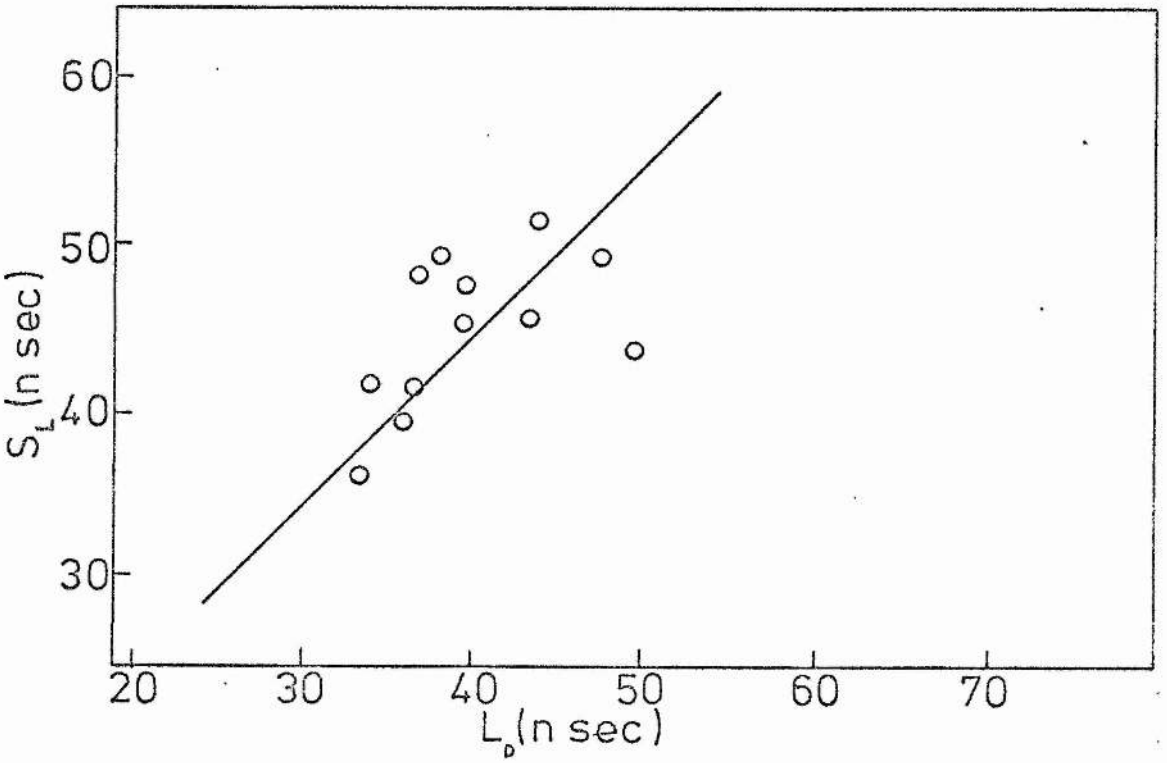

Fig 53 Correlation between Streak Duration of 1st Stokes in Nitrobenzene and Pulse Distortion of Transmitted Laser Pulse

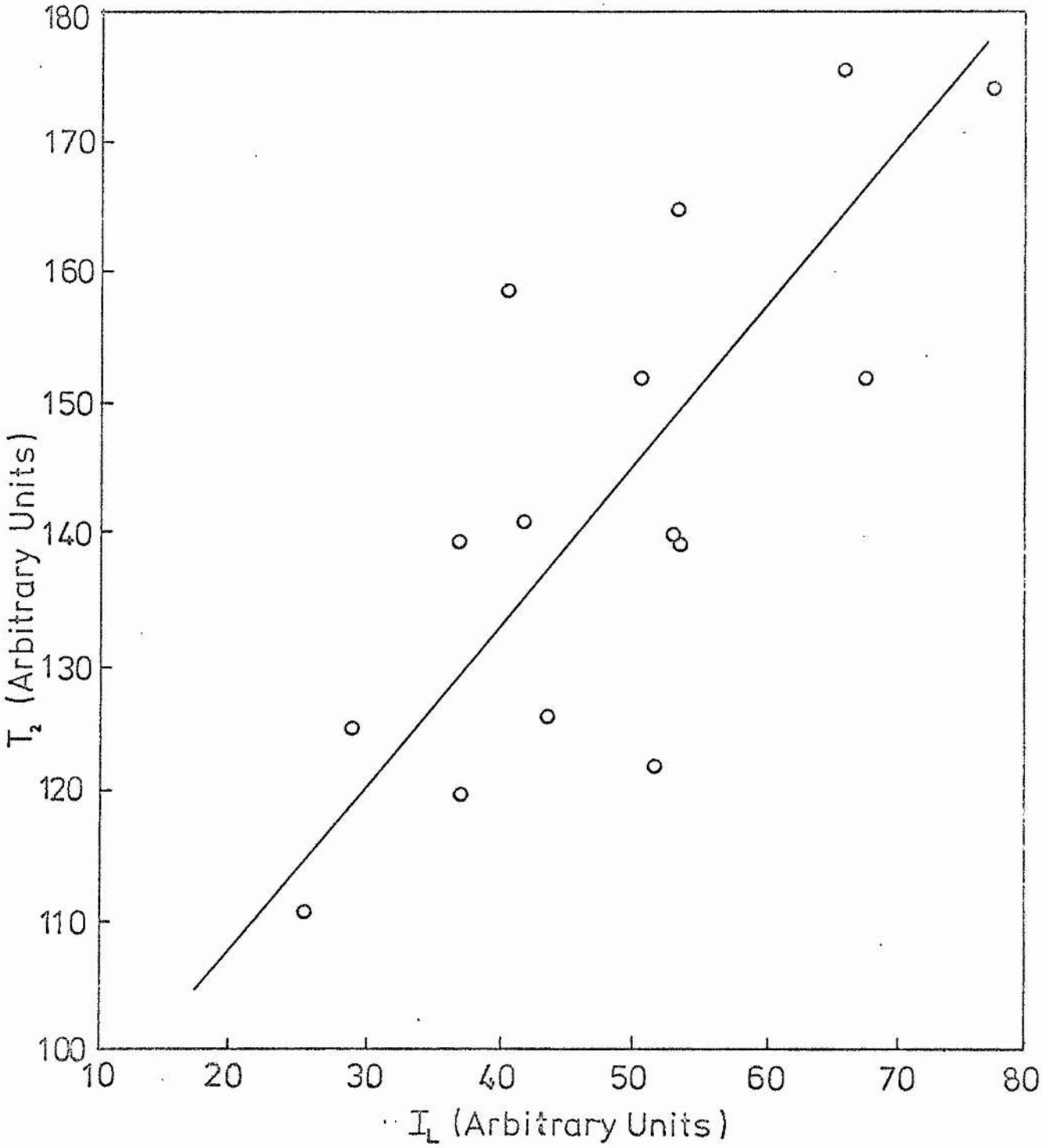

Fig 54 Influence of Input Pulse Amplitude on Pulse Distortion Cut-Off in Nitrobenzene

Typical spectra and line identification for each liquid are shown in Plates 4 - 12. Plate 13 shows the streak camera and the photodiode spectrometer system. Streak pictures are also included of Toluene, Bromobenzene and Benzene/Carbon Disulphide mixtures. These clearly demonstrate the range of the system in studies of this type.

5.11 Summary of Results

5.11(a) Correlation of Pulse Distortion Duration with Streak Duration

For all the liquids investigated there was a strong correlation between the duration of pulse distortion and that of Raman Stokes generation as obtained from the streak photographs. Pulse distortion was observed only if stimulated Raman radiation was generated. For the two liquids in which it was possible to generate second harmonic Stokes radiation, the time delay between the Stokes and the second harmonic Stokes decreased with increasing rate of rise of the exciting pulse. This decrease is difficult to interpret because of the large scatter of the results. The secondary pulse distortion pulse is correlated with harmonic generation, in as much as one was not observed without the other, and the times at which they appear correspond within experimental error. The spectra for all the liquids clearly show that there is a sharp threshold for stimulated Raman and that the harmonics are not generated simultaneously but in sequence.

5.11(b) Pulse Distortion

Each liquid was found to give to the transmitted laser pulse a pulse distortion profile which was characteristic of the particular liquid. The threshold for the onset of distortion was found to increase

Plate 13. Camera Photodiode System

with rate of rise of the exciting pulse, and in the particular case of carbon disulphide, the threshold was shown to approach a constant maximum value. The cut-off value for all the liquids studied (apart from carbon disulphide) showed an increase with the peak amplitude of the exciting pulse. The relative values of the cut-off at the lowest rates of of rise are shown in Table 5 together with a summary of their significant parameters.

5.11(c) Nature of Threshold for Stimulated Raman Radiation

As shown in Plate 4 threshold for the generation of stimulated Raman radiation is not well defined when examined with nanosecond resolution. In general, the threshold consists of one or two very fast pulses before the main generation begins. This behaviour is consistent with the findings of Maier et al (see 4.8) who explained the rapid fluctuations in forward stimulated Raman gain on the basis of observed picosecond Raman pulses in the backward direction. In the case of weak Raman generation, the streaks appear to show a regular train of these pulses.

5.12 Discussion of Results

Although there is a strong correlation between the observed pulse distortion of the transmitted pulse and the streak spectra of the forward stimulated Raman scattering (S.R.S.) it is clear that this is not the dominant process since the time devleopment of the transmitted laser pulse is dictated by the strong backward stimulated Brillouin (S.B.S.) and Raman scattered pulses. A working model of the interaction must be based on the focusing of a slow Q-switched laser pulse into a

TABLE 5

LIQUID	SHIFT	Ndσ	$\Delta\nu_R$(43)	G	$K_\alpha x10^8$(23)	$K_\rho x10^7$	T_{1min}^{exp}
BENZENE	992 cm^{-1}	1.0	2.3 cm^{-1}	1.0	5.73	1.33	23.0
CARBON DISULPHIDE	665 cm^{-1}	2.7	1.4	4.5	32.6	2.53	9.0
CHLORO BENZENE	1002 cm^{-1}	0.7	1.6	1.0	9.93	1.20	55.0
NITRO BENZENE	1345 cm^{-1}	1.1	6.6	0.4	26.4	0.92	27.0

Ndσ is the peak differential scattering cross section relative to BENZENE

$\Delta\nu_R$ is the spontaneous RAMAN linewidth

G is the stimulated gain coefficient defined as $(Nd\sigma/\Delta\nu_R)$

K_α, K_ρ are as defined in CHAPTER 3

T_{1min}^{exp} is the minimum experimental value

non-linear medium where the beam self-traps and then self-focuses within a length given by the distance from the focal plane to the exit surface of the Raman cell. The onset of self-focusing initiates the dominant backward scattering processes which control the effects observed in the forward direction. The model must be such that the observed threshold for the process depends upon the response time. Since the dominant backward scattering processes were not observed directly in the forward direction, and their presence only inferred from other measurements, it is necessary to discuss these effects and their predicted influence on the results obtained in some detail.

5.12(a) Stimulated Brillouin Scattering

Brillouin scattering[45] (i.e. the scattering of thermal density fluctuations) is best viewed as a photon-phonon collision in which a phonon is emitted or absorbed by the incident photon to produce a Stokes or Anti-Stokes photon. Momentum and energy are conserved in the interaction so that the frequency shift is given by

$$\Delta\nu = \nu_s = \pm 2\nu_o(V_s/c)n \sin(\theta/2),$$

where ν_s and ν_o are the frequencies of the phonon and the incident frequency, V_s is the sound velocity at frequency ν_s, (c/n) is the velocity of light in the medium, and θ is the scattering angle. Since backward scattering is the dominant process, θ is 180^o.

As with Raman scattering, stimulated Brillouin scattering occurs in the presence of high photon fluxes. In the liquids of interest the acoustic phonons are heavily damped with attenuation lengths small compared to the interaction region and the distances over which

the intensities of the Stokes waves change appreciably. Under these conditions, Tang[46] showed that S.B.S. could be characterised by two coupled rate equations,

$$(dN_B(z)/dz) = -g'N_L(z)N_B(z),$$
$$(dN_L(z)/dz) = -g'N_L(z)N_B(z) , \qquad 5.12.1$$

where N_L, N_B are the flux densities of the laser and Brillouin light propagating in the +Z and -Z directions respectively, and g' is the gain factor. Maier[47] developed this into his so called quasi- steady state theory where equations 5.12.1 are expressed in terms of intensity, I as follows

$$(dI_B/dz) = -g\, I_L(z)I_B(z) ,$$
$$(dI_L/dz) = -g\, I_L(z)I_B(z) , \qquad 5.12.2$$

The gain factor g is given by

$$g = k_L^2\gamma^2/(2\pi cn^3\rho V\delta\nu) , \qquad 5.12.3$$

where γ is the electrostrictive coupling parameter, V and $\delta\nu$ are the velocity and line width of the acoustic phonons respectively. Solution of the coupled intensity equations gives

$$\frac{I_B(z)}{I_B(o)} = \frac{1 - I_B(o)/I_L(o)}{\exp\{(1-I_B(o)/I_L(o))gI_L(o)z\}-I_B(o)/I_L(o)} \qquad 5.12.4$$

and

$$I_B(o) = I_L(o) - I_L(z) + I_B(z) , \qquad 5.12.5$$

where $I_L(o)$ and $I_B(o)$ are the laser and Brillouin intensities at the entrance to the cell respectively. The conversion of laser into Brillouin light was defined as $I_B(o)/I_L(o) = K$. For large gain in a

cell of length ℓ with $\exp\{1-K\}gI_L(o)\ell >> K$, the above equations simplify to give

$$(1-K)gI_L(o)\ell = \ell n\{(1-K)K\} - \ell n\{(I_B(\ell)/I_L(o)\} \equiv G.$$

Solving this equation for the Brillouin intensity at the cell window gave

$$I_B(0) = I_L(0) - G/(g\ell) \qquad 5.12.5$$

From this equation it is clear that if $G/(g\ell) << I_L(o)$ that a large conversion of the incident laser intensity is possible.

Experimentally, instantaneous power, not intensity, is measured, so that Maier transformed the equations 5.12.4,5 from a knowledge of the intensity distribution of the incident beam and obtained

$$\frac{P_B(Z)}{P_L(o)} = \frac{G}{I_o g\ell}\left\{ \ell n \frac{G}{I_o g\ell} + \frac{1}{1-\exp(-GZ/\ell)} \ell n\left[I_o g\ell/G + (1-I_o g\ell/G) \times \exp(-GZ/\ell)\right]\right\} \quad 5.12.6$$

and

$$P_B(0) = P_L(0) - P_L(Z) + P_B(Z).$$

In an elegant experiment Maier investigated the above equations and found that the value of g agreed with the predicted values for a range of liquids. Investigation of the dependence of conversion upon cell length produced results of particular interest. These are shown in Fig 55. From these experiments, Maier drew the following conclusions.

1. In the quasi-steady state condition the Brillouin power, $P_B(0)$ depends linearly on the incident power, $P_L(0)$. To a first approximation $P_B(0)$ is proportional to $P_L(0)$ and is smaller by a nearly constant amount.

2. The transmitted laser power in the steady state condition

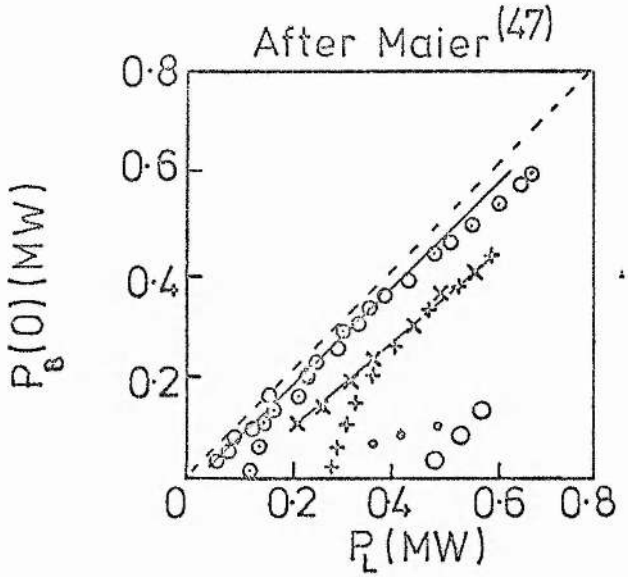

Fig55 Instantaneous Brillouin power P_B versus rising $\overset{\circ}{\underset{\circ}{+}}$ and falling $\overset{\circ}{\underset{\circ}{\times}}$ instantaneous laser power P_L in CS_2 (o) cell length l = 30cm : (+) l = 5cm : (o) l = 25cm. The broken line indicates 100% conversion.

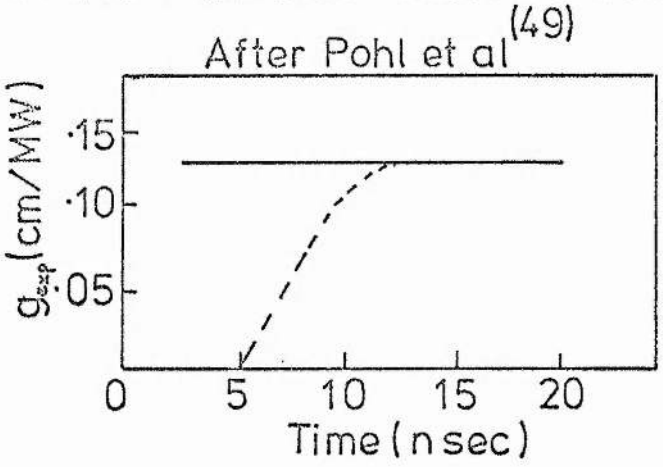

Fig56 Experimental Brillouin gain factor in CS_2 (1) slowly rising input pulse and (2) abruptly rising input pulse.

was found to be approximately constant (c.f. results for Benzene Chapter 4). From equation 5.12.7 with Z = ℓ, Maier showed that this behaviour is expected.

3. Investigation of the Z-dependence of the conversion into stimulated Brillouin showed that conversion occurred in the first few millimetres from the entrance window.

An alternative deduction can be obtained from 5.12.7 with Z = ℓ,

$$P_L(\ell) = P_L(0) - P_B(0) + P_B(\ell) \quad . \qquad 5.12.8$$

Following Maier we note that P_B is small and can therefore be neglected. The results clearly show that in the steady state condition,

$$P_B(0) = K\, P_L(0) \qquad 5.12.8a$$

where K is a constant fraction. Combining 5.12.8a with 5.12.8, we get

$$P_L(\ell) = P_L(0)(1-K) \qquad 5.12.9$$

Once the steady state gain is achieved, the transmitted pulse should therefore follow the incident pulse. Consequently, this should lead to an increase in the forward scattering process of stimulated Raman.

The results shown in Fig 55 indicate that for long cells the steady state condition is achieved for all incident powers whilst for shorter cells this occurs only at higher powers. This means that the sharpness of threshold at which pulse distortion occurs is strongly dependent on the cell length.

5.12(b) Transient Response

The above analysis was based on the steady state theory, but the self-focused threshold is a non-steady condition and the transient

response of the medium is dominant. The early non-steady-state theory developed by Hagenlocker[48] was extended by Pohl[49] in a Brillouin amplifier experiment in which it was shown that the gain factor, g, was time dependent. The response time of the medium was found to be directly related to the phonon life time. Some of the Pohl results are shown in Fig 56. Pohl showed that the dependence of g upon time is of the form

$$g(t) = g(1+e^{-t/2\tau}), \qquad 5.12.10$$

where τ is the phonon life time which is directly related to the line width, $\Delta\nu$ of the excited phonon by the equation

$$\Delta\nu = (2\pi\tau)^{-1} \text{ or } 2\tau = (\pi\Delta\nu)^{-1} \qquad 5.12.11$$

Equation 5.12.10 was verified for a number of liquids including carbon disulphide. For low rates of rise, the gain factor is independent of time whilst for fast rates of rise, the predicted exponential dependence was verified.

Clearly threshold and the time development of forward scattering processes are expected to depend upon the rate of rise of the exciting pulse so that knowledge of the phonon life times for the liquids studied is necessary.

It is clear from the Table6that the phonon life times of the liuqids, apart from carbon disulphide are small, so that, although the phonon life time may significantly effect the minimum time development of forward scattering processes, they are not of sufficient magnitude to explain the dependence of threshold upon the rate of rise of the exciting pulse.

TABLE 6

LIQUID	$\Delta\nu$	2τ (nsec)
Benzene	350[50]	1.8
Carbon disulphide	65[50]	9.8
Chlorobenzene	600[51]	1.06
Nitrobenzene	620[51]	1.02

Since the response time limitations of the Brillouin gain factor cannot explain the observed effects, the self-focusing of a self-trapped beam by the non-linear response of the medium is considered. The exciting pulse is assumed to be triangular with an instantaneous power given by

$$p = M_L t, \qquad 5.12.12$$

where M_L is the rate of rise of the pulse.

For complete generality it is assumed that τ_ρ, the electrostrictive response time (see Chapter 3) is less than t_T, the time at which threshold occurs so that both electrostriction and the optical Kerr effect must be considered in determining the appropriate value of n_2, the non-linear coefficient.

Following Wang[22] the threshold power, P_T is given by

$$P_T^{\frac{1}{2}} = P_{cr}^{\frac{1}{2}} + \alpha/\ell,$$

where P_{cr} and α are as defined in Chapter 3. This expression can be rewritten in the form

$$P_T^{\frac{1}{2}} = (C'/n_2^{\frac{1}{2}}) , \qquad 5.12.13$$

or $$n_2 P_T = \text{constant}.$$

If α and β are the power-dependent components of n_2, then in the absence of time-response limitations, the lowest threshold power obtained satisfies the equation

$$n_2 P_T = (\alpha+\beta)P_o \text{ for } t_T \gg \tau_\rho . \qquad 5.12.14$$

In the absence of electrostriction, i.e., $\tau_\rho \gg t_T$, threshold depends only on the optical Kerr effect, and we have

$$\alpha P_T^K = (\alpha+\beta)P_o$$

or
$$P_T^K = (\alpha+\beta)P_o/\alpha, \qquad 5.12.15$$

where P_T^K is the Kerr-dependent threshold power. Clearly, threshold is strongly dependent upon the value of τ_ρ and lies between the two values given by the inequalities

$$P_o \leqslant P_T \leqslant (\alpha+\beta)P_o/\alpha \ . \qquad 5.12.16$$

Threshold power levels between the two extreme values correspond to values given by $\tau_\rho \lesssim t_T$. In this condition, if an exponential time dependence is assumed for the electrostrictive component, each time increment can be written as $M_L dt(1 - \ell^{-t}/\tau_\rho)$. The total change is found by integrating from 0 to t so that we get

$$n_2^E P = \int_0^t M_L \beta(1-\ell^{-t/\tau_\rho})dt \ ,$$

$$= \beta M_L(t-\tau_\rho) + \beta M_L \tau_\rho \ell^{-t/\tau_\rho},$$

$$= \beta P(t-\tau_\rho) + \beta P(\tau_\rho)\ell^{-t/\tau_\rho}\}. \qquad 5.12.17$$

The total power-dependent change is given by

$$n_2 P = \alpha P(t) + \beta P(t-\tau_\rho) + \beta P(\tau_\rho)\ell^{-t/\tau_\rho} \qquad 5.12.18$$

which at threshold for self-focusing is given by

$$n_2 P \simeq (\alpha+\beta)P_o$$

so that we have

$$P(t_T) = P_o + \frac{\beta}{\alpha+\beta} M_L \tau_\rho (1-\ell^{-t/\tau_\rho}). \qquad 5.12.19$$

For $\tau_\rho \ll t_T$ the above expression indicates that the threshold power increases approximately linearly with rate of rise of the exciting pulse,

$$P(t_T) \simeq P_o + \frac{\beta}{\alpha+\beta} \tau_\rho M_L \ , \qquad 5.12.20$$

where the gradient of the curve is given by

$$\text{gradient} = \beta/(\alpha+\beta).\tau_\rho \qquad 5.12.21$$

In these conditions, if α and β are known , it is possible to determine the value of τ_ρ . The following four predictions are based on electrostriction and the role of electrostriction can be assessed by the extent to which they are proved to be true.

1. If electrostriction is significant then the ratio of thresholds in the limiting conditions should be in the ratio given by $(\alpha+\beta)/\alpha$.

2. A linear rate of rise is expected between these two values with a gradient given by $(\beta/(\alpha+\beta)\tau_\rho$.

3. For slow rates of rise quasi-deconditions the relative thresholds in the absence of time-response limitations should be in the inverse ratio of the summed electrostrictive and optical Kerr coefficients. This is only valid if the constant in equation 5.12.13 is the same for all liquids. This constant is given by

$$C' = \{\frac{(1.22\lambda)^2 C}{256}\}^{\frac{1}{2}} + \frac{n_o}{4} (\frac{a^2}{f}) \frac{C^{\frac{1}{2}}}{\ell} \ .$$

Since the geometrical arrangement was fixed and the mode of operation of the laser was unchanged throughout the experiments described in this thesis, C' should be a constant within experimental error. The refractive index change for the range of liquids is considered small compared to other possible errors so that relative thresholds can be measured.

4. Since the beam diameters in the focal region and the velocity

of the density wave is approximately the same for all the liquids it is predicted that the experimentally determined response time should be approximately constant from liquid to liquid.

5.13 Interpretation of Experimental Results

5.13(a) Threshold as Observed from the Onset of Pulse Distortion

The results clearly show that the threshold for the generation of stimulated Raman radiation is response-time limited. The two possible basic factors in the explanation of the observed effect as discussed above are the time-dependent Brillouin gain factor, $g(t)$, and electrostriction. The values of line-width for the liquids selected indicate that the Brillouin response-time is too small to explain the observed effects in the liquids examined (with the exception of carbon disulphide) where the calculated time could be significant. In this case the alternative mechanism of electrostriction must be considered. The validity of this hypothesis is readily checked from the predictions derived from the simplified treatment above.

From Table 7 it is clear that predictions 1 to 4 above appear to be valid for the liquids studied, within experimental scatter and the limited range of results taken. This strongly indicates that electrostriction is playing a significant role in determining the threshold for self-focusing and the subsequent pulse distortion.

Because of the large experimental scatter of the points and the simplified theory used, the experimentally determined values of τ_ρ are unlikely to be accurate. However, the values obtained appear to

TABLE 7

LIQUID	α	β	$(\alpha+\beta)^{-1}$	$(\alpha+\beta)/\alpha$	$\{\beta/(\alpha+\beta)\}\tau_\rho$	τ_ρ (nsec)	$\frac{T_1 max}{T_1 min}$	$T_1 min$	$(K_\alpha)^{-1}$
BENZENE	3.8	13.3	1.0	4.5	0.78	25.3	>3.0	1.0	1.0
CARBON DISULPHIDE	21.6	25.3	0.39	2.2	0.55	27.0	3.0	0.4	0.18
CHLORO BENZENE	6.6	12.0	0.92	2.82	0.65	27.8	†	1.3	0.58
NITRO BENZENE	17.6	9.2	0.65	1.52	0.3	55.0*	4.0*	0.53	0.27

The value of α is taken as 2/3 K_α (3.2) and the value of β as K_ρ.

The values of $T_1 min$ are relative to BENZENE and have been compared at $M_L = 10$. Those for chlorobenzene and nitrobenzene have been obtained by linear extrapolation.

$T_1 max$ is the estimated terminal value.

† indicates that the experimental scatter makes measurement impossible

* Large discrepancy possibly due to multiphoton absorption

be reasonable since if an incident beam divergence of 1 m radian is assumed, the initial response-time is approximately 100 nsec. This requires a subsequent reduction of a factor 4 as the beam self-focuses. A further experimental check is shown in Fig 57 in which t_T is plotted against M_L. From this it is clear that, for the lowest rates of rise obtained, the electrostrictive term is significant. The results for carbon disulphide, where the time to threshold is less than 20 nsec, indicate that the effective response time is less than that experimentally obtained.

5.13(b) Time Resolution and Pulse Distortion Results

The strong experimental correlation between the duration of first and second Stokes and the pulse distortion clearly shows that the generatio of forward Raman is coupled to the transmitted laser pulse not the exciting pulse. Further, the intensity of forward Raman generation is weak in comparison to this transmitted pulse. This behaviour is consistent with the presence of strong backward Brillouin scattering and the experiments of Maier[47] who showed that the maximum conversion into S.B.S. occurred in the first few millimetres from the entrance window. The initial development of forward stimulated Raman scattering should therefore be related to the pulse distortion through the time dependent gain factor, g, which, from 5.12(b) is a function of the phonon lifetime. From 5.12(a), second Stokes generation occurs when steady state gain conditions are stabilised and the transmitted pulse follows the exciting pulse. The results are clearly consistent with this picture, particularly in

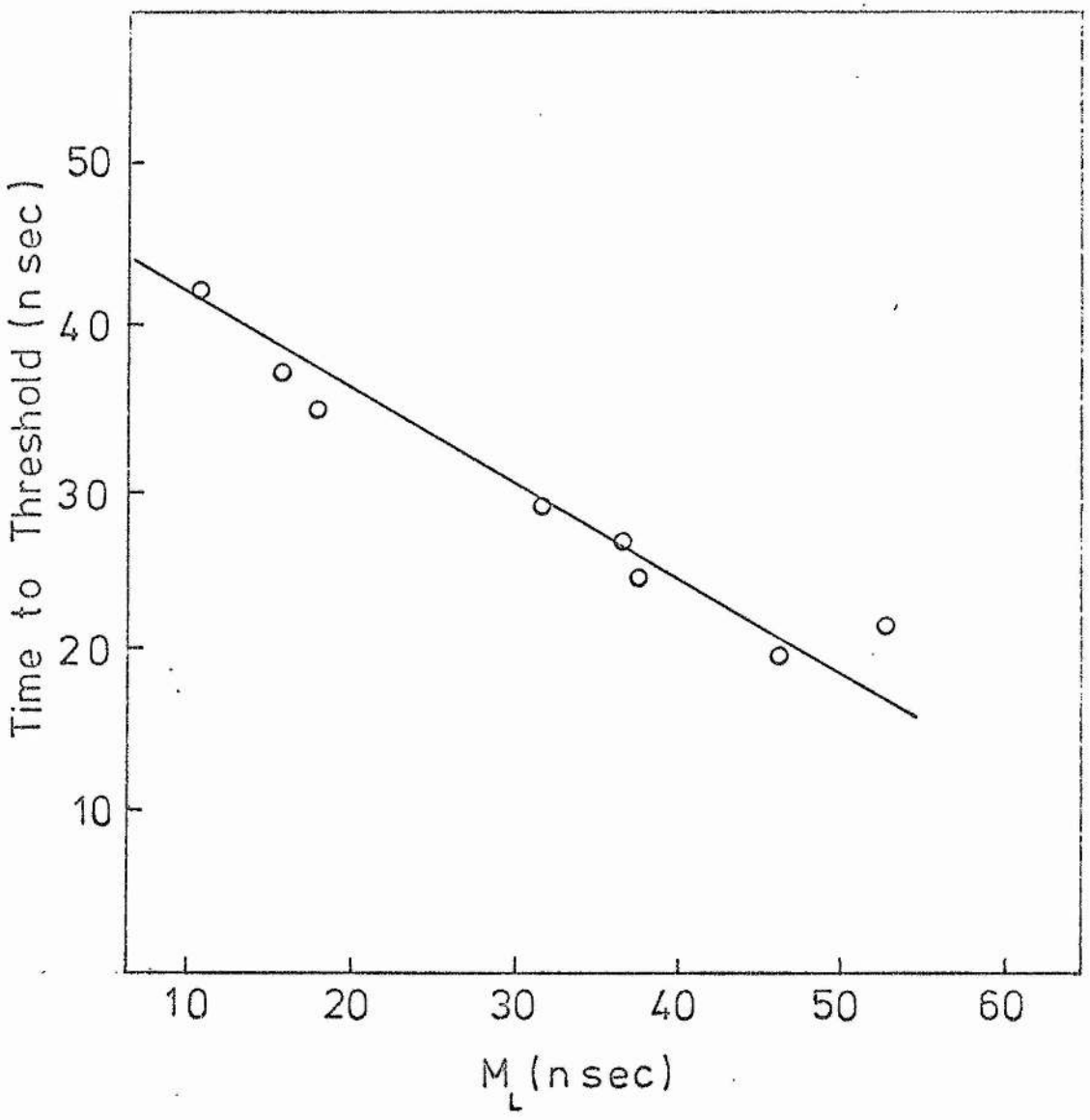

Fig 57 Influence of Rate of Rise of Exciting Pulse on Time to Pulse Distortion Threshold

the case of carbon disulphide which, from Table 6, has the largest phonon lifetime.

In the other liquids, (apart from nitrobenzene, where no harmonics are generated) the effect is masked by a steadily increasing background till the beam apparently defocuses and further forward Raman generation is inhibited. It is significant that this effect is least in carbon disulphide where no correlation is found between T_2, the cut-off threshold, and the input pulse power. The defocusing action is strongest in nitrobenzene. It was found that a freshly distilled sample of this liquid exhibited a marked reduction in the asymmetry of the thresholds suggesting a photon absorption process. Giordmaine[52] showed that multiphoton absorption for the liquids investigated decreased in the order nitrobenzene, benzene, chlorobenzene with the minimum value for carbon disulphide. It appears, therefore, that the defocusing process is due to multiphoton absorption.

The time delay between the fundamental Stokes and the second harmonic for both benzene and carbon disulphide tended to decrease with rate of rise of the exciting pulse. This is readily explained in terms of small signal gain theory for which the exponential term in 2.2.10 can be expanded to give

$$I_R = {}^{o}I_R(1 + G_R I_L + ...),$$

where G_R is the gain coefficient. At threshold, because of the strong backward scattering processes, the forward gain is small and higher order terms in the expansion can be neglected. Since the transmitted laser pulse at threshold is approximately constant and ℓ is small, no

build-up of the fundamental will occur. For slow rates of rise the threshold power is lower and the backward gain is high leading to a slow build-up to the threshold for the harmonics when the steady state gain is reached. For fast rates of rise the threshold power is higher and the backward Brillouin gain is low leading to a more rapid build-up of the fundamental.

For completeness the results must be compared with those of other time resolved investigations, notably those of Hordvik and Collins[53] who, as in the present investigation, studied the time relation between the various orders of stimulated Raman Stokes and Anti-Stokes radiations and the exciting pulse in a similar range of self-focusing liquids. A comparison with their results permits an identification of the time domains in which Raman can be investigated based on the nature of the exciting pulse and the time response of the particular liquid under study. The laser output in their experiments consisted of an irregular series of resolved pulses each lasting a few nanoseconds. The rate of change of the exciting pulse therefore prohibited any significant build up of backward stimulated Brillouin scattering since insufficient time was available to establish the steady state gain factor. Stimulated Raman scattering was therefore dominant and the time development was related to the incident exciting pulse not the transmitted pulse. This behaviour is consistent with the findings of Kaiser[54] who used subnanosecond pulses and obtained high conversion into stimulated Raman radiation. In other words, in an excitation system where the incident

radiation consists of pulses, whose rate of change is fast compared to the phonon life-time, stimulated Raman generation is dominant in the interaction. In the present experiments, however, stimulated Raman scattering is weak and follows the transmitted laser pulse, not the exciting pulse, suggesting that backward stimulated Brillouin scattering is dominant. Although the time response of the oscilloscopes used prohibited observation of nanosecond oscillations in the incident pulse, any significant modulation of the slow Q-switched envelope would have been clearly evident on the streak records. The effects observed are therefore a function of the envelope of the exciting pulse and not any nanosecond fine structure. The present experiments are in a time domain where the rate of charge of the exciting pulse is slow compared to the phonon life time and stimulated Brillouin scattering is dominant. Further, it seems unlikely that the power dependent time shifts[53] between the peak of the exciting pulse and the peak outputs of various orders of Stokes radiation are significant to the present experiments since, here, Raman generation is controlled by the severely attenuated transmitted pulse so that the shifts would be of the order of a nanosecond.

5.13(c) Stimulated Raman Gain Coefficient

Stimulated Raman gain, as can be seen from the above is not

the most significant parameter in the effects observed, and the forward stimulated Raman effect appears merely to record the other processes in the interaction. The spectra obtained show that the gain is highest for carbon disulphide and lowest for nitrobenzene where only the fundamental Raman-shifted line is observed. It is difficult to make any quantitative deductions from the observed effects and the known gain coefficients because of the presence of multiphoton absorption effects.

5.13(d) Anomalous Effects Due to Focused Excitation

Two effects occur in a focused system which are not present in a parallel excitation experiment. The backward travelling Brillouin and Raman pulses do not have access to the whole of the incident pulse so that once the waves pass the focal region only a fraction of the incident beam is available. Secondly, as the field increases, the diameter of the focal spot increases, which may lead to an enhancement of the observed increase in the transmitted laser pulse[54]. This effect should, however, be small. It is difficult to estimate the significance of the former.

5.14 Concluding Remarks

The conclusion, that there is a significant electrostrictive

contribution to the results is, perhaps, surprising, but it must be remembered that the dynamics of filament formation, even in a parallel excitation system, are not yet understood. Several authors have reported terminal filament sizes of the order of 5μ in carbon disulphide[54] which would give an electrostrictive time constant of ∿3 nanoseconds. The observation of short pulses of duration 1 nanosecond is still possible under the above scheme as the Kerr-dependent component could relax to cause defocusing, whilst the electrostrictive component only partially relaxes and the beam can then refocus.

The forward scattering process of stimulated Raman is clearly coupled to the transmitted pulse and not the exciting pulse. This is not surprising, as Maier showed that the maximum conversion into Brillouin occurred in the first few millimetres from the entrance window, so that the dynamics of the focused beam and the forward gain are controlled by the pulse transmitted through this region.

The experimental system developed to study the transient effects in the stimulated Raman process has obvious assets since a large amount of data can be collected for each giant pulse emitted by the laser. The system could be improved by using faster oscilloscopes and by monitoring pulses in the backward direction thus giving a complete time record of all the scattering processes.

RESULTS - BENZENE

I_L	M_L	T_D,S-2S	T_D,S-AS	S_L	$2S_L$	AS_L	T_D,2S-S	S-AS	T_1	T_2	L_D	L_{2D}
30.6	11.0	-	∿	30.0	-	∿	-	∿	22.0	25.0	35.0	-
55.5	15.0	-	-	32.0	-	14.0	-	4.0	33.0	31.0		-
40.0	16.0	-	16.0	50.0	-	28.0	-	7.0	25.0	37.0	49.0	-
42.3	18.0	12.0	8.0	42.0	14.0	28.0	14.0	4.0	32.0	27.0	53.0	13.0
58.0	19.0	-	6.0	30.0	-	20.0	-	∿	34.0	52.0	36.0	-
77.0	29.0	9.0	5.0	38.0	14.0	25.0	12.0	6.0	44.0	76.0	45.0	14.0
61.5	30.0	14.0	6.0	38.0	12.0	28.0	12.0	4.0	44.0	52.0	42.0	19.0
49.5	32.0	8.0	4.0	44.0	13.0	26.0	18.0	8.0	45.0	55.0	45.0	
80	35.0	10.0	8.0	44.0	18.0	28.0	8.0	15.0	42	106	46	21.0
100	37.0	10.0	10.0	10.0	45.0	23.0	32.0	13.0	53.0	103.0		
47.7	38.0	10.0	8.0	42.0	14.0	30.0	14.0	6.0	39.0	45.0	46.0	16.0
66.0	47.0	10.0	8.0	48.0	23.0	35.0	15.0	6.0	37.0	84.0	61.0	20.0
97.5	53.0	5.0	5.0	38.0	22.0	30.0	12.0	6.0	65.0	104.0	47.0	21.0
133	70.0	5.0	2.0	34.0	20.0	25.0	6.0	8.0	97.0	152	34	18.0

All in units of one nanosecond.

∿ = Feature too indefinite to measure

L_{2D} corresponds to duration of secondary distortion of the transmitted pulse.

RESULTS - CARBON DISULPHIDE

I_L	M_L	T_D,S-2S	T_D,S-AS	S_L	$2S_L$	AS_L	T_1	T_2	L_D	L_{2D}
95	11	1	9.0	62.0	56.0	50.0	9.0	37.0	80.0	60.0
121	12	9.0	8.0	54.0	32.0	46.0	13.0	53.0	80.0	∿
98	12	6.0	∿	64.0	52.0	30.0	12.0	41.0	76.0	60.0
142	14	6.0	6.0	61.0	50.0	54.0	13.0	58.0	80.0	
93.5	15	6.0	4.0	61.0	52.0	26.0	11.0	38.0	77.0	55.0
44.0	15	10.0	2.0	48.0	30.0	36.0	15.0	34.0	59.0	35.0
95	16	5.0	8.5	62.0	51.0	51.0	10.0	45.0	80.0	60.0
63.5	17	6.0	4.0	66.0	52.0	20.0	12.0	29.0	80.0	55.0
49.5	19	12.0	2.0	62.0	41.0	50.0	18.0	43.0	82.0	
66.5	20.0	6.5	3.0	64.0	48.0	50.0	17.0	40.0	80.0	60.0
39.2	22	8.0	2.0	54.0	34.0	40.0	21.0	37.0	74.0	50
31.6	25	8.0	3.0	48.0	38.0	38.0	24.0	40.0	70.0	45.0
77.0	28	8.0	4.0	56.0	44.0	45.0	23.0	43.0	70.0	57.0
41.5	28	10.0	1.0	52.0	38.0	46.0	32.0	49.0	70.0	47.0
29.2	30	11.0	3.0	47.0	26.0	36.0	29.0	62.0	59.0	43.0
42.5	37	10.0	4.5	46.0	31.0	37.0	27.0	63.0	56.0	42.5
36.6	37	11.0	3.0	46.0	26.0	35.0	32.0	49.0	55.0	
50.0	41.0	9.0	2.0	43.0	28.0	36.0	38.0	63.0	52.0	45.0
46.0	46.0	8.0	2.5	59.0	40.0	46.0	32.0	49.0		
38.6	48.0	12.0	4.0	44.0	38.0	36.0	32.0	61.0	58.0	38.4
50.0	50.0	10.0	1.0	43.0	25.0	38.0	38.0	63.0	50.0	

RESULTS - CARBON DISULPHIDE

Streak speed changed from 2 nsec/mm to 1 nsec/mm

M_L	19.0	19.0	22.0	23.0	27.0	28.0	31.0	40.0	47.0	53.0
T_D, S-2S	10.0	8.0	4.5	5.0	3.0	5.0	4.0	7.0	6.0	4.0

RESULTS - CHLOROBENZENE

I_L	50.0	82.0	44.0	99	102.0	81.0	113.0	70	52.5	58.2
M_L	34	41.0	57.0	63.0	70.0	71.0	75.0	76	89	91
T_D, S-2S	-	-	-	-	8	6	-	-	-	-
S_L	27	26.0	22.0	35.0	38	35	26.0	24.0	22	24
T_1	55.0	65.0	89.0	78.0	80	71	91.0	90.0	119	121
T_2	87.0	88.0	99.0	169.0	131	119	139.0	128	133	120
L_D	∿	28.0	24.0	-	43	34	27.0	27	15	23

RESULTS - NITROBENZENE

I_L	M_L	S_L	T_1	T_2	L_0
42.0	25.2	46.0	26.0	104.5	44.0
78.0	25.8	44.0	28.2	129	50.0
54.0	27.6	50.0	27.4	122.0	47.5
66.0	28.0	49.0	31.8	130	37.0
37.1	28.4	52.0	32.6	103.5	44.5
53.7	33.4	50.0	37.8	103.5	38.6
29.6	31.4	43.0	35.0	107.2	37.0
25.6	48.0	42.0	44.5	82.5	37.0
54.3	48.2	48.0	29.0	103.0	40
48.4	48.5	-	46.5	112.5	-
52.0	51.5	42	49.5	90.5	34.0
40.4	53.0	-	45.4	107.2	-
38.0	56.5	46	48.2	89.0	40.0
44.4	61.0	40	52.0	93.4	35.6
68.2	61.0	36.0	52.0	112.5	34.0

APPENDIX A

A NEW BRIDGE FOR THE COMPARISON OF TWO "EQUAL" RESISTORS

Abstract

A simple, stable and inexpensive bridge has been constructed which compares two nominally equal resistors with a detection sensitivity of 1 part in 10^6.

Introduction

It is general practice when comparing two equal resistances to use an equal arm Wheatstone bridge. This method produces thermal stability but loses in sensitivity. Increased sensitivity can be attained by reducing the value of the resistors in the ratio arms but this is at the cost of a significantly increased power consumption for resistances less than 1 K. The new bridge operates at the maximum sensitivity of a Wheatstone with an order of magnitude less power consumption than the equivalent Wheatstone bridge (see below). The bridge has been used to compare standard resistances in the range 10-1000 Ω and as part of a Rat's nest system (Baker 1963) for the measurement of energy from a Q-switched laser. In both of those applications high sensitivity and stability are required. The bridge has been found capable of detecting changes in resistance of 1 in 10^6

Theory

An equivalent Wheatstone bridge and the new bridge are shown in Figs 1 and 2, respectively.

The new bridge relies for its operation on the equality of the

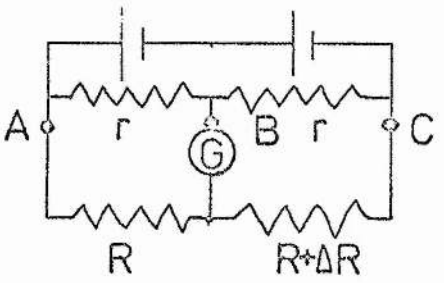

Fig 1

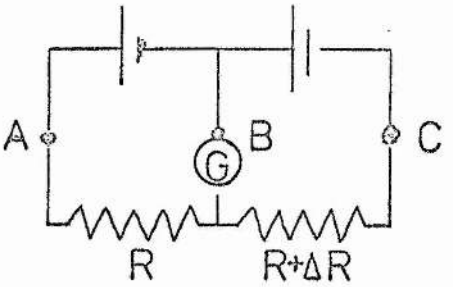

Fig 2

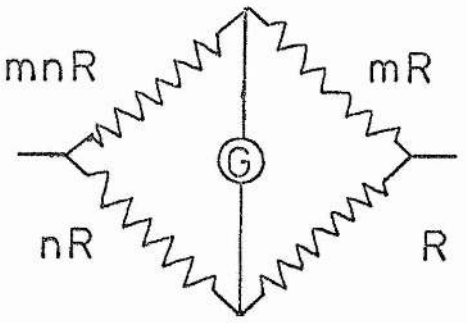

Fig 3

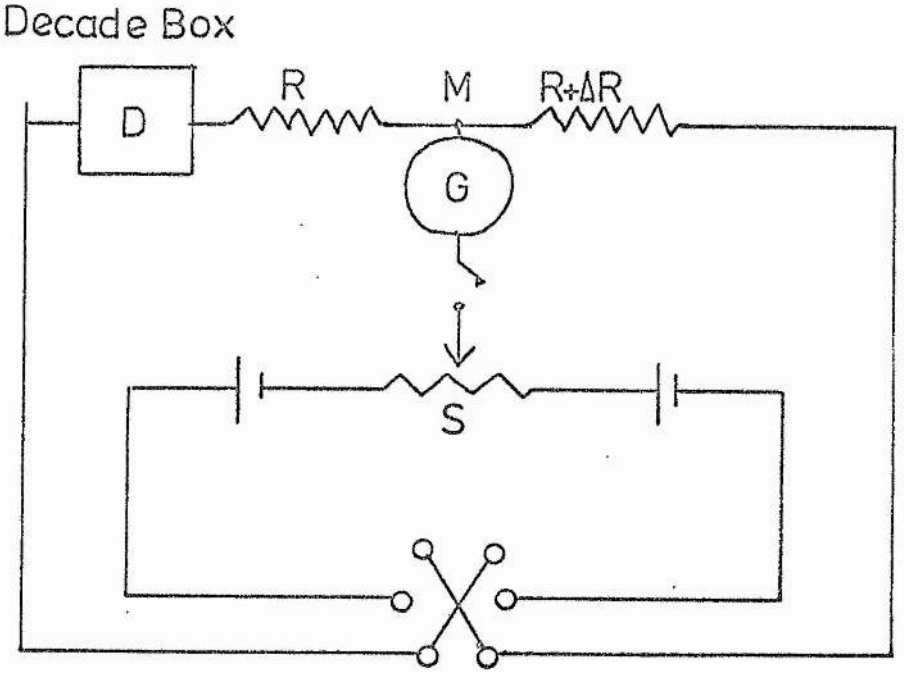

Fig 4

voltages, therefore only resistance unbalance is indicated by the galvanometer. Provided r<<R, the two circuits are electrically identical at the three terminals A, B, C and Callendar's theory can be applied to both.

The theory for the Wheatstone bridge shown in Fig 3 gives the sensitivity S,

$$S = i_g/R = i/\{(G/n)(1+n) + (1+m)R\} \qquad (1)$$

where R is the unknown resistance,

G is the galvanometer resistance,

i is the current through R,

i_g is the galvanometer current,

m,n are the coefficients shown in Fig 3,

and the optimum galvanometer resistance is given by

$$G = Rn(1+m)/(1+n) \qquad (2)$$

Substituting (2) into (1) with n = 1 gives

$$S_{max} = i/\{2R(m+1)\} \qquad (3)$$

Since the new bridge is effectively a Wheatstone bridge with zero ratio arms (i.e. m = 0), the sensitivity of the new bridge is equal to the maximum sensitivity of the Wheatstone bridge.

Since the power dissipated in the ratio arms of the Wheatstone bridge is given by,

$$P = v^2/mR, \qquad (4)$$

it is clear that maximum sensitivity cannot be achieved in practice. A more practical comparison can be made by choosing m = 0.1 which

gives 90% of maximum sensitivity. In this case the current drawn from the batteries of the Wheatstone bridge is an order of magnitude greater than that of the new bridge, and the power dissipation in the ratio arms of the Wheatstone bridge is 10 times that in the measurement arms.

The deflection (D) produced in a galvanometer of sensitivity S_g mm/μamp by a change ΔR is given by $D = S_g.S.\Delta R$. We define the resistance sensitivity of the bridge as $S_R = D/\Delta R$ and obtain for the maximum resistance sensitivity of the new bridge the value

$$S_R = (S_g i/2R) \times 10^6 = (S_g v/2R^2) \times 10^6 \text{ mm/ohm} \qquad (5)$$

As a typical application, consider the measurement of 100Ω standards using a 90Ω galvanometer with a deflection sensitivity of 71 mm/μamp and 2 volt batteries, the resistance sensitivity, S_R, is, for this case, $S_R = 5$ mm/millohm. Since a deflection of half a millimetre is readily detected, the bridge is capable of detecting 10^{-4} ohm or 1 part in 10^6. In practice, however, battery drift and thermal instability limit the accuracy attainable.

Construction

The practical circuit is shown in Fig 4. If the resistances are equal and the voltages applied to them differ, then, by operating the reversal switch, a deflection d_V, will be obtained on the same side of zero. If the voltages are equal and the resistances differ, reversal should produce asymmetric deflections, d_1 and d_2, where $d_1 = d_R - d_V$, and $d_2 = d_R + d_V$. The null point corresponding to equal resistances is then given by

$$R_N = (d_2 - d_1)/2 = d_V. \qquad (6)$$

Voltage unbalance, therefore, acts to shirt the resistance zero from the galvanometer zero. The voltage sensitivity of the bridge is defined by $S_V = D/\Delta V = D/i\Delta R$. Thus, from equation 5, we get

$$S_V = (S_g/2R) \times 10^6 \text{ mm/}\mu\text{volt} ,$$

so that an unbalance of 2 mV under the conditions of the example discussed above produces a full scale deflection. Care must therefore be taken to ensure that this voltage, caused by differences in battery voltage, circuit resistance, and thermal effects is small and constant. Convenient sources have proved to be Exide, 2 volt batteries with an internal resistance of 0.002 ohm. By selecting a pair which are equal to within 200 μvolts and storing these in parallel for 24 hours or so: the unbalance is typically reduced to 5 μvolts. Using two of these cells under a loading of 200 ohms, the drift has been found to be of the order of 1 μvolt/minute or 10^{-4} ohms/minute. Final compensation is made by the variable resistance, R_s, between the two batteries which acts as a zero adjustment. The value of this resistance is usually such that it has a 2 m volt drop along its length of 50 cm.

Thermal Effects

At a sensitivity of 1 ppm (Dunn 1967) has shown that thermal effects must be considered in detail. Following this work the circuit was designed as follows.

1. Heavy copper connecting leads were used .
2. A circuit arrangement which is symmetrical about SM was used.
3. There was a minimum number of dissimilar metal contacts.

4. The switch was fabricated from heavy copper strip (resistance less than 10^{-3} ohms).

The temperature stability of a resistor is given by

$$R = R_o\{1 + \alpha(T-T_o) + \beta(T-T_o)^2 + ...\},$$

which produces a resistance change of 10 ppm/degree C for manganin. Dunn (1967) has shown that the value of a stancard resistance is dependent on the power P dissipated and is given by

$$R = R_o\{1 + \alpha(kP) + \beta(kP)^2 .....\}$$

where we have

$$k(\text{oil filled resistor}) = \frac{0.5}{L}\{1-\ell^{-0.001t} + (13\pm10)10^{-4}/(r_2 d)\}$$

$$k_{air} = \frac{2.7}{L}\{1 - \ell^{-0.18t} + \frac{(14 + 10)10^{-3}}{r_2 d}\},$$

and L, r_2, d are dimensional constants for Dunn's idealised resistor construction. t is time in seconds.

These expressions indicate that there will be a sudden small rise in temperature followed by a larger change with a much longer time constant. Resistances used in the new bridge have been found to take periods of up to two hours to reach equilibrium.

Typical values of k_{oil} is 2.5 degrees C/watt corresponding to a resistance change of 25.0 ppm; thus there is a large uncertainty unless the power level is low. Their calculations were made for a particular resistance geometry so that the loading factor is dependent on the particular resistance used. In the new bridge, since the loading factor is the same for both resistors, they are compared under a given load condition. In the table given below the temperature stability

R	P_m watts	P_r watts	T_m °C oil	T_r °C oil	T_r °C air	T_r °C air
10	0.4	4	1	10	10	100
100	0.04	0.4	0.1	1	1	10
1000	0.004	0.04	0.01	0.1	0.1	1

P_m is the power dissipation in the measurement arm.

P_r is the power dissipation in the ratio arm of the Wheatstone bridge

T_m is the temperature rise in the measurement arm

T_r is the temperature rise in the ratio arm

and the power dissipation for the new bridge and for a Wheatstone with m = 0.1 are compared under normal operating conditions using two Exide batteries. In the new bridge the figures for power dissipation correspond to that of the measurement arm in the Wheatstone bridge. These values are calculated for oil and air filled resistors using the loading constants 2.5 degrees/watt and 25 degrees/watt respectively.

For a Wheatstone bridge, the loading factors of all four resistors must be considered, whereas, in the new bridge, where the ratio arms are effectively zero, only the measurement arm is important. From the table it is clear that the loading factor of the Wheatstone is prohibitive since the temperature rise and corresponding resistance change is large.

Operation

As with other bridges, the new bridge can be used in either the deflection or null deflection mode. The null method has proved most satisfactory for standard resistances, whereas the deflection mode is more suitable for the Rat's nest.

References

BAKER, R.M., Electronics, 36, (1963), 36.

DUNN, A.F., I.E.E.E. Trans. Of Instrum., (1966), 220.

REFERENCES

1. RAMAN, C.V. and KRISHNAN, K.S., Ind. Journ. Phys., 2, (1928), 387.

2. SMEKAL, A., Naturwiss, 11, (1923), 8.

3. PLACZEK, G., Handbuch der Radiologie, Vol VI, (1934), 209. Translated, U.S. Atomic Energy Comm., by Ann Werbin, UCRL-526(L) 1962.

4. DIRAC, P.A.M., Proc. Roy. Soc. A114, (1927), 710.

5. MCCLUNG, F.J. and HELLWARTH, R.W., J. App. Phys. 33, No. 3, (1962), 828.

6. WOODBURY, E.S. and Ng, W.K., Proc. I.R.E. 50, (1962), 2367.

7. ECKHARD, G., HELLWARTH, R.W. et al, Phys. Rev. Letters, 9, No. 11, (1962).

8. TERHUNE, R.W., Bull. Americ. Phys. Soc., 8, (1963), 359.

9. STOICHEFF, B.P., Phys. Letters, 7, (1963), 186.

10. HELLWARTH, R.W., App. Opt., 2, No. 8, (1963), 847.

11. HELLWARTH, R.W., Phys. Rev., 130, No. 5, (1968), 1850.

12. GARMIRE, E., PANDARESE, F. and TOWNES, C.H., Phys. Rev. Letters, 11, No. 4, (1963), 160.

13. TAKUMA, H. and JENNINGS, D.A., Proc. I.E.E.

14. BLOEMBERGEN, N. and SHEN, Y.R., Phys. Rev. Letters, 13, No. 24, (1964), 720.

15. LALLEMAND, P. and BLOEMBERGEN, N., Appl. Phys. Letters, 6, No.10, (1965), 210.

16. McCLUNG, F.S., WAGNER, W.G. and WEINER, D., Phys. Rev. Letters, 15, No. 3, (1965), 96.

17. CHIAO, R.Y., GARMIRE, E. and TOWNES, C.H., Phys. Rev. Letters, 13, No. 15, (1964), 477.

18. SHEN, Y.R. and SHAHAM, Y.S., Phys. Rev. Letters, 15, No. 26, (1965), 1008.

19. LALLEMAND, P. and BLOEMBERGEN, N., Phys. Rev. Letters, 15, No. 26, (1965), 1010.

20. CHIAO, R.Y., Phys. Rev. Letters, 13, No. 15, (1964), 477.

21. KELLEY, P.L., Phys. Rev. Letters, 15, No. 26, (1965), 1005.

22. WANG, C.C., Phys. Rev. Letters, 16, No. 9, (1966), 344.

23. SHEN, Y.R., Phys. Letters, 20, No. 4, (1966), 378.

24. BLEANEY and BLEANEY, Electricity and Magnetism, Second Edition Oxford University Press, 1965.

25. RAMAN, C.V. and KRISHNAN, K.S., Phil. Mag., 3, (1927), 724.

26. KAISER, W. and MAIER, M., Phys. Letters, 21, No. 5, (1966), 530.

27. PILEPETSKII, N.F. and RUSTAMOV, A.R., JETP Letters, 2, (1965), 55.

28. CHIAO, R.Y., Phys. Rev. Letters, 13, No. 15, (1964), 477.

29. BAKER, R.M., Electronics, 36, (1963), 36.

30. MAIER, M. and KAISER, W., Phys. Letters, 23, No. 1, (1966), 83.

31. GIORDMAINE, J.A. and HOWE, J.A., Phys. Rev. Letters, 11, (1963), 207.

32. McCLUNG, F.J., WAGNER, W.G. and WEINER, D., Phys. Rev. Letters, 15, (1965), 96.

33. WEINER, D., J. App. Phys., 36, (1965), 2395.

34. DAMEN, T.C., LEITE, R.C. and PORTO, S.P., Phys. Rev. Letters, 14, No. 9, (1965).

35. BRET, G., COMPT. REND., 260, (1965), 5323.

36. DALTON, M.L., App. Opt. 4, No. 5, (1965), 603.

37. MILLER, R.C., LABUDA, E.F. and GORDON, E.I., 22nd Conf. Electron Device Research, Ithica, (1964).

38. LABUDA, E.F., GORDON, E.I. and MILLER, R.C., I.E.E.E. J. of Quantum Electronics, Q.E. - 1, (1965), 273.

39. LOEB, L.B., J. Appl. Phys., 29, (1958), 1369.

40. BLOOM, A.L., App. Phys. Letters, 2, No. 5, (1963), 101.

41. Princeton Applied Research Manual, (1965).

42. McCLUNG, F.J. and WEINER, D., J. Opt. Soc. Amer., 54, 5, (1964), 641.

43. SKINNER, J.G. and MILSEN, W.G., J. Opt. Soc. Amer., 58, No. 1, (1968), 113.

44. BOYDE, G.D. and GORDON, G.P., Bell. Syst. Tech. J., 41, (1962), 347.

45. BRILLOUIN, L., ANN. PHYS. (Paris), 17, (1922), 88.

46. TANG, C.L., J. Appl. Phys., 37, (1966), 2945.

47. MAIER, M., Phys. Rev., 166, No. 1, (1968), 113.

48. HAGENLOCKER, E.E., MINCK, R.W. and RADO, W.G., Phys. Rev., 154, (1967), 226.

49. POHL, D., MAIER, M. and KAISER, W., Phys. Rev. Letters, 20, No. 8, (1968), 366.

50. FLEURY, P.A., and CHIAO, R.Y., J. Accoust. Soc. Am., 39, (1966), 751.

51. CRADDOCK, H., PhD Thesis, University of Kent, (1969).

52. GIORDMAINE, J.A. and HOWE, J.A., Phys. Rev. Letters, 11, (1963), 207.

53. HORDVIK, A. and COLLINS, R.J., IEEE J. Quantum Electronics, Vol QE-4, No. 5, (1970), 254.

54. KAISER, W., IEEE J. Quantum Electronics (Abstract), Vol QE-4, (1968), 381.

55. LOY, M.M.T. and SHEN, Y.R., Phys. Rev. Letters, 22, No. 9, (1969), 994.